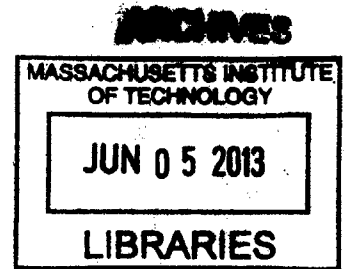


Solution-Gated Graphene Transistors for Chemical and Biological Sensing Applications

By

Benjamin Mailly

B.S., École Polytechnique, 2010



SUBMITTED TO THE DEPARTMENT OF MATERIALS SCIENCE AND
ENGINEERING IN PARTIAL FULFILLMENT OF THE REQUIREMENTS FOR THE
DEGREE OF

MASTER OF SCIENCE IN MATERIALS SCIENCE AND ENGINEERING
&
MASTER OF SCIENCE IN TECHNOLOGY AND POLICY

AT THE

MASSACHUSETTS INSTITUTE OF TECHNOLOGY

FEBRUARY 2013

©2013 Massachusetts Institute of Technology. All rights reserved

Signature redacted

Signature of Author: _____

Department of Materials Science and Engineering

January 14, 2013

Signature redacted

Certified by: _____

 Tomás Palacios
Professor of Electrical Engineering and Computer Science
Thesis supervisor

Signature redacted

Accepted by: _____

Gerbrand Ceder
Professor of Materials Science and Engineering
Chair, Departmental Committee on Graduate students

Solution-Gated Graphene Transistors for Chemical and Biological Sensing Applications

By

Benjamin Maily

Submitted to the Department of Materials Science and Engineering
On January 18, 2013 in Partial Fulfillment of the
Requirements for the Degree of Master of Science in
Chemical Engineering and Master of Science of the Technology Policy Program

ABSTRACT

Various fabrication processes were developed in order to make graphene-based chemical and biological sensors on different substrates. Single-layer graphene is grown by chemical vapor deposition and then transferred to silicon dioxide as well as PolyEthylene Naphthalate (PEN) substrate, where graphene solution-gated field-effect transistors (SGFET) are fabricated. The graphene on SiO₂ and PEN SGFETs exhibit high transconductances of 5 and 1 mS.mm⁻¹ respectively. They can be used as pH sensors in an aqueous environment with sensitivity at the Dirac point of 22 mV/pH. No significant influence of the nature of the substrate and the amount of residues on top of the graphene surface was found. This paves the way for developing low cost, flexible and transparent graphene sensors on plastic. The functionalization of graphene with glucose oxidase enables to build a graphene glucose sensor. The sensor exhibits reliably a high sensitivity of 15mV/pG (pG=point of glucose concentration) at the Dirac point and the lower detection limit found is 0.1 mM. Then, as the noise is the second crucial parameter along with sensitivity for biosensors, it was characterized in graphene SGFETs. The noise measured at the gate is very good around 20 μ V, which is an order of magnitude lower than conventional silicon SGFET.

Bilayer sensors were also investigated since they could potentially exhibit lower noise than monolayer devices. A transfer method was designed to stack two monolayer graphene films in order to make a bilayer film. Bilayer devices could also be used as pH sensor with similar sensitivity compared to monolayer devices. However, the noise performance of bilayer devices around 15 μ V is slightly better than monolayer devices and bilayer graphene is therefore also a promising candidate for sensing applications.

Finally, the commercialization of graphene sensors as well as innovative biosensors is hampered in the US by an ill-adapted FDA regulation. The consequences of this regulation are very negative with an outflow of capital from the US to Europe. Policy recommendations are made to restore the US leadership in the biosensor market, especially the implementation of an adaptive FDA regulation with a limited-launch, living-license process in which the effectiveness requirement is removed.

Thesis Supervisor: Tomás Palacios

Title: Professor of Electrical Engineering and Computer Science

Contents

Chapter 1- Introduction

- 1- Graphene properties
- 2- Electrochemistry principles
- 3- Solution gated field effect transistor technology
- 4- Commercialization of innovations in the biosensor market

Chapter 2- Fabrication Technology of graphene SGFETs

- 1- Graphene growth and transfer on SiO₂
- 2- Fabrication of graphene SGFET
- 3- Fabrication of graphene sensors on plastic PEN
- 4- Measurement set up

Chapter 3- Characterization of single-layer graphene sensors

- 1- Electrical characteristics on different substrates
- 2- pH sensing
- 3- Glucose sensing
- 4- E. Coli detection
- 5- Noise characterization in monolayer graphene sensors

Chapter 4- Bilayer graphene sensors

- 1- Fabrication process
- 2- Bilayer graphene sensor characterization
- 3- pH sensing
- 4- Noise in bilayer graphene devices

Chapter 5- The policy implications of moving from research to commercialization in the biosensor market

- 1- Policy controversies around the commercialization of biosensors
- 2- The biosensor technological revolution
- 3- Key drivers and restraints in the market
- 4- Two high barriers: development costs and regulatory approval
- 5- Policy recommendations

Conclusion

Chapter 1-Introduction

Carbon is one of the most fascinating elements in the periodic table. It can form allotropes of all dimensionalities: three-dimensional graphite, two-dimensional graphene, one-dimensional carbon nanotubes and zero-dimensional fullerenes. The most recent carbon material to have been discovered is graphene¹, isolated for the first time in 2004. Graphene is a two-dimensional material of sp^2 -bonded carbon atoms arranged in a honeycomb lattice. Since its discovery, graphene has been intensively investigated within the scientific and industrial communities. Indeed, its two-dimensional structure with each carbon atom connected to its neighbors through strong covalent bonds, results in outstanding electrical, optical, and mechanical properties²⁻⁴. Especially a unique property of its band structure is the strictly linear energy dispersion relation at low energies where electrons and holes behave like massless relativistic particles². This leads to very high charge carrier mobility in the graphene sheet with mobility exceeding $15000\text{ cm}^2\text{V}^{-1}\text{s}^{-1}$ at room temperature^{5,6}. In addition, with regards to its future applications, graphene possesses the attractive advantage of enabling large area integration thanks to the high quality and uniform graphene growth by Chemical Vapor Deposition⁷. Thus, numerous electronic applications are being targeted by this material, including high frequency transistors⁸, frequency multipliers⁹ and mixers,¹⁰ solar cells¹¹ and flexible displays¹².

Furthermore, graphene, being an all-surface material with very high carrier mobility, is also very promising for chemical and biological sensing applications¹³⁻¹⁵ that require high sensitivity, low noise and a fast response. Graphene is extremely sensitive to its environment and atomic or molecular adsorption on its surface can dope graphene. Indeed, the use of graphene quantum Hall effect (QHE) devices has allowed the demonstration of single molecule detection for some gases¹⁶. When a gas molecule attaches to or detaches from graphene's surface, the adsorbed molecules change the local carrier concentration in graphene electron at a time, which leads to step-like changes in resistance. In addition to the outstanding achieved sensitivity, graphene is also a low-noise electronic material due to its very high carrier mobility¹⁷. Such sensitivity has been beyond the reach of any detection technique until now, including solid-state gas sensors hailed for their exceptional sensitivity¹⁸⁻²¹.

In spite of the outstanding sensitivity of QHE devices, the high magnetic fields required to get QHE prevent the use of these devices in low cost applications. A second sensing mechanism, more suitable for detection of liquid analytes, consists in the use of solution-gated field effect transistors²² to sense the surface potential of a graphene channel exposed to an analyte of interest. Solution-gated transistor technology has numerous advantages compared to conventional electrode-based sensors²³, such as intrinsic signal amplification and straightforward integration with microelectronics. Therefore, the design and fabrication of a graphene solution gated transistor array technology is very promising especially for applications in medical implantable sensors. For example, the functionalization of graphene to allow glucose sensing could enable a new generation of high performance implantable glucose sensors. Furthermore, graphene can be easily transferred to plastic substrates. This integration on flexible substrates will expand the

range of sensing applications for graphene, including low cost, flexible and easily disposable sensors.

After reviewing the main properties of graphene in section 1, we will describe in section 2, some fundamental electrochemistry principles in order to explain the concept of solution gated transistor technology. Finally, as graphene holds great potential for chemical and biological sensing applications, we will introduce the issues that are raised around the commercialization of innovative and new biosensors like graphene sensors especially with regards to the US regulation for market approval that is too stringent and not adapted to support innovation. These issues will be analyzed thoroughly in chapter 5.

1- Graphene properties

Graphene is a two-dimensional material formed by sp^2 -bonded carbon atoms arranged in a honeycomb lattice. It has been studied theoretically for a long time but it was presumed that graphene is not stable in single layer form and therefore could not exist²⁴. It was only in 2004 that Novoselov and Geim demonstrated that graphene was actually stable and characterized experimentally its properties on silicon dioxide¹. Its outstanding characteristics rapidly capture the intense interest of the scientific community⁵ envisioning its use for future electronic devices applications.

- **Atomic structure of graphene**

The atomic structure of graphene is a one atom-thick layer of carbon atoms densely packed in a honeycomb structure. Its structure has been studied with Atomic Force Microscope (AFM)²⁵, Scanning Tunneling Microscope (STM)²⁶ and Transmission electron microscopy (TEM)²⁷. It has an atomic distance of 0.14 nm and a height of 0.33 nm.

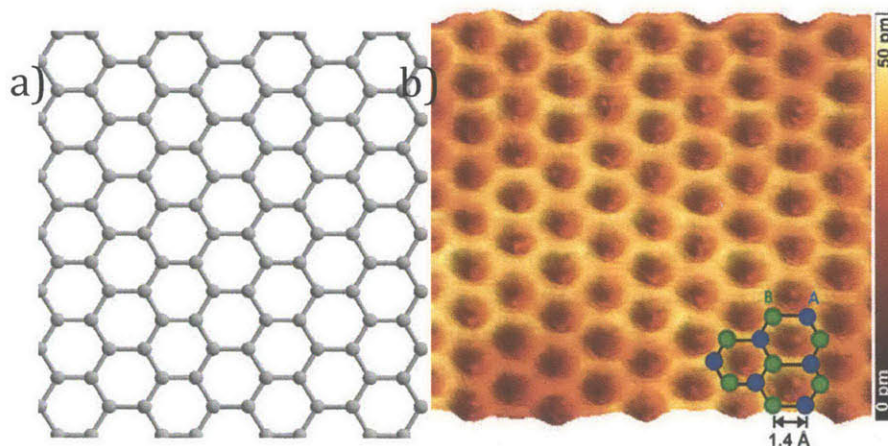


Figure 1: a) Atomic structure of graphene, from scientific report 2007 IMEC⁵⁴, b) STM topography revealing atomically resolved graphene lattice, from group of Prof Roland Wiesendanger, university of Hambourg⁵⁵

The atomic p_z orbitals that are perpendicular to the plane give rise to the energy bands, conduction band π^* and valence band π for graphene's electronic properties. The energy dispersion can be described by the following equation in the first Brillouin zone using the tight binding model with the \vec{k} vector²⁸:

$$E = \pm \gamma_0 \sqrt{1 + 4\cos^2\left(\frac{k_y a}{2}\right) + 4\cos\left(\frac{k_y a}{2}\right)\cos\left(\frac{k_x \sqrt{3}a}{2}\right)}$$

Where the nearest-neighbor hopping energy $\gamma_0 \approx 2.8$ eV and the lattice constant $a = 2.46$ Å. This energy dispersion causes the conduction band and the valence band to touch at the six corners of the hexagonal Brillouin zone called the "Dirac points". Close to the Dirac point, at low energies, the energy dispersion becomes linear:

$$E = \hbar v_F \sqrt{k_y^2 + k_x^2}$$

where v_F is the Fermi velocity, $v_F = 10^6$ m.s⁻¹. Due to this linear dispersion relation at low energies, electrons and holes near these six points behave like massless Dirac relativistic particles. That's why the six corners of the Brillouin zone are called the Dirac points. The linear energy dispersion relation makes graphene quite different from most conventional three-dimensional semiconductors that exhibit parabolic bands and band gap. Therefore, graphene is a semi-metal or zero-gap semiconductor.

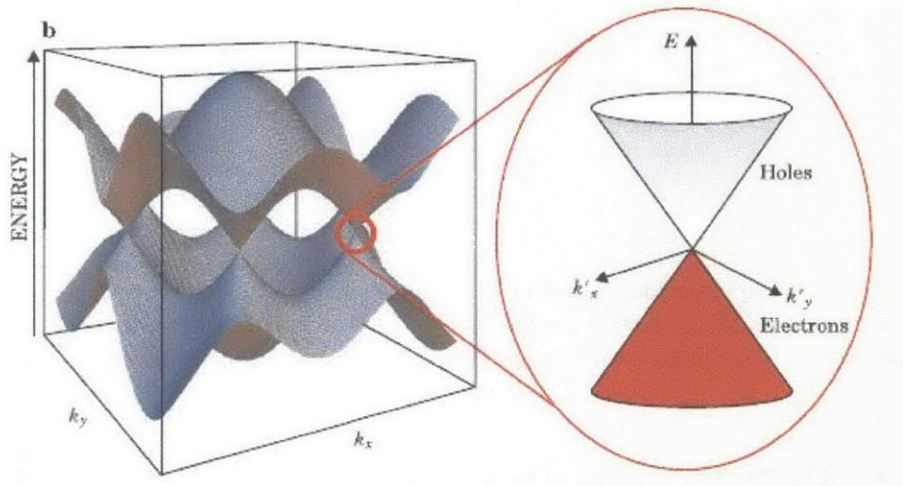


Figure 2: Energy bands of graphene. On the left side, the energy spectrum in units of 2.7 eV (nearest neighbor hopping energy). On the right side, zoomed portion of the linear energy band near the Dirac point. From M. Wilson, Phys. Today (janv. 2006, p. 21-23).

- **Electronic properties of graphene**

The most striking feature of the electronic properties of graphene is its extremely high electron mobility at room temperature, with reported experimental values for exfoliated graphene on silicon dioxide in excess of 15 000 cm².V⁻¹.s^{-1.5}. Scattering of electrons by optical phonons of the

substrate is a larger effect at room temperature than scattering by graphene's own phonons, and limits the mobility to $40\,000\text{ cm}^2\cdot\text{V}^{-1}\cdot\text{s}^{-1}$ ²⁹. However, by suspending graphene, the carrier mobility can gain an order of magnitude and reach $200\,000\text{ cm}^2\cdot\text{V}^{-1}\cdot\text{s}^{-1}$ ³⁰. In addition, by transferring graphene onto a smoother substrate than SiO_2 , especially hexagonal boron nitride, carrier mobility can also very significantly increase and reach up to $140\,000\text{ cm}^2\cdot\text{V}^{-1}\cdot\text{s}^{-1}$ ³¹.

Another important feature of graphene is its ambipolar electric field effect⁵ so that charge carriers can be turned continuously between holes and electrons, as shown on figure. Indeed, by fabricating a graphene transistor, the position of the Fermi energy E_F can be adjusted by applying a top gate voltage V_{GS} . Positive V_{GS} induces electrons whereas negative V_{GS} induces holes. Minimum charge carrier concentration and maximum sheet resistance is achieved with a gate voltage that puts the Fermi level in the graphene exactly at the Dirac point⁵. A sharp and linear decrease in resistance is observed on adding charge carriers of either sign.

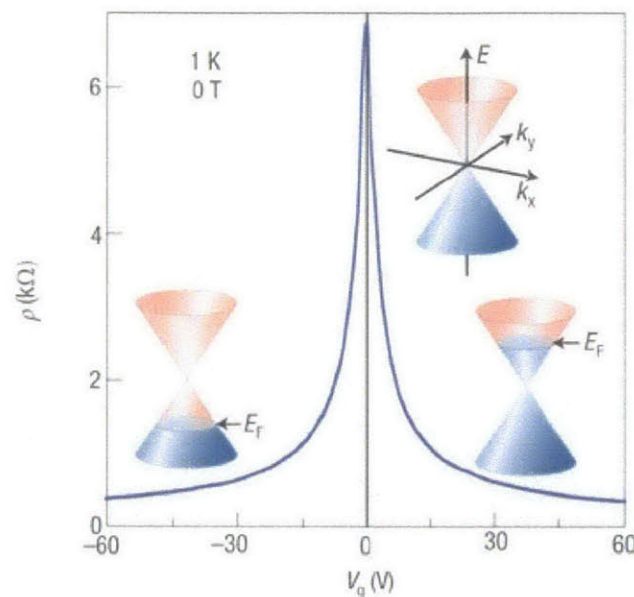


Figure 3: Graphene resistance in terms of the top gate voltage V_{GS} that enables to modulate the Fermi energy E_F . The ambipolar electric field effect is observed charge carriers can be turned continuously between holes and electrons. Positive gate voltage V_{GS} induces holes and negative gate voltage V_{GS} induces electrons⁵.

- **The different ways of producing graphene**

There are three main techniques of producing graphene. The first way is the mechanical exfoliation of graphite. This was the method invented by K.S Novoselov and A.K Geim when they isolated graphene for the first time¹. It consists in sandwiching highly oriented pyrolytic graphite (HOPG) between two pieces of sticky tape and then peeling the tapes apart. In this way, the graphite flake is sliced into two parts, each one of them being thinner than the original one. Repeating this method many times produce thinner and thinner flakes until some flakes reach the single atom thickness. These one atom thick flakes are made of graphene. The flakes are then transferred on a Si/SiO_2 substrate by peeling off the tapes directly on the substrate. The single

layer graphene flakes can then be identified directly by optical microscopy^{32, 33}. Confirmation of the number of layers can be done using Raman measurements³². The great advantage of this method is that the quality of the graphene is the highest of any method^{5, 34}, carrier mobility in excess of $15\,000\text{ cm}^2\text{ V}^{-1}\text{ s}^{-1}$ on SiO_2 substrates has been achieved. However, this method has a great disadvantage, in terms of applications for the industry. It is not reproducible and the large-scale production is impossible. Therefore exfoliated graphene cannot be used for any industrial application but only for research purposes.

The second method for obtaining graphene is to heat silicon carbide (SiC) to high temperatures ($>1100\text{ }^\circ\text{C}$) to reduce it to graphene³⁵. This process produces epitaxial graphene with dimensions dependent upon the size of the SiC substrate (wafer) so that is a scalable method for industrial use. The surface of the SiC used for graphene formation, silicon- or carbon-terminated, highly influences the thickness, mobility and carrier density of the graphene. Thus, although graphene grown on the carbon face has higher mobility (values of $\sim 5,000\text{ cm}^2\text{ V}^{-1}\text{ s}^{-1}$ have been reported³⁶, compared with $\sim 1,000\text{ cm}^2\text{ V}^{-1}\text{ s}^{-1}$ for graphene grown on the silicon face³⁷, it is easier to grow single-layer and bilayer graphene on the silicon face, which makes the silicon face of SiC better suited for electronic applications. However, recently, hydrogenation method has enabled to increase the carrier mobility of graphene of interest for industrial applications from $1,000\text{ cm}^2\text{ V}^{-1}\text{ s}^{-1}$ to around $2000\text{ cm}^2\text{ V}^{-1}\text{ s}^{-1}$ ³⁸. A disadvantage of epitaxial graphene is the fact that graphene is bound to the SiC substrate which limits the range of its applications especially because silicon carbide wafers are very expensive, around 100 times the price of silicon wafers³⁹.

The third method for producing graphene is growing it by Chemical Vapor Deposition (CVD) on metal substrates. The metals considered for industrial applications are copper or nickel foils because they are relatively inexpensive. The metal foil is first brought to very high temperatures around $1000\text{ }^\circ\text{C}$ and then methane gas is flowed in the CVD tube. The methane decomposes on the surface of the metal and carbon atoms solubilize in the metal. By cooling down the metal afterwards, some carbon atoms precipitate at the surface of the metal and assemble to form graphene. Graphene growth by CVD on nickel produces large area graphene films but the films are not uniformly single layer⁴⁰. On the contrary, graphene growth by CVD on copper foils produces large areas of graphene films that are uniformly single layer (more than 95 %)⁷. Then, thanks to the etching of the catalyst metal, the graphene film can be transferred to any arbitrary substrate. That is one of the most important advantages of graphene grown by CVD notably because it enables the integration of graphene on plastic and flexible substrates, which opens up a wide new range of applications for graphene. Another important advantage is that the graphene film quality is quite high with carrier mobilities that can reach $4,000\text{ cm}^2\text{ V}^{-1}\text{ s}^{-1}$ at room temperature.

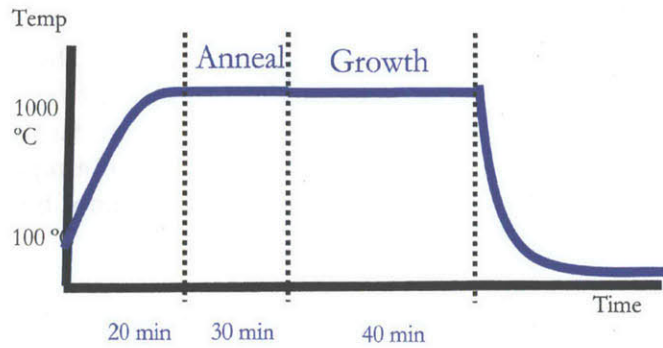


Figure 4: Temperature-Time diagram of the growth technique used to grow graphene by CVD on copper foil

In conclusion, the CVD growth of graphene is the most promising method for producing graphene at large scale for industrial applications because it has high carrier mobility and can be transferred to any substrate.

- **Other outstanding properties of graphene**

Graphene has not only amazing electronic properties but it also has outstanding mechanical, thermal, optical and chemical properties. First, graphene is the strongest material known. Indeed, it has been found that graphene is harder than diamond and about 300 times harder than steel⁴¹. Thus, the tensile strength of graphene exceeds 1TPa. Furthermore, graphene is also very stretchable⁴ and can be stretched up to 20 % of its initial length. These mechanical properties combined with the chemical properties of graphene are very promising for very high performance flexible biosensors. Graphene has also impressive optical properties. Thus, despite being the thinnest material ever made, it is still visible to the naked eye. Graphene absorbs 2.3 % of light that passes through it, which makes it optically transparent⁴². Graphene is also an excellent thermal conductor. Its thermal conductivity was measured recently at room temperature and is around $5 \times 10^3 \text{ W.m}^{-1}.\text{K}^{-1}$ ⁴³. Thus, graphene could even outperform carbon nanotubes in heat conduction^{43,44}. This very high thermal conductivity may have important implications in graphene-based electronic devices. Indeed, as devices continue to shrink and circuit density increases, high thermal conductivity plays an increasingly larger role in device reliability since it is essential for dissipating heat efficiently to keep electronics cool. Finally, we already mention that graphene has outstanding chemical properties for sensing applications since it is very sensitive to its environment where weakly attached adsorbates can change its carrier concentration and doping. However, graphene has other important chemical properties. It is remarkable stable, chemically inert and crystalline under ambient conditions.

2- Electrochemistry principles

Electrochemistry is the branch of chemistry concerned with the interrelation of electrical and chemical effects. The field of electrochemistry encompasses a large array of different phenomena (like electrophoresis and corrosion), devices (like electroanalytical sensors, batteries or fuel cells) and technologies (like electroplating of metals or chlorine)⁴⁵. In electrochemical systems, electrochemists are concerned with processes and factors that affect the transfer of charges across the interface between chemical phases, for example, between an electronic conductor (an electrode) and an ionic conductor (an electrolyte). In an electrode, charge is transported through the movement of electrons and holes. In the electrolyte phase, charge is transported through the movement of ions. Many electrochemical processes involve chemical phenomena where charge separation or charge transfer takes place at electrode surfaces. In an electrochemical system, in order to preserve charge neutrality, there are always at least two charge transfer reactions or charge separation phenomena taking place, and each of them correspond to what is called a half reaction at a different electrode. The two different electrodes, the electrolyte and the external circuit form an electrochemical cell. Each electrode in contact with the electrolyte where the half reaction takes place at the interface electrode/electrolyte, is called a half cell. Thus, in an electrochemical cell, when the sum of free energy changes at the electrodes is negative, electrochemical energy is converted into electrical energy and therefore the cell behaves like a battery. When the sum of free energy is positive, electrical energy from the external circuit is provided for the reactions at the electrodes to occur. Electrical energy is converted into electrochemical energy and the process is called electrophoresis.

- **The electrode-electrolyte interface**

When a semiconductor or metal electrode is in contact with an electrolyte, an electrode-electrolyte interface is formed at which the electrochemical reaction process occurs. The structure of the interfacial region is crucial because the thermodynamic driving forces and the kinetics of the reactions depend on it. This interface has been shown experimentally to behave like a capacitor. At a given potential, a charge q^M exists on the semiconductor or metal electrode and a charge q^S in the solution. Depending on the potential across the interface and the composition of the solution, the charge on the metal can be positive or negative compared to the one in the solution but at all times, $q^M = -q^S$. The space-charge region in the metal represents an accumulation of electrons or holes and resides in a very thin layer ($<0.1 \text{ \AA}$) in the metal surface. The charge in the solution is made up of an excess or deficiency of anions or cations in the vicinity of the electrode surface. The whole arrangement of charged species and orientated dipoles at the metal/solution interface is called the electrical double layer. At a given potential, the interface is characterized by a double layer capacitance C_D , typically in the range of $10\text{-}40 \mu\text{F}\cdot\text{cm}^{-2}$. The space-charge region in the solid phase of the semiconductor or metal is comparable to the one in a classic semiconductor-oxide-metal interface. On the contrary, the structure of the solution side of the electrical double layer in contact with the semiconductor is specific to semiconductor-electrolyte interface and is described below⁴⁵.

The solution side of the double layer is thought to be made of by several layers, as shown in figure 4. The well-accepted final model for the structure of the double layer was elaborated by Bockris and Devanathan (1963)⁴⁶. The layer closest to the electrode is the Helmholtz layer and

contains solvent molecules and sometimes ions or molecules that are said to be specifically adsorbed. The so-called inner Helmholtz plane (IHP) is defined by the plane going through the centers of these specifically adsorbed ions. The total charge density, which represents the charge by electrode area unit, from specifically adsorbed ions in the Helmholtz layer is often denoted σ^i . The second closest layer to the electrode and next to the Helmholtz layer is composed of solvated ions with a primary hydration shell and the plan going through the centers of these nearest solvated ions is called the outer Helmholtz plane (OHP). The interaction of the solvated ions with the charged semiconductor involves only long-range electrostatic forces so that their interaction is independent of the chemical properties of the ions contrary to the case of specifically adsorbed ions. These ions are said to be nonspecifically adsorbed. With thermal agitation, the nonspecifically adsorbed ions are distributed in the region called diffuse layer that extends from the OHP into the bulk of the solution. The charge density in the diffuse layer is often denoted σ^d . Therefore, the total charge density in the solution σ^s is

$$\sigma^s = \sigma^i + \sigma^d = -\sigma^M$$

The thickness of the diffuse layer depends on the total ionic concentration in the solution, for concentrations greater than 10^{-2} M, the thickness is less than 100 Å.

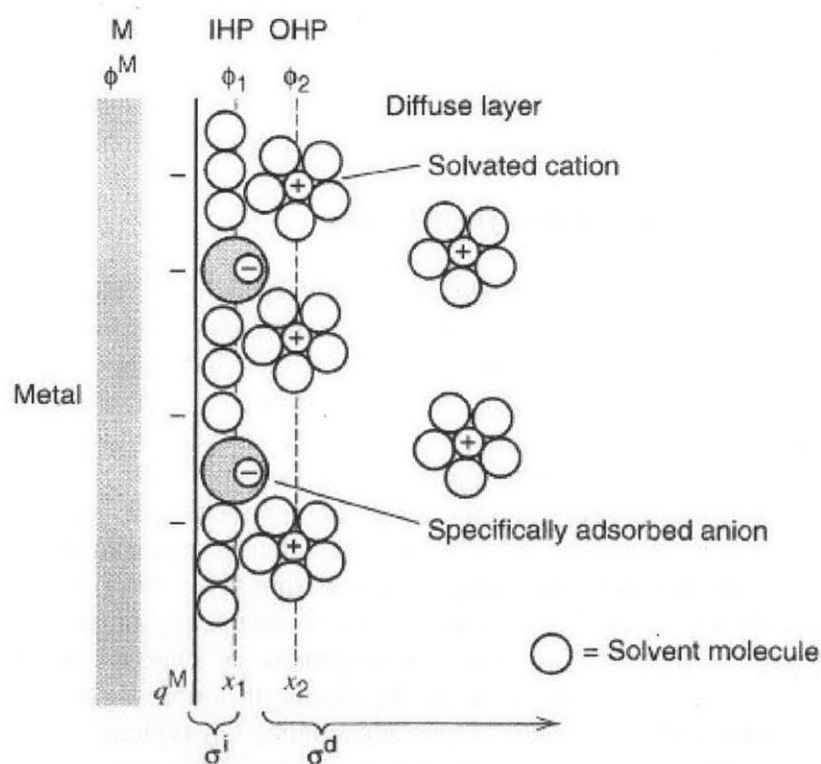


Figure 5: Model of the electrical double layer structure formed at a metal-electrolyte interface. Specifically adsorbed anions can be seen at the IHP and solvated cations are nonspecifically adsorbed at the OHP. ⁴¹

- **Thermodynamics of electrochemical reactions**

The thermodynamics of electrochemical reactions describes the change in energy and entropy during a reaction. These two fundamental state functions will determine to what extent a reaction will process. Information about these functions can only be obtained at equilibrium and therefore, thermodynamics does not give any information about the rate at which an equilibrium state is approached or the mechanism of the reaction. In electrochemistry, the reference point for the chemical potential is defined by convention with the standard hydrogen electrode (SHE) as zero potential. In an electrochemical cell, each of the half reaction occurring at an electrode is characterized by a standard redox potential E^0 of the half cell measured relative to the SHE potential. The real electrochemical potential of the half-cell E is related to E^0 by the Nernst equation:

$$E = E^0 + \frac{RT}{nF} \ln\left(\frac{a^r}{a^i}\right)$$

Where F is the Faraday constant: $9.6485 \times 10^4 \text{ C} \cdot \text{mol}^{-1}$, R is the gas constant: $8.3145 \text{ J} \cdot \text{K}^{-1} \cdot \text{mol}^{-1}$, n is the number of electrons exchanged in the reaction, a^i is the activity of the ions or molecules that are reactants at the initiation of the reaction and a^r is the activity of the ions or molecules that are products of the reaction. For small concentrations, the activity of ionic or molecular species in the solution is approximately its concentration.

In this regard, a reference electrode is a half-cell for which the potential is stable and well known. The potential of reference electrode are therefore used as a reference to measure the potential of other electrodes in terms of potential differences. The commonly used reference electrodes are the SHE ($E^0=0\text{V}$), the saturated calomel electrode ($E^0=0.242\text{V}$ against the SHE) and the silver/silver chloride electrode ($E^0=0.197\text{V}$ against the SHE).

- **Polarizable and non polarizable electrodes**

Before introducing the concept of polarizable and non polarizable electrodes, it is worth noticing that in electrochemistry, there are two types of processes occurring at electrodes: Faradaic and non Faradaic processes⁴⁵. Faradaic processes concern reactions in which electrons are transferred across the semiconductor/solution interface and cause oxidation or reduction. However, under some conditions, an electrode/solution interface exhibit a range of potentials under which no charge-transfer occurs because such reactions are thermodynamically or kinetically unfavorable. And yet, processes such as adsorption, desorption and the formation of the electrical double layer still occur. Furthermore, the structure of the double layer can change with changing potential or solution composition, even though no charge transfer occurs. These processes are called non-Faradaic processes. Even though charge does not cross the interface, external currents can still flow (at least transiently) with a change in the potential or solution composition. In most cases, these currents originate from charging of the electrode and of the double layer capacitor. During this charging, species in the electrolyte may absorb or desorb from the interface, and therefore, the structure of the interface may change.

One of the most important properties of the interface is what electrochemists call its polarizability. The definition of polarizable⁴⁷ is to what extent an interface resists or accepts potential changes. There are two ideal limiting cases of electrode-electrolyte interfaces:

- The ideal polarizable interface at which no charge transfer can occur across the electrode/solution interface regardless of the potential imposed by an outside source of voltage.
- The ideal nonpolarizable interface at which an infinitesimal change in the voltage drop across the interface causes a very large (ideally infinite) faradaic DC current and therefore a very strong charge transfer. In an electrochemical cell with one ideal nonpolarizable interface, changes of total voltages applied to a circuit must be distributed among the other sections of the circuit until new equilibrium concentrations are established across the interface.

No real electrode has ideal polarizable or nonpolarizable properties. However, some interfaces can approach these ideal extreme behaviors over limited potential ranges. For example, a mercury electrode in contact with deaerated potassium chloride solution approaches the behavior of an ideal polarizable interface over a potential range about 2V wide⁴⁵. A good example of an ideal nonpolarizable interface is the reference Ag/AgCl electrode. In figure 6, the equivalent circuit and current-potential curves of an ideal polarizable and nonpolarizable interface are shown.

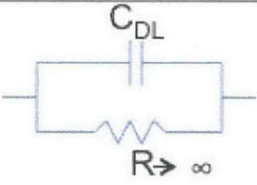
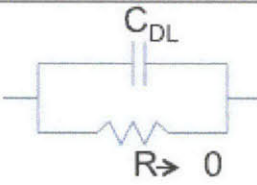


	Ideal polarizable electrode: leak proof interface	Ideal non polarizable electrode: infinitely strong leaking interface
Equivalent circuit		
Current-potential curves		

Figure 6: Tab representing the equivalent circuit and current potential curves of ideal polarizable and non polarizable electrodes

3- Solution gated field effect transistor technology

To explain how a solution gated field effect transistor (SGFET) works, it is important to first describe the basic operating principles of a metal-oxide-semiconductor FET (MOSFET) because both types of devices work quite similarly.

- **MOSFET**

A field effect transistor (FET) is a three-terminal semiconductor device and it is used for amplifying or switching electronic signals. The three terminals are source, drain and gate. In a FET, the resistance between drain and source is controlled by the gate via an electric field effect. The MOSFET is a particular type of FET, characterized by the presence of a metal-oxide-semiconductor (MOS) structure. The MOSFET is by far the most common transistor in digital and analog circuits. The traditional MOS structure is obtained by growing a layer of silicon dioxide on top of a silicon substrate and depositing a layer of metal on top to form the gate. As the silicon dioxide is a dielectric material, the MOS structure is equivalent to a planar capacitor, with one of the electrodes replaced by a semiconductor. When a voltage is applied across a MOS structure, it changes the distribution of charges in the semiconductor. If we consider a p-type semiconductor, a positive gate voltage V_{GS} , from gate to the body of the semiconductor creates a depletion layer by forcing the positively charged holes away from the oxide/semiconductor interface, leaving exposed a carrier-free region of immobile, negatively charged acceptor ions. If V_{GS} is high enough, a high concentration of negative charge carriers forms in an inversion layer located in a thin layer next to the interface between the semiconductor and the insulator.

The principle of a MOSFET is based on the modulation of charge concentration by a MOS capacitance between the body of a semiconductor and a gate electrode located above the body, separated and insulated from all other device regions by a gate dielectric layer that is an oxide. The drain and source terminals are made by the creation of two highly doped regions separated by the body region of the semiconductor. The two highly doped regions must be of the same doping type (either p or n type) and the body of the opposite type. An n-MOSFET structure is shown in figure 7.

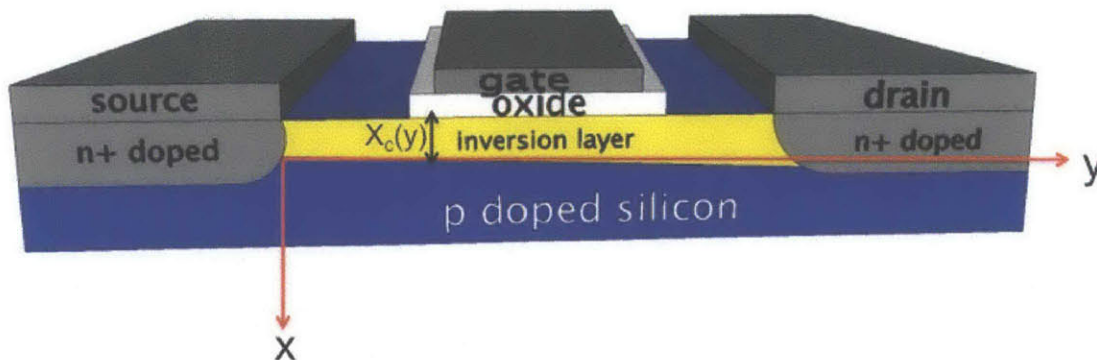


Figure 7: Structure of an n-MOSFET device

In the case of an n-MOSFET as represented above, in the body of the semiconductor, the position of the Fermi level relative to the edges of the semiconductor energy-bands sets the occupancy of the energy bands. As shown in figure 8, with a sufficient positive gate voltage, close to the oxide-semiconductor interface, the Fermi level is driven away from the edge of the valence band and closer to the conduction band. For gate voltage biases above the threshold voltage V_T , the Fermi level becomes closer to the conduction band edge than to the valence band,

populating the surface with electrons in a so called inversion layer that is n-doped, as shown on figure 7. This inversion layer is a conducting channel that extends between drain and source and, current can flow through it by applying a voltage between drain and source. For gate voltages below the threshold value, the conducting channel disappears and the source-channel-drain structure is a n-p-n junction. Therefore only an extremely small subthreshold current can flow between the source and the drain.

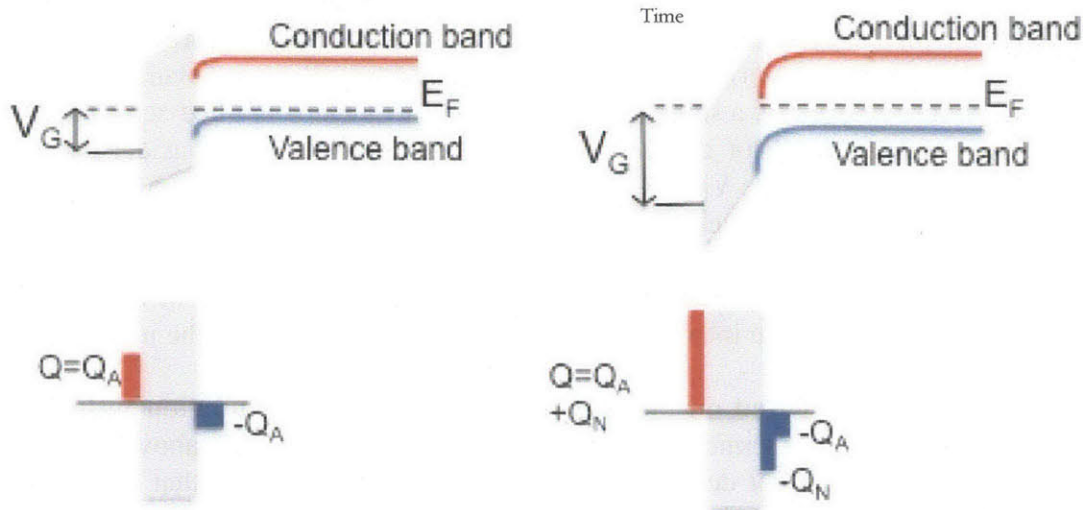


Figure 8: Channel formation in an n-MOSFET. Energy band diagram and charge distribution for a) positive gate voltage bias lower than the threshold voltage, which bends the bands, depleting holes from the oxide-semiconductor surface, the charge inducing the bending is balanced by a layer of negative charge. b) positive gate voltage bias above the threshold voltage, which further bends the bands, depleting holes enough so that the conduction band is closer to the Fermi level than the valence band and creates a conducting n doped channel.

We can now derive a quantitative analysis of operation of an n-MOSFET. As shown in figure 6, the direction from source to drain is defined as y-axis, and the x coordinate is to be downward, perpendicular to the channel. Now consider the current flowing across the channel (in yellow). According to the gradual channel approximation, the current flow is assumed to be one dimensional⁴⁸. Then in an incremental length dy at position y in the channel, we can derive the total mobile channel charge⁴⁹:

$$(1.1) \quad \left(\int_0^\infty \rho_{ch}(x, y) dx \right) \cdot W dy = \sigma_{ch}(y) \cdot W dy$$

where $\rho_{ch}(x, y)$ is the charge per unit area in the channel at position (x, y) , W is the width of the transistor and $\sigma_{ch}(y)$ is the total charge density in the channel in the plan transversal to the y axis at the position y . The current being the amount of charge passing through a given area per unit time, the channel current I_{DS} at a given position y is:

$$(1.2) \quad I_{DS} = - \sigma_{ch}(y) W \frac{dy}{dt} = - \sigma_{ch}(y) W v(y)$$

where $v(y)$ is the average channel hole velocity at position y .

Let's consider first the case where $V_{DS} = 0$ V corresponding to the case of the chemical equilibrium within the channel. An electrostatic potential $V_0(x, y)$ is established such that $eV_0(x, y)$ is the energy of the semiconductor with reference to the gate electrode Fermi level as an equipotential plane. This potential establishes a detailed balance of drift and diffusion currents leading to a vanishing total current density everywhere. When a finite non-zero drain source voltage V_{DS} is applied, the potential profile changes such that the sum of the modified diffusion and drift currents leads to a uniform and non zero current. Usually in MOSFET devices, this sum of currents can be approximated by the drift current itself. Then the velocity in (1.2) can be replaced by the drift velocity so that:

$$v(y) = \mu(y)E(y) = -\mu(y) \frac{dV}{dy}$$

where $\mu(y)$ is the average channel mobility and $E(y)$ is the longitudinal electric field. Therefore, the current density can be written:

$$I_{DS} = \sigma_{ch}(y) W \mu(y) \frac{dV}{dy}$$

However, the current is independent of y as it is constant through out the channel. In the MOSFET structure, the mobile channel charge density $\sigma_{ch}(y)$ depends only implicitly via the voltage $V(y)=V(y, x_{ch})$ on the position y , with $x_{ch}(y)$ the width of the channel in the x direction. $V(y)$ is in general monotonous function of y so that the integration of equation (6.6) over the channel length L from source to drain can be transformed to an integration over voltage and yields:

$$I_{DS} \cdot L = W \int_0^L \sigma_{ch}(y) \mu(y) \frac{dV}{dy} dy = W \mu \int_{V(0)}^{V(L)} \sigma_{ch}(V) dV$$

In the last step of the equation above, the average mobility was taken as an approximation and extracted from the integral. With $V(0)=-V_{GS}$ and $V(L)=-V_{GS}+V_{DS}$, this gives

$$I_{DS} = \frac{W \mu}{L} \int_{-V_{GS}}^{-V_{GS}+V_{DS}} \sigma_{ch}(V) dV$$

Then, with V_T being the channel threshold potential where inversion begins and C_{ox} the oxide capacitance, we have in the MOS structure $\sigma_{ch} = -C_{ox}(V - V_T)$. Therefore, the current can be expressed as:

$$(1.3) \quad I_{DS} = \frac{W \mu}{L} C_{ox} [(V_{GS} - V_T)V_{DS} - V_{DS}^2]$$

Note that V_T and the inversion region corresponds to $V_{GS} > V_T$.

- **Solution gated transistors**

The concept of the traditional Solution Gated Field Effect Transistor (SGFET) ^{22, 50, 51} is based on the concept of MOSFET. The fabrication of a SGFET consists in removing the metal gate from a MOSFET and replacing it with a reference electrode and an electrolyte. SGFET are usually used for sensing the concentration of certain ions and can be determined from the characteristics of the transistor. That is why these devices are also called ISFET (Ion Sensitive Field Effect Transistor) when the SGFET is used for sensing ion concentration.

In a MOSFET, it is the metal oxide semiconductor structure that induces the “field effect”, while in SGFET this is achieved by the electrolyte-semiconductor interface. The reference electrode is used to apply the gate voltage through the solution. Both the MOS structure and the solution-semiconductor interface serve as planar capacitors to induced the required electric field. Thanks to the similarities of these devices, their resulting current-voltage characteristics are very similar. The figure 9 shows the structure of a SGFET compared to a MOSFET.

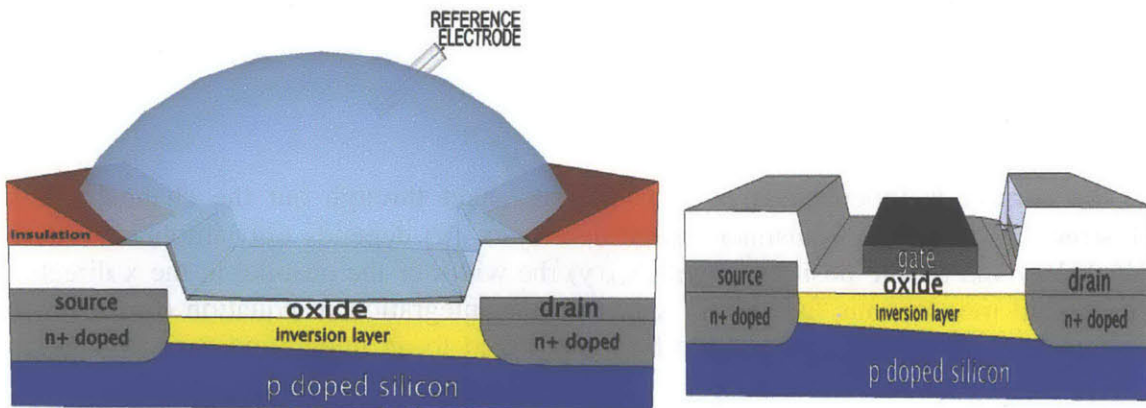


Figure 9: Schematic structure of a) a semiconductor-oxide SGFET and b) a MOSFET

For the correct operation of a Si SGFET, a stable interface between the silicon and silicon dioxide is key, just like in the case of a MOSFET device. Indeed, an operational MOSFET couples in a stable way an electric field, penetrating the oxide, to the current I_{DS} between drain and source in the channel underneath the oxide. In the case of a semiconductor-oxide SGFET, the outer surface of the oxide is in equilibrium with an ionic solution in contact with the oxide. The resulting interfacial potential will modulate the electric field applied through the solution by

the reference electrode and penetrating the oxide. Thus, an operational SGFET couples in a stable manner the electric field induced by the solution/oxide interfacial potential to the current I_{DS} between drain and source in the channel underneath the oxide. Thus, in a semiconductor-oxide SGFET, the modulation of the electric field by the solution/oxide interfacial potential, which is directly related to the concentrations of certain ions in the solution, enables to sense these ions by recording the I_{DS} current.

Here we are going to explain more quantitatively how a specific type of SGFET, the semiconductor-oxide SGFET works, as shown in figure 9. Thanks to the similarities between a MOSFET and a SGFET, the equation (1.3) is valid for both devices²² and can be rewritten:

$$(1.4) \quad I_{DS} = \beta \left[V_{GS} - V_T - \frac{1}{2} V_{DS} \right] V_{DS}$$

where $\beta = \frac{W\mu}{L}$ is a geometric sensitivity parameter. The threshold voltage V_T is given by:

$$V_T = V_{FB} - \frac{Q_B}{C_{ox}} + 2\phi_F$$

where V_{FB} is the flat-band voltage, Q_B is the depletion charge in the silicon and ϕ_F is the Fermi potential.

In the case of a MOSFET, the flat band potential is then given by:

$$V_{FB} = \frac{\Phi_M - \Phi_{sc}}{e} - \frac{Q_{ss} + Q_{ox}}{C_{ox}}$$

with the silicon work-function, the work-function of the gate metal, Q_{ss} the surface state density at the silicon surface, and Q_{ox} the fixed oxide charge.

From equation (1.4), it can be seen that the threshold voltage of a MOSFET is determined by material properties such as the workfunction and charge accumulation. For the stable operation of a MOSFET it is of importance that the threshold voltage is constant which can be achieved by applying an appropriate MOS process such as ion implantation.

In the case of a semiconductor-oxide SGFET the gate voltage is the voltage at the reference electrode but the threshold voltage contains also terms that reflect the interfaces between the liquid and the gate oxide on the one side as well as between the liquid and the reference electrode at the other side. The latter term is in fact the reference electrode potential relative to vacuum E_{ref} , which includes Φ_M . The interface potential at the gate oxide-electrolyte interface is determined by the surface dipole potential of the solution X_{sol} , which is a constant, and the surface potential Ψ_0 , which results from a chemical reaction, usually governed by the dissociation of oxide surface groups²². This results in a change in the expression of the flat-band voltage:

$$V_{FB} = E_{ref} - \Psi_0 + X_{sol} - \frac{\Phi_{sc}}{e} - \frac{Q_{ss} + Q_{ox}}{C_{ox}}$$

Because all the terms are constant except Ψ_0 , it is this term that makes the ISFET sensitive to the electrolyte pH, which is controlling the dissociation of the oxide surface groups. This dissociation of the oxide surface groups modulates the surface charge density of the oxide and can yield both a negatively charged (due to SiO^-) and a positively charged (due to SiOH_2^+) surface. As shown in figure 10, according to the site-binding model⁵², during this reaction, the hydroxyl sites bind or release hydrogen ions. This reaction creates a charge on the oxide surface that is opposite to the ion charge in the solution. In this way a double layer structure is created with capacitance C_{dl} and a variable potential drop Ψ_0 , which is operating as a serial voltage source with the gate electrode, and is linearly dependent on the hydrogen concentration in the solution. That is why a semiconductor-oxide SGFET can be used as pH sensor. Their electrical response depends on the pH linearly via the surface potential Ψ_0 . Fig. 10 shows the SGFET equivalent electrical circuit containing the FET, the double layer capacitance C_{dl} and the current source representing the charge resulting in the potential drop.

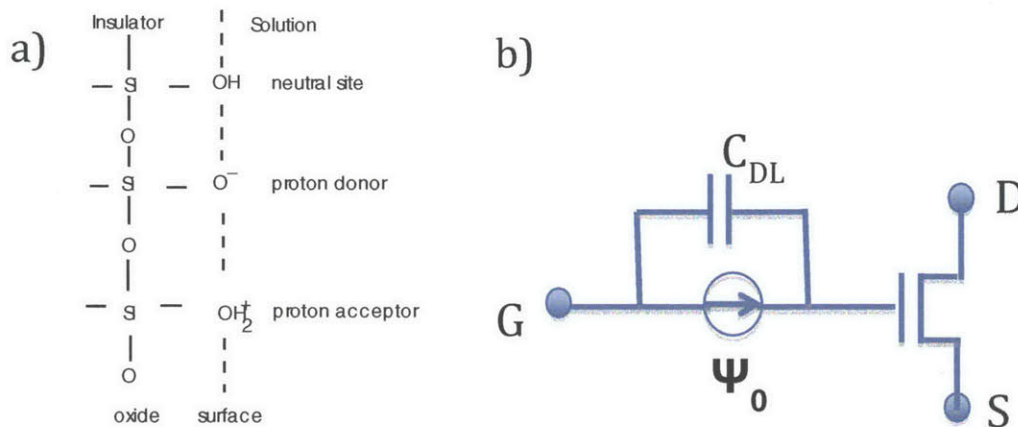


Figure 10: a) Schematic representation of the site-binding model b) equivalent circuit of a semiconductor-oxide SGFET

The sensitivity of a semiconductor-oxide SGFET is defined by the linear dependency between pH and channel potential, and for high performance sensors can be up to 59 mV/pH at room temperature.

As we will see in the next chapter, in the graphene SGFETs that we have built, there is no oxide layer between the electrode and the sample surface, since the graphene surface is directly touching the electrolyte. Thereby nearly no hydroxyl groups bind on the semiconductor surface. As a result, the “site-binding model” does not work for these new type of SGFETs devices. In this case, the semiconductor/electrolyte interface should be polarizable. In graphene, the hydrophobic surface of graphene, when in contact with an aqueous electrolyte, indeed forms a polarizable interface with most electrolytes and thus can be adopted without any further gate insulation processes for SGFETs. The operating principle of graphene SGFET will be discussed in chapter 3.

In conclusion, MOSFETs and all types of SGFETs share much in common because both devices operate following similar charge control mechanisms. However, in graphene sensors, as the graphene is directly in contact with the electrolyte without any oxide in between, the mechanisms for sensing are different than the ones described for conventional semiconductor-

oxide SGFETs.

4- Commercialization of innovations in the biosensor market

Graphene holds great potential for many applications in chemical and biological sensing applications. Research for the integration of this newly discovered carbon nanomaterial into a biological sensor (biosensor) is part of an important research effort worldwide for the convergence of nanotechnology, biotechnology and bioelectronics into exploration of radically innovative biosensors. The success of this effort could bring many new applications to revolutionize the way of doing medicine⁵³. However, commercialization of the revolutionary innovations of biosensors lags several years behind research demonstrations and faces serious hurdles due to the stringent regulation for market approval in the US. The US regulation is indeed challenged by the need to support the fast paced-research needed for innovation while maintaining the high safety standards of America's health. This regulatory challenge is of crucial importance because it may seriously hamper innovations in the field from reaching the market. Therefore, significant policy controversies have been raised around the US regulation implemented by FDA. Some policy recommendations may need to be formulated to make the regulation more efficient and supportive of innovations in order to make the commercialization of graphene sensors viable within a sensible timeline. The regulatory challenge as well as policy recommendations to address it will be discussed in Chapter 5.

References

- (1) Novoselov, K.; Geim, A.; Morozov, S.; Jiang, D.; Zhang, Y.; Dubonos, S.; Grigorieva, I.; Firsov, A. Electric field effect in atomically thin carbon films. *Science* **2004**, *306*, 666-669.
- (2) Novoselov, K. S.; Geim, A. K.; Morozov, S. V.; Jiang, D.; Katsnelson, M. I.; Grigorieva, I. V.; Dubonos, S. V.; Firsov, A. A. Two-dimensional gas of massless Dirac fermions in graphene. *Nature* **2005**, *438*, 197-200.
- (3) Zhang, Y.; Tan, Y. W.; Stormer, H. L.; Kim, P. Experimental observation of the quantum Hall effect and Berry's phase in graphene. *Nature* **2005**, *438*, 201-204.
- (4) Kim, K. S.; Zhao, Y.; Jang, H.; Lee, S. Y.; Kim, J. M.; Kim, K. S.; Ahn, J. H.; Kim, P.; Choi, J. Y.; Hong, B. H. Large-scale pattern growth of graphene films for stretchable transparent electrodes. *Nature* **2009**, *457*, 706-710.
- (5) Geim, A. K.; Novoselov, K. S. The rise of graphene. *Nature materials* **2007**, *6*, 183-191.

- (6) Bolotin, K. I.; Sikes, K.; Jiang, Z.; Klima, M.; Fudenberg, G.; Hone, J.; Kim, P.; Stormer, H. Ultrahigh electron mobility in suspended graphene. *Solid State Commun.* **2008**, *146*, 351-355.
- (7) Li, X.; Cai, W.; An, J.; Kim, S.; Nah, J.; Yang, D.; Piner, R.; Velamakanni, A.; Jung, I.; Tutuc, E.; Banerjee, S. K.; Colombo, L.; Ruoff, R. S. Large-area synthesis of high-quality and uniform graphene films on copper foils. *Science* **2009**, *324*, 1312-1314.
- (8) Lin, Y. M.; Jenkins, K. A.; Valdes-Garcia, A.; Small, J. P.; Farmer, D. B.; Avouris, P. Operation of graphene transistors at gigahertz frequencies. *Nano Lett.* **2009**, *9*, 422-426.
- (9) Wang, H.; Nezich, D.; Kong, J.; Palacios, T. Graphene frequency multipliers. *Electron Device Letters, IEEE* **2009**, *30*, 547-549.
- (10) Wang, H.; Hsu, A.; Wu, J.; Kong, J.; Palacios, T. Graphene-based ambipolar RF mixers. *Electron Device Letters, IEEE* **2010**, *31*, 906-908.
- (11) Wang, X.; Zhi, L.; Mullen, K. Transparent, conductive graphene electrodes for dye-sensitized solar cells. *Nano Lett.* **2008**, *8*, 323-327.
- (12) Verma, V. P.; Das, S.; Lahiri, I.; Choi, W. Large-area graphene on polymer film for flexible and transparent anode in field emission device. *Appl. Phys. Lett.* **2010**, *96*, 203108-203108-3.
- (13) Ang, P. K.; Chen, W.; Wee, A. T.; Loh, K. P. Solution-gated epitaxial graphene as pH sensor. *J. Am. Chem. Soc.* **2008**, *130*, 14392-14393.
- (14) Ohno, Y.; Maehashi, K.; Yamashiro, Y.; Matsumoto, K. Electrolyte-gated graphene field-effect transistors for detecting pH and protein adsorption. *Nano Lett.* **2009**, *9*, 3318-3322.
- (15) Cheng, Z.; Li, Q.; Li, Z.; Zhou, Q.; Fang, Y. Suspended graphene sensors with improved signal and reduced noise. *Nano Lett.* **2010**, *10*, 1864-1868.
- (16) Schedin, F.; Geim, A. K.; Morozov, S. V.; Hill, E. W.; Blake, P.; Katsnelson, M. I.; Novoselov, K. S. Detection of individual gas molecules adsorbed on graphene. *Nat. Mater.* **2007**, *6*, 652-655.
- (17) Dankerl, M.; Hauf, M. V.; Lippert, A.; Hess, L. H.; Birner, S.; Sharp, I. D.; Mahmood, A.; Mallet, P.; Veuillen, J. Y.; Stutzmann, M. Graphene Solution-Gated Field-Effect Transistor Array for Sensing Applications. *Adv Mater* **2010**, *20*, 3117-3124.
- (18) Moseley, P. Solid state gas sensors. *Measurement Science and technology* **1997**, *8*, 223-238.

- (19) Capone, S.; Forleo, A.; Francioso, L.; Rella, R.; Siciliano, P.; Spadavecchia, J.; Presicce, D.; Taurino, A. Solid state gas sensors: state of the art and future activities. *Journal of Optoelectronics and Advanced Materials* **2003**, *5*, 1335-1348.
- (20) Kong, J.; Franklin, N. R.; Zhou, C.; Chapline, M. G.; Peng, S.; Cho, K.; Dai, H. Nanotube molecular wires as chemical sensors. *Science* **2000**, *287*, 622-625.
- (21) Collins, P. G.; Bradley, K.; Ishigami, M.; Zettl, A. Extreme oxygen sensitivity of electronic properties of carbon nanotubes. *Science* **2000**, *287*, 1801-1804.
- (22) Bergveld, P. In *In ISFET, theory and practice*; IEEE Sensor Conference Toronto; 2003; Vol. 10, pp 1.
- (23) Lu, C. H.; Yang, H. H.; Zhu, C. L.; Chen, X.; Chen, G. N. A graphene platform for sensing biomolecules. *Angew. Chem. Int. Ed Engl.* **2009**, *48*, 4785-4787.
- (24) Wallace, P. The band theory of graphite. *Physical Review* **1947**, *71*, 622.
- (25) Huang, P. Y.; Ruiz-Vargas, C. S.; van der Zande, A. M.; Whitney, W. S.; Levendorf, M. P.; Kevek, J. W.; Garg, S.; Alden, J. S.; Hustedt, C. J.; Zhu, Y. Grains and grain boundaries in single-layer graphene atomic patchwork quilts. *Nature* **2011**, *469*, 389-392.
- (26) Ishigami, M.; Chen, J.; Cullen, W.; Fuhrer, M.; Williams, E. Atomic structure of graphene on SiO₂. *Nano Letters* **2007**, *7*, 1643-1648.
- (27) Meyer, J. C.; Kisielowski, C.; Erni, R.; Rossell, M. D.; Crommie, M.; Zettl, A. Direct imaging of lattice atoms and topological defects in graphene membranes. *Nano letters* **2008**, *8*, 3582-3586.
- (28) Neto, A. H. C.; Guinea, F.; Peres, N.; Novoselov, K.; Geim, A. The electronic properties of graphene. *Reviews of modern physics* **2009**, *81*, 109.
- (29) Fang, T.; Konar, A.; Xing, H.; Jena, D. Mobility in semiconducting graphene nanoribbons: Phonon, impurity, and edge roughness scattering. *Physical Review B* **2008**, *78*, 205403.
- (30) Bolotin, K. I.; Sikes, K.; Jiang, Z.; Klima, M.; Fudenberg, G.; Hone, J.; Kim, P.; Stormer, H. Ultrahigh electron mobility in suspended graphene. *Solid State Commun.* **2008**, *146*, 351-355.
- (31) Dean, C.; Young, A.; Meric, I.; Lee, C.; Wang, L.; Sorgenfrei, S.; Watanabe, K.; Taniguchi, T.; Kim, P.; Shepard, K. Boron nitride substrates for high-quality graphene electronics. *Nature nanotechnology* **2010**, *5*, 722-726.

- (32) Ferrari, A.; Meyer, J.; Scardaci, V.; Casiraghi, C.; Lazzeri, M.; Mauri, F.; Piscanec, S.; Jiang, D.; Novoselov, K.; Roth, S. Raman spectrum of graphene and graphene layers. *Phys. Rev. Lett.* **2006**, *97*, 187401.
- (33) Blake, P.; Hill, E.; Castro Neto, A.; Novoselov, K.; Jiang, D.; Yang, R.; Booth, T.; Geim, A. Making graphene visible. *Appl. Phys. Lett.* **2007**, *91*, 063124-063124-3.
- (34) Schwierz, F. Graphene transistors. *Nature nanotechnology* **2010**, *5*, 487-496.
- (35) Sutter, P. Epitaxial graphene: How silicon leaves the scene. *Nature Materials* **2009**, *8*, 171-172.
- (36) Kedzierski, J.; Hsu, P. L.; Healey, P.; Wyatt, P. W.; Keast, C. L.; Sprinkle, M.; Berger, C.; de Heer, W. A. Epitaxial graphene transistors on SiC substrates. *Electron Devices, IEEE Transactions on* **2008**, *55*, 2078-2085.
- (37) Emtsev, K. V.; Bostwick, A.; Horn, K.; Jobst, J.; Kellogg, G. L.; Ley, L.; McChesney, J. L.; Ohta, T.; Reshanov, S. A.; Röhrl, J. Towards wafer-size graphene layers by atmospheric pressure graphitization of silicon carbide. *Nature materials* **2009**, *8*, 203-207.
- (38) Robinson, J. A.; Hollander, M.; LaBella III, M.; Trumbull, K. A.; Cavalero, R.; Snyder, D. W. Epitaxial graphene transistors: enhancing performance via hydrogen intercalation. *Nano letters* **2011**, *11*, 3875-3880.
- (39) M.Loboda **Design Considerations for SiC-based Power Electronics**
http://powerelectronics.com/power_semiconductors/sic/design-considerations-for-sic-based-power-electronics-1106/. *Power electronics technology* **2012**.
- (40) Reina, A.; Jia, X.; Ho, J.; Nezich, D.; Son, H.; Bulovic, V.; Dresselhaus, M. S.; Kong, J. Large area, few-layer graphene films on arbitrary substrates by chemical vapor deposition. *Nano letters* **2008**, *9*, 30-35.
- (41) Lee, C.; Wei, X.; Kysar, J. W.; Hone, J. Measurement of the elastic properties and intrinsic strength of monolayer graphene. *Science* **2008**, *321*, 385-388.
- (42) Nair, R.; Blake, P.; Grigorenko, A.; Novoselov, K.; Booth, T.; Stauber, T.; Peres, N.; Geim, A. Fine structure constant defines visual transparency of graphene. *Science* **2008**, *320*, 1308-1308.
- (43) Balandin, A. A.; Ghosh, S.; Bao, W.; Calizo, I.; Teweldebrhan, D.; Miao, F.; Lau, C. N. Superior thermal conductivity of single-layer graphene. *Nano letters* **2008**, *8*, 902-907.
- (44) Chen, S.; Wu, Q.; Mishra, C.; Kang, J.; Zhang, H.; Cho, K.; Cai, W.; Balandin, A. A.; Ruoff, R. S. Thermal conductivity of isotopically modified graphene. *Nature Materials* **2012**.

- (45) Bard, A. J.; Faulkner, L. R. *Electrochemical methods: fundamentals and applications*; Wiley New York: 1980; Vol. 2.
- (46) Bockris, J. O. M.; Devanathan, M.; Muller, K. On the structure of charged interfaces. *Proceedings of the Royal Society of London. Series A. Mathematical and Physical Sciences* **1963**, 274, 55-79.
- (47) Bockris, J. O. M.; Reddy, A. K. N. *Modern Electrochemistry 2B: Electroics in Chemistry, Engineering, Biology and Environmental Science*; Springer: 2001; Vol. 2.
- (48) Ayers, J. E. *Digital integrated circuits: analysis and design*; CRC: 2003; .
- (49) Anderson, B.; Anderson, R. *Fundamentals of semiconductor devices*; McGraw-Hill, Inc.: 2004; .
- (50) Bergveld, P. Thirty years of ISFETOLOGY: What happened in the past 30 years and what may happen in the next 30 years. *Sensors Actuators B: Chem.* **2003**, 88, 1-20.
- (51) Bergveld, P. Development of an ion-sensitive solid-state device for neurophysiological measurements. *Biomedical Engineering, IEEE Transactions on* **1970**, 70-71.
- (52) Yates, D. E.; Levine, S.; Healy, T. W. Site-binding model of the electrical double layer at the oxide/water interface. *J.Chem.Soc., Faraday Trans.1* **1974**, 70, 1807-1818.
- (53) Bohunicky, B.; Mousa, S. A. Biosensors: the new wave in cancer diagnosis. *Nanotechnology, Science and Applications* **2011**, 4, 1-10.
- (54) Nano-enhanced wholesale technologies Atomic structure of graphene
<http://www.nano-enhanced-wholesale-technologies.com/faq/carbon-forms.htm>.
- (55) Roland Wiesendanger group STM topography of graphene
<http://www.nanoscience.de/nanojoom/index.php/en/research/current-topics/graphene.html>.

Chapter 2- Fabrication Technology of graphene SGFETs

In this chapter, we will describe the fabrication methods of graphene SGFETs on silicon dioxide as well as on plastic substrates. In this fabrication technology, it was very important to adopt steps to ensure the complete removal of photoresist residues from the top of the graphene surface. Indeed, the removal of photoresist residues could have an impact on the sensing performance of graphene as was suggested elsewhere¹ and will be discussed in chapter 3. Finally, the measurement set up is described.

1- Graphene growth and transfer on SiO₂

The first step towards the fabrication of SGFET arrays is the growth of large areas of monolayer graphene films by CVD on copper foils. For this purpose, we first anneal at 1000°C and low pressure the copper foil in a CVD furnace for 30 min while flowing hydrogen (10 sccm) in order to remove any copper oxide layer that would have formed at the surface of the copper foil. Subsequently, graphene is grown at the surface of the copper foil by flowing methane gas (50 sccm) with hydrogen gas (20sccm) for 40 minutes. Finally, we cool down the foil by opening the furnace while still flowing hydrogen (10 sccm). As a result, a mostly single layer (~90% single layer) and continuous graphene film covers the entire top surface of the copper foil.

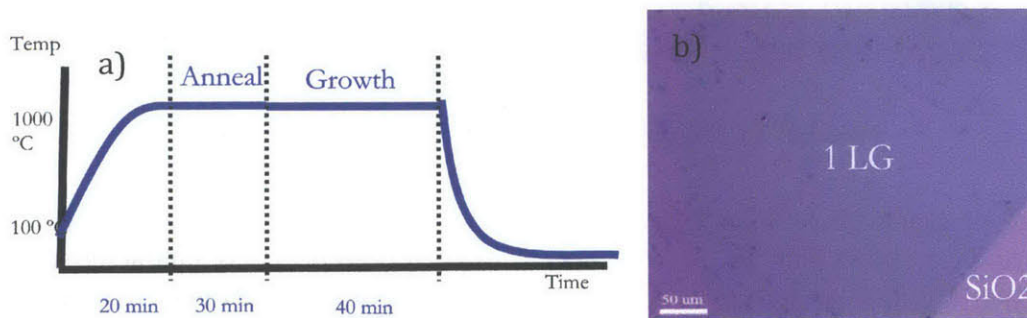


Figure 1: a) schematic of the graphene growth recipe on copper foil. b) Optical image of continuous monolayer graphene film transferred on silicon dioxide

Prior to the transfer of the graphene film on the substrate, metal contacts are deposited on the Si/SiO₂ substrate (290 nm of SiO₂). This bottom-contact process ensures that the metal-graphene interface is clean of any polymer residue from the transfer process or photo resist. Photo resist residue is typically found in top-contact electrodes, which increases the contact resistance². However, in the bottom-contact technology, it is easy to remove any photo resist residues layer due to the deposition of metal contacts before transferring graphene. Indeed, after deposition of the metal contacts, an O₂ plasma etch on the surface with an Asher is performed in order to

remove any photo resist residues on the silicon dioxide surface. This cannot be done in the case of top contact electrodes, as the plasma treatment would completely destroy the graphene layer.

In our bottom contact process, two subsequent metal depositions are performed. First, Ti/Au (10nm/300nm) contact pads are deposited by optical lithography using AZ5214 resist and e-Beam evaporation on the substrate. These contact pads will serve for the wirebonding to the chip carrier later on. Consequently, Ti/Pd/Au (2.5nm/45nm/15nm) drain and source Ohmic contacts are deposited on the substrate.

The next step consists in transferring the graphene film onto the substrate with the already deposited metal contacts. For this purpose, a Poly(methyl methacrylate) (PMMA) layer (PMMA A9 from Microchem diluted 1:1 with anisole) is first spin coated on the copper foil. An O₂ plasma etch of the back side of the foil is done to remove the graphene layer grown also on the back side of the foil. Then, the copper foil is etched away with commercial Cu etchant (Transene CE-100). After rinsing several times the graphene film in water, the film is cleaned in a hydrochloric acid solution. Then, the film is finally transferred on the substrate.

In order to remove the PMMA layer, our approach is to first expose the sample to acetone vapors instead of immersing directly in acetone because direct immersion would be a harsh process and the graphene could come off from the substrate. The acetone vapors do a preliminary removal of the PMMA but gently so that the graphene sticks well to the substrate. Then some liquid acetone is flowed for 10 seconds to finish dissolving the PMMA. Finally, in order to completely remove any PMMA residues left, the sample is put in a furnace for an annealing at 500 degree C for 2 hours with argon (400 sccm) and hydrogen (700 sccm).

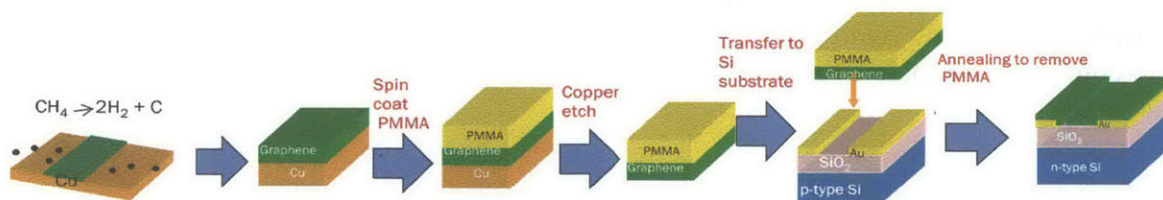


Figure 2: Transfer technique process

The optical image of graphene SGFET arrays in figure 3 a) shows that the graphene film is continuous. Figure 3 b) shows that the Raman spectrum of the graphene is characteristic of monolayer graphene. The D peak is very weak showing that our graphene has very few defects. In addition, the graphene surface is completely clean of any PMMA residues with this process as shown on the AFM image in figure 3 c). The RMS surface roughness is 0.5 nm, consistent with clean graphene surface.

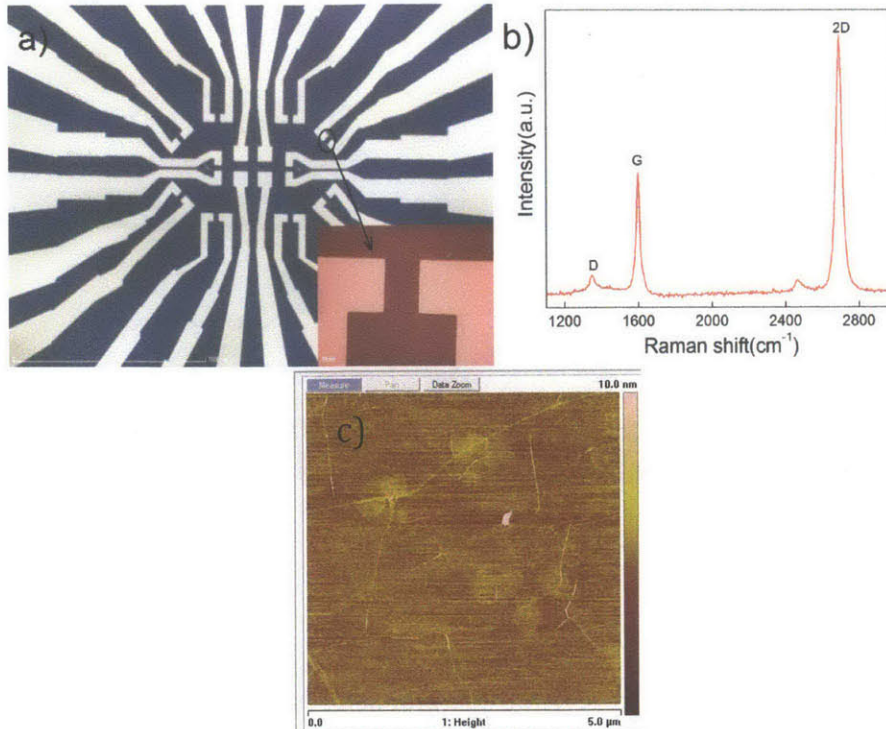


Figure 3: a) Optical micrograph of a sensor array on Si/SiO₂. The inset on the bottom right corner shows the detail of a CVD-grown graphene-on-SiO₂ transistor before depositing the insulation. (b) Raman spectrum for a wavelength $\lambda=532\text{nm}$ confirms the presence of mono-layer graphene. (c) AFM image obtained with a Veeco Dimension 3100 system, of the graphene surface after transfer.

2- Fabrication of graphene SGFET

- **Graphene patterning**

The next step consists on patterning the graphene. In order to protect the graphene layer from any photo resist contamination, a thin layer of MMA is deposited on top of the graphene. Subsequently, a layer of OCG photo resist is spin-coated and exposed to pattern the graphene. An O₂ plasma etch is done to etch subsequently the MMA layer first and then the graphene. The remaining OCG photoresist and MMA layer are removed by acetone cleaning. To remove any MMA residues on top of graphene, a 2 hours annealing at 500 degree C is performed with flowing hydrogen (700 sccm) and argon (400 sccm) gases.

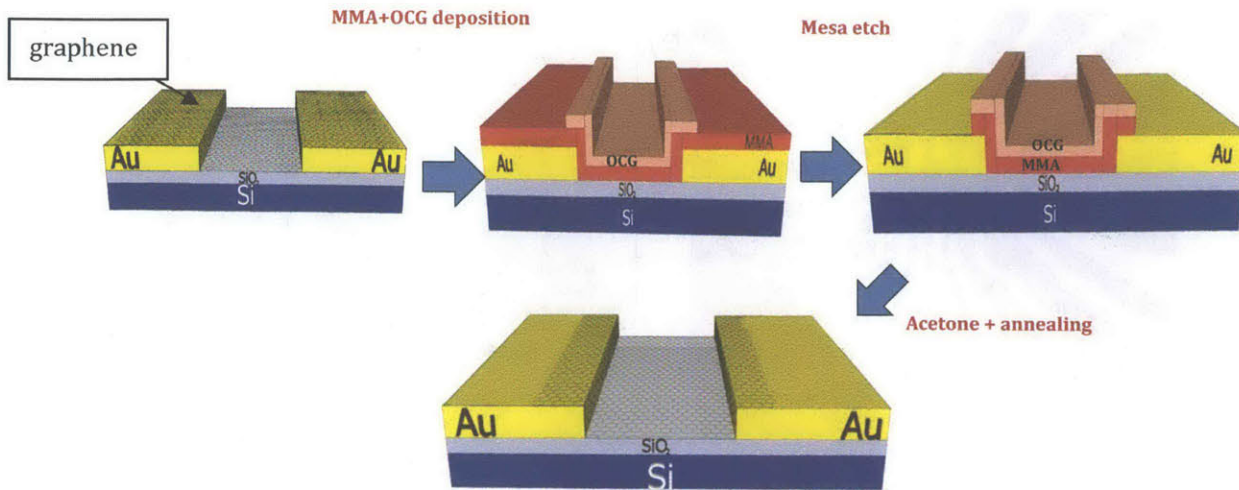


Figure 4: Graphene patterning process

As shown in figure 5, the graphene surface is still completely clean of residues and the use of a MMA protective has thus enabled to perform the graphene patterning without contaminating the graphene layer with OCG photo resist residues. The AFM images of the graphene before and after the graphene patterning step are very similar and exhibit an almost identical RMS surface roughness. At this stage, we have fabricated graphene-on-SiO₂ transistors.

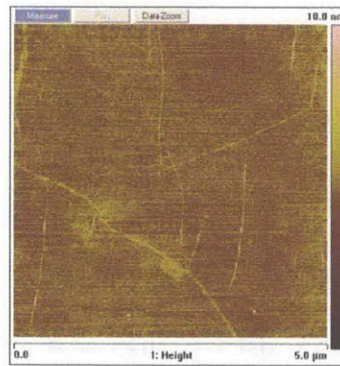


Figure 5: AFM image obtained with a Veeco Dimension 3100 system, of the graphene surface of after patterning.

- **Method 1: Insulation of devices with a small part of the metal contacts exposed**

After fabricating the device, the graphene-on-SiO₂ transistors are glued to a 28-pin chip carrier and wire-bonded using a wet aluminum wire bonder. Then, it is very important to insulate the device, which consists in avoiding and minimizing the contact of the solution with any metal contacts or wires on the chip. Indeed, the contact of the solution with metals can significantly increase the gate leakage of the device. This gate leakage not only perturbs significantly the sensing measurements but also very quickly the device can break at high gate leakage. The first

and most straightforward method insulation consists in applying manually on metal contacts a Room Temperature Vulcanization (RTV) non-flowing silicone rubber (Dow Corning K738) that cures at room temperature and will serve as an insulation barrier. Nearly all of the metal contact area is covered with the rubber except the very end of the metal contacts that are in direct contact with graphene because it is not possible manually to reach the necessary precision without taking the risk of covering the entire graphene transistor with the silicon rubber. With this silicon rubber technology, a well surrounding the contact pads is then built.

Finally, a flowing epoxy from Epoxy Technologies (OE 303-M) that cures at room temperature is applied on the exteriors of the well in order to insulate the wires connecting the contact pads to the chip carrier. The well is used to contain the flowing epoxy outside of its walls and avoid that it flows on the graphene devices. Figure 6 illustrates the final insulation step.

With this insulation method, the gate leakage is generally around 1 nA at $V_{DS}=50$ mV and is four orders of magnitude lower than the current going through the graphene sheet and therefore is negligible. This insulation method is therefore appropriate. However, a second method was developed in order to cover entirely the metals, which decreases further the gate leakage.

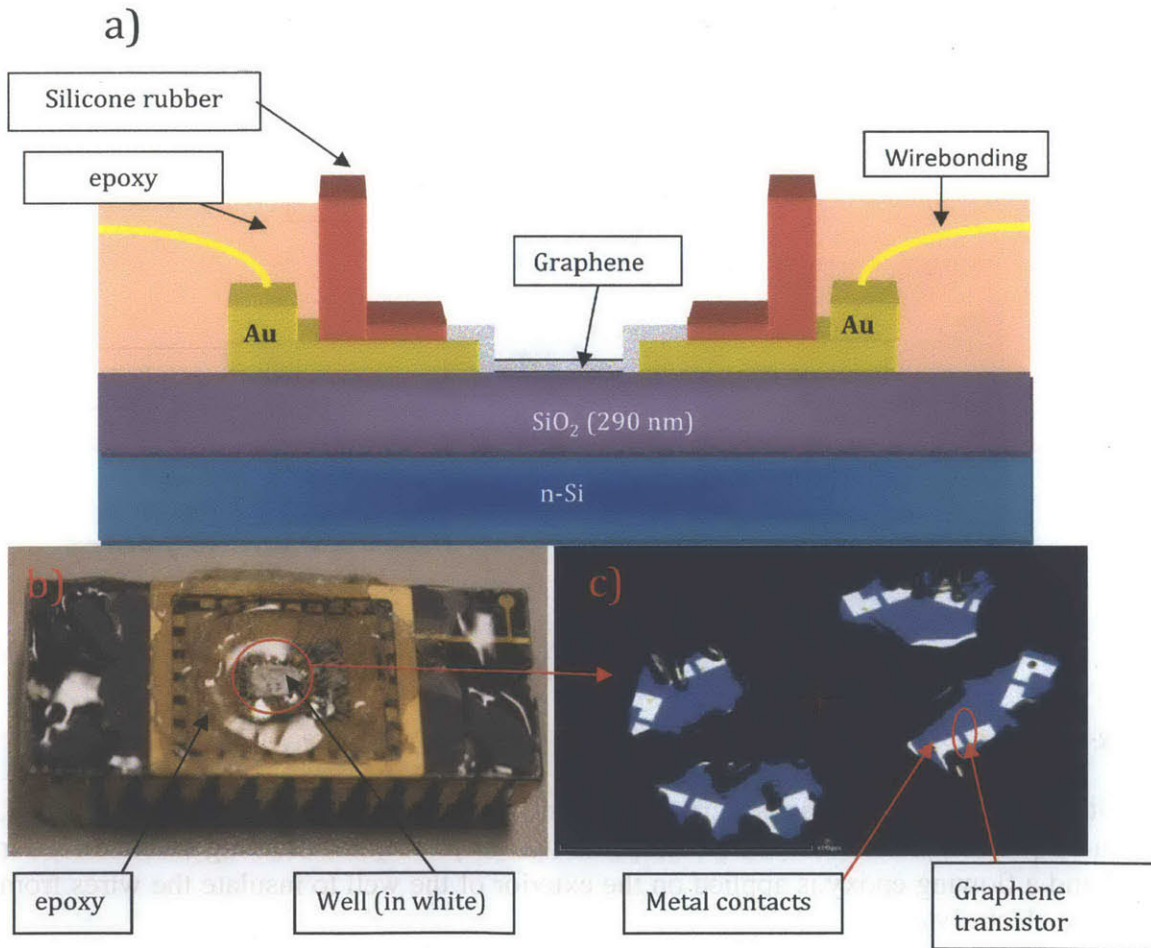


Figure 6: a) Schematic structure of the device wire bonded to a chip carrier and encapsulated. b) Optical image of a chip carrier with the built-up well and the epoxy for insulation. c) Zoomed in image showing the manual application of the rubber insulation on the metal contacts of the graphene transistors. A tiny part of the metals are going to be exposed to the electrolyte

- **Method 2: Insulation of devices with metal contacts completely insulated**

This fabrication method has the advantage of totally insulating the metal contacts, which enables to decrease, usually by an order of magnitude, the gate leakage due to the total lack of contact between metals and the electrolyte. Indeed, gate leakage is around the nA in the case described above where a tiny portion of the metals are exposed to the electrolyte whereas in the case of total insulation of the metals, the gate leakage is around 100 pA.

In order to totally insulate the metals, we use an insulating SU 8 layer to cover the contacts. However, in order to have a graphene surface clean of SU 8 residues, a sacrificial aluminum oxide layer is used. Thus, we deposit a 5 nm thick layer of Al_2O_3 on top of the graphene-on- SiO_2 transistors. Two subsequent layers of 1.5 μm thick SU 8 are then spin coated. Then, the SU 8 layers are exposed and developed in order to create window openings in the graphene transistors. Finally we remove the Al_2O_3 layer in the openings by wet etch. The graphene in these openings will be consequently directly exposed to the electrolyte. The graphene surface again is clean of any SU 8 residues thanks to the use of the Al_2O_3 protective layer. The use of SU 8 leads to the creation of an access region, which is the area of the graphene channel covered by SU 8 that cannot be biased by the gate voltage through the electrolyte. The length of this region is 3 μm on each of the two metal contacts. This access region increases the global contact resistance and decreases the transconductance.

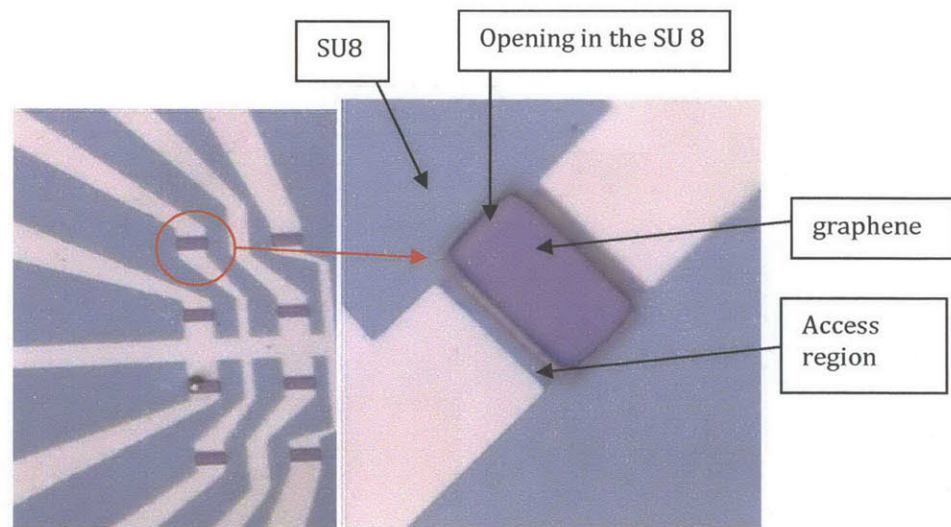


Figure 8: Optical images of graphene transistors arrays with a zoomed in on a single transistor.

The chip with the graphene transistors arrays is then, as in the previous fabrication method, mounted to a 28-pin chip carrier and wire-bonded. A well of (RTV) non-flowing silicone rubber is fabricated and a flowing epoxy is applied on the exterior of the well to insulate the wires from contact with the electrolyte.

3- Fabrication of graphene sensors on plastic PEN

As explained in Chapter 1, the integration of graphene sensors on plastic substrates is very promising for the fabrication of high performance flexible and low cost sensors. The successful fabrication of graphene sensors on plastic substrate would significantly increase the range of sensing applications for graphene.

In our work, a Polyethylene naphthalate (PEN) substrate was chosen because it is already used for flexible electronics and has the advantage of being transparent. The substrate that we used is a PEN Teonex® (Teijin DuPont) substrate 125 μm thick. The first step is to deposit metal contacts on the PEN substrate. As with the fabrication on silicon dioxide, a bottom-contact process is chosen so that the metal-graphene interface is clean of any polymer residue (e.g. PMMA) from the transfer process. For this purpose, metal Ohmic electrodes (Ni/Au, 20nm/40nm, Ni being used as the adhesion layer) were fabricated on the PEN substrate by a low temperature thin film metallization process, photolithography patterning and subsequent local wet etching of both Au and Ni layers.

Subsequently, the graphene is transferred to the PEN substrate in the same way than on silicon dioxide. The removal of PMMA is done by using acetone vapors and subsequent flowing of acetone on the sample in the exact way as described previously for transfer on silicon dioxide. However, in this case we cannot use the high temperature annealing to completely remove the PMMA residues, as the PEN starts melting at 120 C.

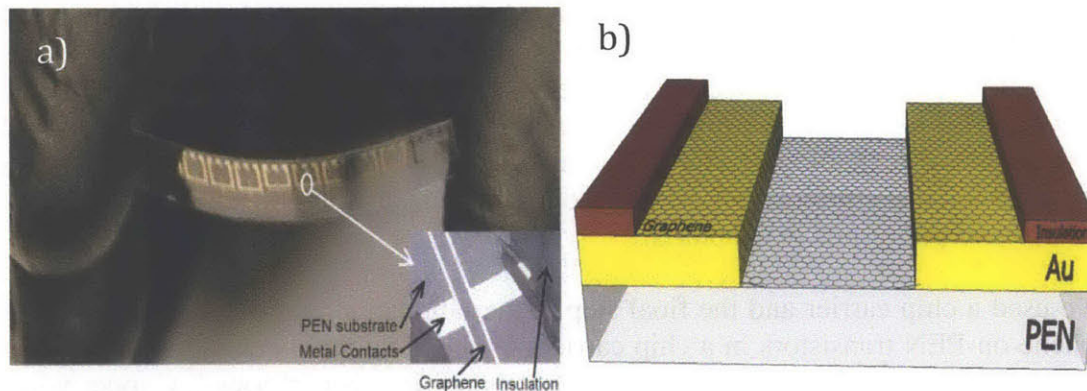


Figure 9: a) Optical image of an array of graphene chemical sensors on plastic substrate. The inset on the bottom right corner shows a detail of one of the devices. b) Schematic illustration of a graphene-on-PEN transistor

Therefore, in the case of fabrication of graphene sensors on plastic substrate, some residues may remain on the graphene substrate. However, due to the very rough surface of PEN (~10 nm in RMS roughness), AFM could not be used to characterize the amount of residues. In order to have an idea of the amount of residues on top of the graphene surface, the same fabrication treatment based on acetone vapors and acetone flow and no high temperature annealing was used with graphene on silicon dioxide. Figure 10 shows an atomic force microscope image of the resulting surface. The RMS roughness of the graphene surface indeed increases significantly with these

residues on the surface (2.11 nm) compared to the graphene surface clean of any residues that we obtain after annealing (0.8 nm).

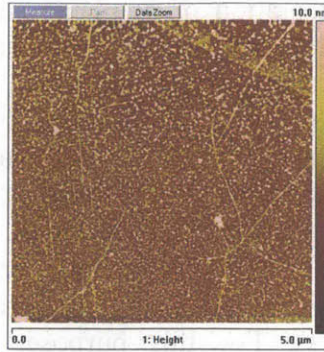


Figure 10: AFM image obtained with a Veeco Dimension 3100 system, of the graphene surface on silicon dioxide after acetone vapors and acetone flowing treatment

Different methods were used to try to characterize the structural quality of graphene on PEN. Unfortunately Raman spectroscopy does not work in this case because the graphene Raman signature is hidden by the PEN signature. However, the electrical performance of the fabricated devices is excellent, which shows that graphene was successfully transferred and that the graphene film is continuous and of good quality.

In order to make a totally flexible sensor, the packaging used for graphene-on-SiO₂ transistors as well as the measurement set up should have been adapted. Especially the design and fabrication of micro fluidics to put on top of the device would have been needed for this purpose. In this work, we were more interested in characterizing the graphene-on-PEN SGFETs than actually proving that it was possible to make a completely flexible sensor. However, in the future, it will be interesting to adapt the technology to make the sensor totally flexible. Using micro fluidics will definitely work in this outlook but it will not change in any way the validity of the characterization that we performed in chapter 3.

In our work we used a chip carrier and the final step in the fabrication process was to therefore place the graphene-on-PEN transistors in a chip carrier. As the aluminum wet etch wirebonding on a flexible plastic substrate does not work, manual wirebonding was performed. Copper wires were positioned so that they connect the pads of the transistors to the pads of the chip carrier. Then silver epoxy was used to glue the copper wire as well electrically connect the wire to the contact pads. RTV non flowing silicone rubber insulation was then used to protect the wires and also the metal contacts from contact with the electrolyte, as shown in figure 11.



Figure 11: a) Optical image of the manual wirebonding. b) Schematic illustration of a graphene-on-PEN solution-gated transistor.

4- Measurement set up

All the different fabrication methods described above lead to the fabrication of graphene sensors with differences in the amount of residues on top of graphene as well as the degree of insulation coverage of metal contacts. After the encapsulation of the sensors, the very last step in the fabrication of the sensors is to glue a glass ring onto the chip carrier and then a beaker to the glass ring. This will enable to contain the electrolyte solution that will contact the graphene of our SGFETs. At this point, the devices are ready to be used as a graphene SGFETs.

The graphene devices are then immersed in the solution we wanted to sense and an Ag/AgCl reference electrode (WPI flexible dri-ref reference electrode), put inside the solution, is used to apply the top gate voltage. The drain and source contacts of the devices, as well as the reference electrode, are all connected through an interface to an Agilent 4155C Semiconductor Parameter Analyzer in order to measure the transistor characteristics, as shown in figure 12 below.

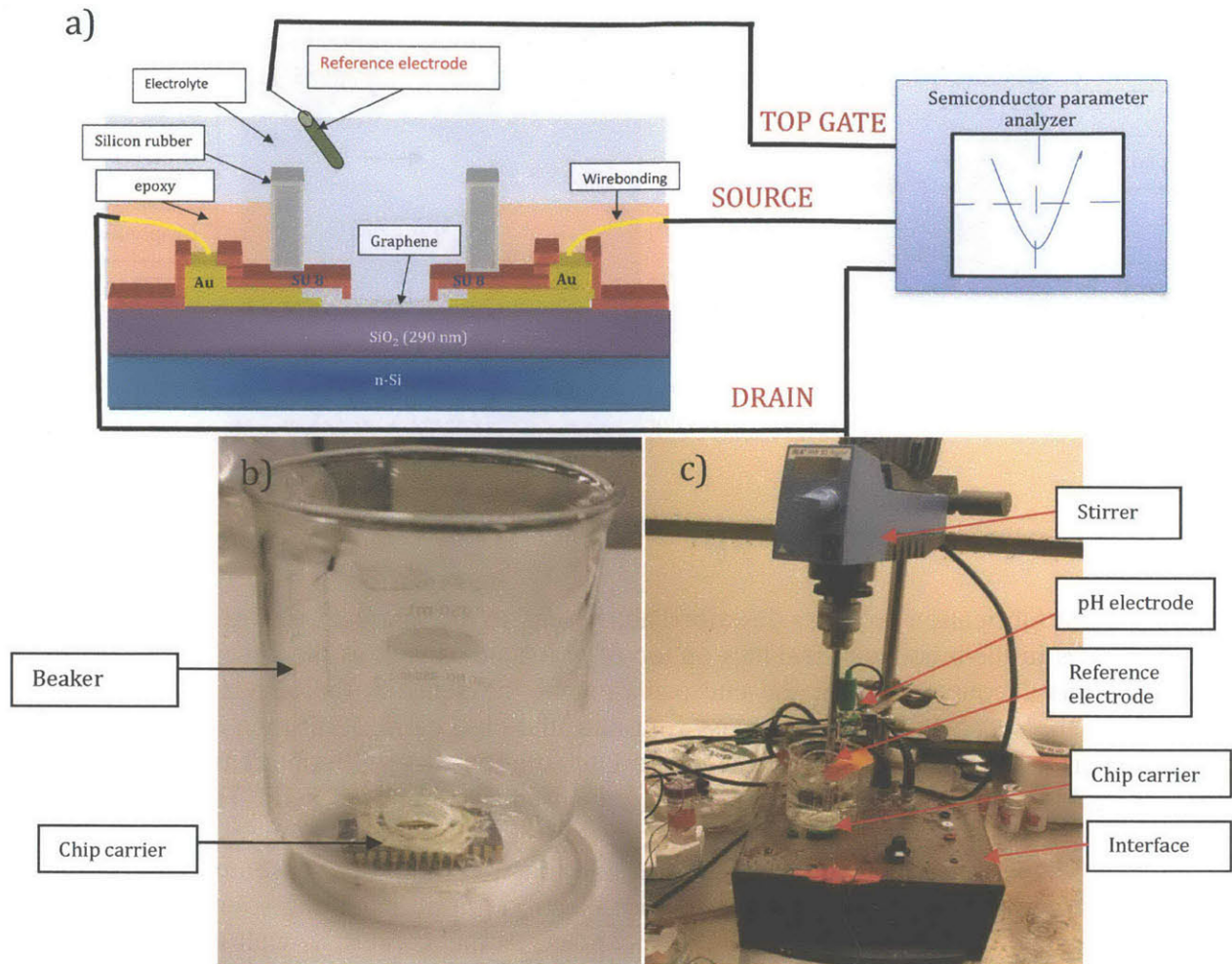


Figure 12: a) Schematic illustration of the measurement set up, b) Photography of the chip carrier and the beaker mounted on top. c) Photography of the measurement set up

References

- (1) Heller, I.; Chatoor, S.; Mannik, J.; Zevenbergen, M. A.; Dekker, C.; Lemay, S. G. Influence of Electrolyte Composition on Liquid-Gated Carbon Nanotube and Graphene Transistors. *J. Am. Chem. Soc.* **2010**.
- (2) Hsu, A.; Wang, H.; Kim, K. K.; Kong, J.; Palacios, T. Impact of Graphene Interface Quality on Contact Resistance and RF Device Performance. *Electron Device Letters, IEEE* **2011**, *32*, 1008-1010.

Chapter 3- Characterization of single-layer graphene sensors

1-Electrical characteristics on different substrates

This section discusses the electrical characteristics of graphene SGFETs in electrolyte-gated configuration and compared back-gated configuration measurements. In electrolyte-gated configuration, the top gate voltage V_{GS} is applied to the solution with a reference electrode whereas in back-gated configuration, the top gate voltage V_{GS} is applied to the SiO_2 layer underneath graphene through the conductive silicon back of the wafer. Then, we will compare the electrical characteristics of graphene sensors on different substrates, especially silicon dioxide and plastic PEN, in order to understand the influence of the substrate on the electrical performance.

- **Graphene on SiO_2 devices**

To characterize the performance of the fabricated devices in electrolyte-gated configuration, the drain and source contacts of the graphene transistors, as well as an Ag/AgCl reference electrode, are connected to an Agilent 4155 Semiconductor Parameter Analyzer. Then, the devices are immersed in a 10 mM phosphate buffer solution pH 7 with an ionic strength adjusted to 100 mM with sodium chloride. The solution was constantly stirred at 140 rpm. The drain-source voltage V_{DS} is set to 50 mV and the gate-source voltage V_{GS} sweep was limited between 0.1 V and 0.5 V to avoid the creation of surface defects as mentioned elsewhere¹. In the back-gated configuration the gate-source voltage V_{GS} is applied between 0 V and 100 V at the back of the chip through a 300 nm thick SiO_2 layer and the active graphene channel is exposed to ambient air.

Figure 1 shows the transfer characteristics, i.e. the modulation of the drain-source current I_D with the top gate voltage V_{GS} , of a device with dimensions $10 \times 60 \mu m^2$ (Length \times Width) in the back-gated and electrolyte-gated configurations.

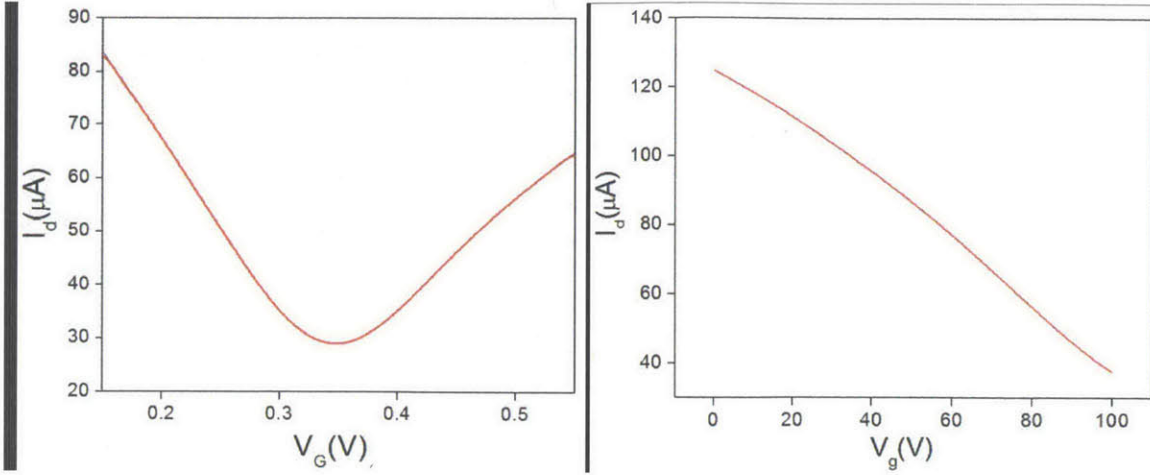


Figure 1: Graphene transistor, $10 \times 60 \mu\text{m}^2$ in size; a) back-gated transfer characteristics in air; b) electrolyte-gated transfer characteristics in 10 mM phosphate buffer. For all measurements, $V_{DS}=50\text{mV}$.

In the back-gated configuration, the minimum conductivity point V_{GSmin} cannot be observed in the measured range of voltages, which indicates the p-type nature of the CVD grown graphene. The substrate induced doping is commonly observed in graphene grown by CVD and is due to negatively charged impurities trapped at the interface between graphene and SiO_2 , attributed to the doping effect of a water layer underneath the graphene². The high temperature annealing further p-dopes the graphene sheet. In the electrolyte-gated configuration, on the other hand, the transport properties are significantly different. First, the minimum conductivity point V_{GSmin} shifts towards lower voltages to a value around 0.3 V.

The transconductance $g_m = \frac{\partial I_d}{\partial V_{gs}}$ is a key parameter for sensors because it determines the current response, which is the sensor output for a small modulation of the gate voltage due to the modification of the surface potential, i.e. a change in analyte concentration. Therefore, the transconductance directly gives the sensitivity of the sensor. For the measurements in the electrolyte-gated configuration, there is an asymmetry in transconductance values in the hole conduction and electron conduction regimes. The maximum transconductance of the device in the hole conduction regime is $5 \text{ mS}\cdot\text{mm}^{-1}$ when normalized by gate width whereas it is only $3.8 \text{ mS}\cdot\text{mm}^{-1}$ in the electron conduction regime. This is a very high transconductance, twenty times higher than for common silicon SGFETs³⁻⁵. This is due to the high interfacial capacitance⁶ at the graphene/electrolyte interface as well as the high carrier mobility in graphene³. Therefore our graphene sensors have the potential to be much more sensitive than the silicon ones.

In addition, the transconductance $g_m = \frac{\partial I_d}{\partial V_{gs}}$, is more than 300 times higher when the graphene is in operated in the electrolyte-gated configuration. This increase in the transconductance is mainly due to the much larger gate capacitance in the electrolyte-gated configuration compared to the back-gated configuration.

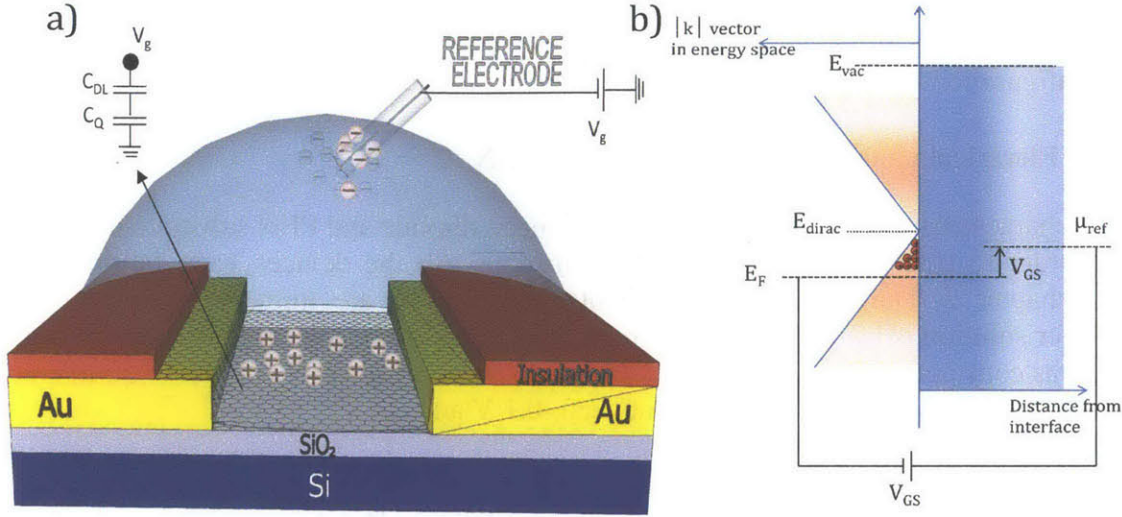


Figure 2: a) Model of the graphene SGFET with the double layer and quantum capacitances; b) Modulation of the charge carrier density by the electrolyte gate: the applied gate voltage shifts the Fermi level E_F in graphene below (shown) or above the Dirac point (E_{dirac}), defining the density and type of charge carriers.

For the electrolyte-gated configuration, the top gate voltage drops at the electrostatic double layer formed by the accumulation of ions near the graphene/electrolyte interface to maintain charge neutrality, leading to the formation of a double layer capacitance C_{DL} . Actually, the graphene/electrolyte interface capacitance C_{int} is formed by the series combination of the double layer capacitance C_{DL} and the quantum capacitance of graphene C_Q so that $\frac{1}{C_{int}} = \frac{1}{C_{DL}} + \frac{1}{C_Q}$. For the back-gate configuration, the total capacitance C_{BG} is formed by the series combination of the oxide capacitance C_{ox} and the quantum capacitance of graphene C_Q : $\frac{1}{C_{BG}} = \frac{1}{C_{ox}} + \frac{1}{C_Q}$. It is worth noticing here that the back-gated measurements were performed without any solution on top of the graphene that was exposed to air in order to avoid any influence of the solution on the measurement due to the electric field applied to the back gate that would penetrate into the solution⁷. Assuming that the capacitance is, in first order, described by $C \approx \frac{\epsilon_0 \epsilon A}{d}$, with ϵ the dielectric constant, d the thickness of the capacitance and A the area, differences in both dielectric constant and thickness of the capacitance are responsible for the difference in capacitance in the two configurations.

Indeed, the very small thickness of the double layer is only limited by the size of the ions (~ 1 nm) whereas the back gate capacitance C_{BG} is limited by the 300-nm-thick backside oxide. In addition, the dielectric constant of the electrolyte is around 80, similar to water, whereas the dielectric constant of the SiO_2 is only 3.9. Thus, by taking into account that the quantum capacitance is around $2 \mu F \cdot cm^{-2}$, and since C_{ox} is nearly three orders of magnitude lower, we have $C_{BG} \sim C_{ox} = 1.4 nF \cdot cm^{-2}$. For the interfacial capacitance in the electrolyte-gated configuration, the quantum capacitance is of the order of the double layer capacitance and we found that $C_{int} = 1.6 \mu F \cdot cm^{-2}$, which is in agreement with what was obtained by a more complex model⁶.

Therefore, this substantial difference in capacitances between the configurations accounts for the increase by 300 times in transconductance in the electrolyte-gated configuration compared to the back-gated configuration.

- **Electrical characteristics on SiO₂ and PEN**

The electrical characteristics of graphene sensors on silicon dioxide and PEN substrate have been compared in order to study the influence of the substrate. All the devices were fabricated as described in chapter 2. During the measurements, the devices are immersed in a 10 mM phosphate buffer solution pH 7 with an ionic strength adjusted to 100 mM with sodium chloride. The solution was constantly stirred at 140 rpm. The drain-source voltage V_{DS} is set to 50 mV and the gate-source voltage V_{GS} sweep is limited between -0.1 V and 0.4 V.

Figure 2 shows the transfer characteristics of a graphene-on-PEN transistor, compared to a graphene-on-SiO₂ device, for a 10 mM phosphate buffer solution pH 7.2.

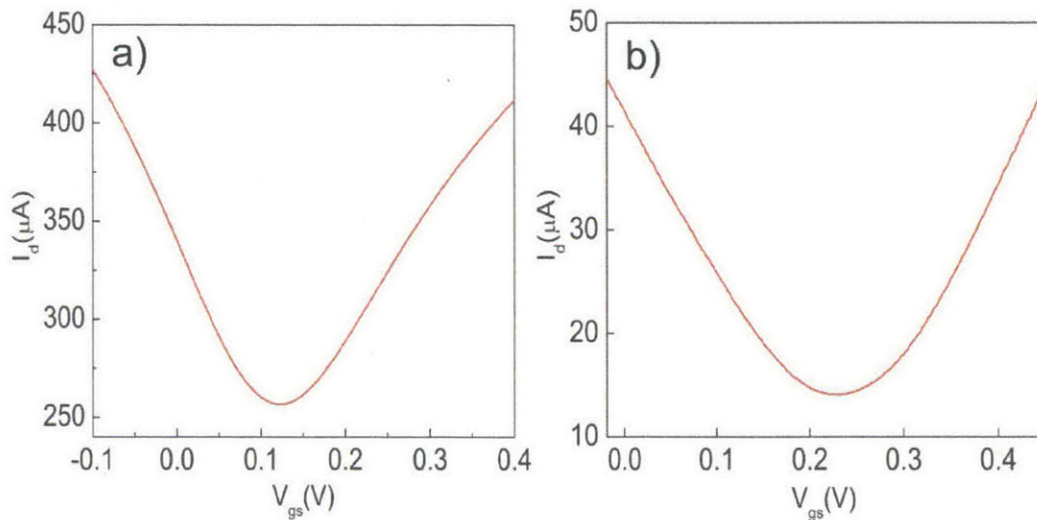


Figure 3: Transfer characteristics in a 10 mM phosphate buffer solution of a) $20 \times 1000 \mu\text{m}^2$ graphene transistor on PEN as well as of b) $20 \times 40 \mu\text{m}^2$ graphene transistor on SiO₂ for a drain-source voltage $V_{DS}=50\text{mV}$.

The gate-source voltage V_{GSmin} at minimum conductivity point, which corresponds to the Dirac point, is 0.12 V for the graphene-on-PEN transistor and 0.22V for the graphene-on-SiO₂ transistor. This indicates that in both cases, the graphene is p-doped, as usually observed for graphene grown by CVD. The more significant p-doping effect observed in the case of graphene on SiO₂ is mainly due to the additional annealing at 500 degree C in hydrogen atmosphere performed in order to totally remove the PMMA residues.

The maximum transconductance of the graphene-on-PEN device is 1020 μS in the hole conduction regime and 716 μS in the electron conduction regime. When normalized by the transistor width, the maximum transconductance of the transistor is then $1 \text{ mS}\cdot\text{mm}^{-1}$. This transconductance value is 5 times smaller than the maximum transconductance of the reference graphene-on-SiO₂ devices ($5 \text{ mS}\cdot\text{mm}^{-1}$). It should be noted that the transconductance of our

graphene transistors on PEN substrate is quite high compared to conventional planar silicon SGFET technology, about 4 times higher³⁻⁵. This is due to the high interfacial capacitance at the graphene/electrolyte interface as well as the high carrier mobility in graphene even on PEN substrate.

The higher transconductance in graphene-on-SiO₂ devices can be attributed to the higher carrier mobility on silicon dioxide than on PEN. Indeed, the field effect carrier mobility of the transistor μ_{FE} can be calculated using $\mu_{FE} = \frac{1}{C_{int}} \frac{d\sigma}{dV_{gs}}$, where C_{int} is the interfacial graphene/electrolyte capacitance and σ is the conductance. Following our previous estimation of the interfacial capacitance, we can extract a maximum hole mobility of 300 cm².V⁻¹.s⁻¹ and an electron mobility of 220 cm².V⁻¹.s⁻¹ for the graphene-on-PEN transistor, while for the graphene-on-SiO₂ transistor, the maximum hole mobility is 1095 cm².V⁻¹.s⁻¹ and the electron mobility is 1250 cm².V⁻¹.s⁻¹. The lower carrier mobility in the graphene-on-PEN devices as compared to devices on SiO₂ is expected for two reasons: first the PEN substrate has more than 10 times higher RMS surface roughness (~5-10 nm) than SiO₂(~0.4-0.5 nm) and secondly, the graphene transfer technique on PEN leaves more PMMA residue on the graphene due to the lack of a high temperature annealing, which increases the carrier scattering and degrades the transport properties^{9, 10}.

2- pH sensing

In this section, we demonstrate the use of graphene SGFETs for pH sensing. Devices fabricated on different substrates were evaluated, which gives very important insight about the pH sensing mechanism for graphene sensors.

We first compare the pH sensing mechanisms taking place in graphene SGFET and the one in Si/SiO₂ ISFET. This comparison emphasizes the differences in the two mechanisms and the different pH sensitivities that they induce as well as it underlines the specificity of the graphene pH sensing mechanism. The study focuses then particularly on the impact of the substrate on which the graphene is transferred or the amount of residues left on top of graphene during device processing since they are not well understood. Understanding the influence of these different elements on the sensor response is of paramount importance since it will enable to improve the intrinsic graphene sensor response to targeted molecules. Indeed, graphene-based chemical sensors show an intricate response of their transfer characteristics to changes in electrolyte properties such as salt concentration, type of ions or pH¹¹. And yet, in sensing experiments, the specific electric signal from targeted biomolecules could be obscured by signal perturbations like substrate charging effects as well as charging effects of ionizable groups of residue on top of the graphene surface^{9, 11, 12}. Finally, some experiments confirm that, contrary to the case of Si/SiO₂ ISFET, no chemical bonding is taking place between HO⁻ ions and the graphene surface in the pH sensing mechanism.

- **pH sensing on silicon dioxide**

In this section, the pH sensing of graphene sensors on silicon dioxide is described and the comparison in pH sensing between a graphene surface with or without PMMA residues highlights the influence of residues on the pH sensing mechanism. Indeed, it was hypothesized

that the presence of ionizable acidic groups of organic absorbents such as resist residue or amorphous carbon on top of the graphene surface could create pH-dependent surface charges in the vicinity of graphene, which would be responsible for the electrical response of the graphene devices with pH¹¹. Our experiments will test the validity of this hypothesis.

The graphene-on-SiO₂ devices are fabricated according to the technology described in chapter 2 section 2). The graphene surface is completely clean of residues but part of the metals are exposed to the electrolyte since we did not use SU 8. The gate leakage is negligible around 1nA, e.g. 4 orders of magnitude smaller than the drain-source current I_D . The dependence of the graphene-on-SiO₂ transistor transfer characteristics with the pH was evaluated. For these measurements, the device was immersed in a 10 mM phosphate buffer solution with an ionic strength adjusted to 100 mM with NaCl. Then, aliquots of 0.5 M HCl and NaOH were added to change the pH of the solution.

The dependence of the graphene-on-SiO₂ transistor transfer characteristics with pH is shown in Figure 3.

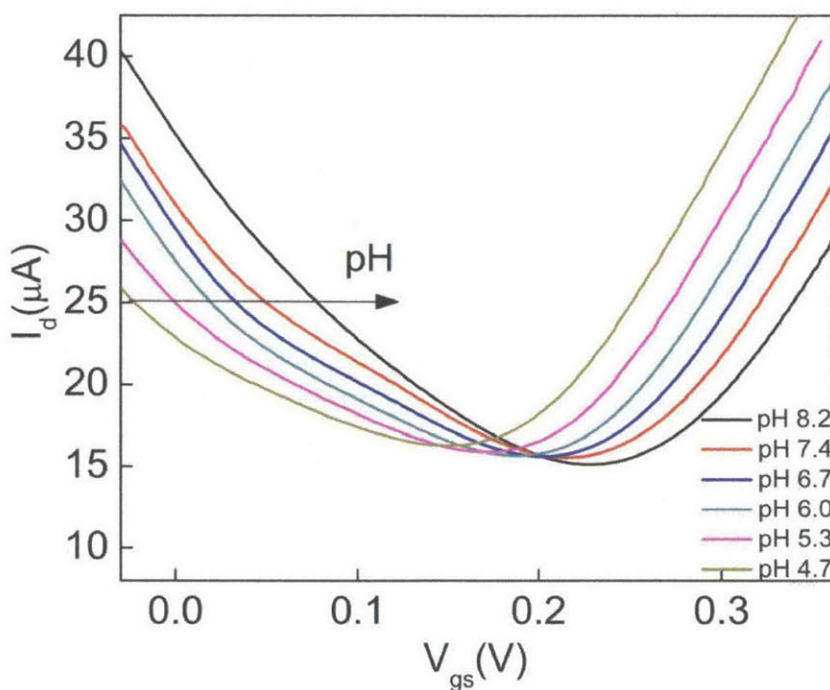


Figure 4: Transfer characteristics of a $20 \times 40 \mu\text{m}^2$ graphene-on-SiO₂ SGFET at a constant drain-source voltage of $V_{DS}=50\text{mV}$, for different pH

The Dirac point in the graphene transistor shifts towards more positive voltages when the pH is increased. This allows pH sensing by measuring the graphene electrical characteristics. The shift of the Dirac point is due to the increase in negative charge close to the graphene when the pH increases and indicates that the electrochemical double layer at the graphene/electrolyte interface is sensitive to pH allowing the capacitive charging of the surface by H_3O^+ or HO^- ions¹³¹⁴. As shown on Figure 5, the Dirac point shifts linearly with the pH, with a sensitivity of 22 mV/pH. The same sensitivity at the Dirac point was found with transistors of other sizes confirming that the graphene pH sensing is independent of the transistor size. Besides, this sensitivity is quite

similar to the one reported at the Dirac point for mechanically exfoliated graphene on SiO₂(26 mV/pH)¹⁵ and for epitaxial graphene on silicon carbide (19mV/pH)¹. It should be noted that the graphene sensor is very stable and that after the pH experiment, the device was washed in water, dried in nitrogen stream and put a day later in phosphate buffer exhibiting the same transfer characteristics.

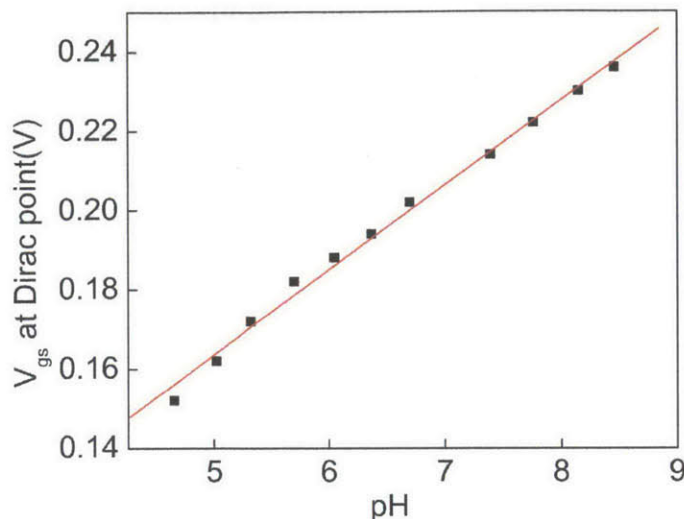


Figure 5: Voltage at Dirac point shift with the pH for the 20x40 μm² graphene-on-SiO₂ SGFET

- **Comparison of pH sensing mechanisms in graphene and Si/SiO₂ SGFETs**

It is worth comparing the pH sensing mechanisms in graphene and Si/SiO₂ SGFETs in order to better understand the specificity of graphene pH sensing mechanism. We are going to see that these two pH-sensing mechanisms are indeed different and this explains why the pH sensitivities in the two devices are different.

Graphene is a sp² arrangement of carbon atoms densely packed and the pristine graphene surface has no dangling bonds sticking out of the graphene plane¹⁶. Therefore, hydroxide or hydronium ions that physically adsorb on the graphene surface¹⁴ in pH sensing experiments, cannot attach to the graphene surface by a chemical bonding as there are no dangling bonds on the graphene surface. On the contrary, in the case of Si/SiO₂ SGFETs, the outer surface of the silicon dioxide in contact with the solution has dangling bonds. That's why, hydroxide or hydronium ions that adsorb to the SiO₂ surface can attach to the SiO₂ surface by forming chemical bonding with the dangling bonds. As shown in figure 6, the attachment of hydroxide or hydronium ions change the concentration of the 3 surface groups of SiO₂: SiO⁻, SiOH and SiOH₂⁺, according to the site binding model^{17, 18}. It therefore changes the surface oxide charge of SiO₂ and induces a pH dependence of Si/SiO₂ SGFETs with a pH sensitivity of 30 mV/pH.

Now, in the case of graphene SGFETs, the graphene surface has no dangling bonds and so the ions cannot bind chemically to its surface. However, the fact that the graphene has a significant pH dependent response with a sensitivity of 22 mV/pH emphasizes that there is some electron transfers between the graphene surface and the hydroxide or hydroniums ions. Therefore, it strongly suggests that the pH dependence is due to a chemical doping mechanism of graphene by the physical adsorption of ions as graphene is very sensitive to its environment. Out of the two possible chemical doping mechanisms that are surface transfer doping and substitutional doping¹⁹, the doping mechanism taking place here is a surface transfer doping. Surface transfer doping is already at stake in gas sensing experiments with graphene²⁰. Thus, the hydroxide and hydronium ions when adsorbed will interact electronically with the graphene surface and dope it. Therefore, surface transfer doping very likely induce the pH dependent response of graphene with a pH sensitivity of 22 mV/pH.

In conclusion, the very different pH sensing mechanisms taking place in graphene and Si/SiO₂ SGFETs explain the different pH sensitivity observed. The observations about the graphene pH sensing mechanism that are done below are all in agreement with a surface transfer doping mechanism for pH sensing.

It is worth noticing here that even though graphene is only a one atom thick membrane, there is no direct interaction of the ions in the solution with the Si/SiO₂ substrate underneath graphene since graphene is believed to be impermeable to most gases and liquids ^{21, 22}. Therefore, no chemical bonding between the ions in solution and the substrate underneath graphene can occur as graphene covers the dangling bonds of the substrate.

- **pH sensing on silicon dioxide for graphene surface with and without residues**

An interesting hypothesis that we wanted to test experimentally was whether or not residues on top of the graphene had an influence on the pH sensing. Indeed, it was suggested that the presence of ionizable acidic groups of organic absorbents such as resist residues or amorphous carbon on top of the graphene surface could create pH-dependent surface charges in the vicinity of graphene, which would be responsible for the electrical response of the graphene devices with the pH.

In order to understand the influence of residues on pH sensing, we compare these results with the pH sensing obtained for a graphene surface with residues on top. For this purpose, the PMMA removal after graphene transfer is only done using acetone vapors and acetone flowing. No annealing at high temperature was performed so that PMMA residues remained on top of the graphene surface. Likewise, the graphene etch is done without the high temperature annealing to remove the MMA residues only with acetone. Figure 6 shows the residues on top of the graphene surface at the end of the fabrication of the graphene-on-SiO₂ transistors.

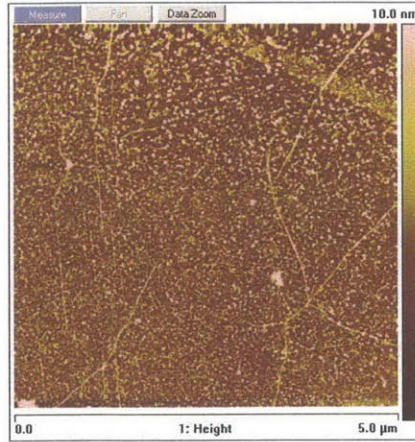


Figure 6: AFM image obtained with a Veeco Dimension 3100 system, of the graphene surface on silicon dioxide after acetone vapors and acetone flowing treatment

For a graphene surface with residues on top, the dependence of the graphene-on-SiO₂ transistor transfer characteristics with pH is shown in Figure 7.

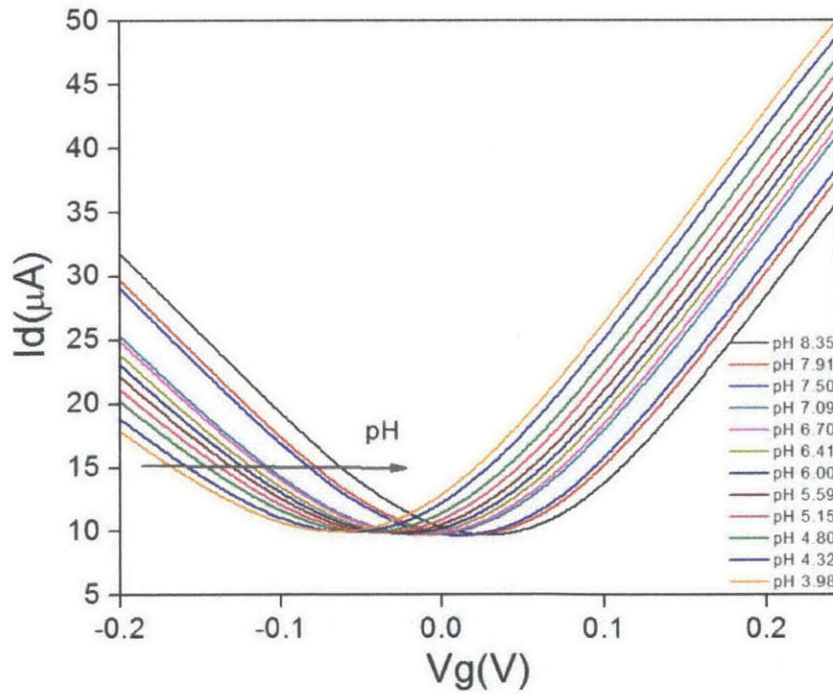


Figure 7: Transfer characteristics of a 20x40 μm² graphene-on-SiO₂ SGFET, with residues on top of the graphene surface, at a constant drain-source voltage of $V_{DS}=50mV$, for different pH

It can be noticed that the graphene is a much less p-doped than the graphene processed with a high temperature annealing, which emphasizes that most of the p-doping induced in graphene originates from impurities added during the high temperature annealing. For a graphene surface with residues on top, the pH sensitivity is 21 mV/pH, as shown in figure 8.

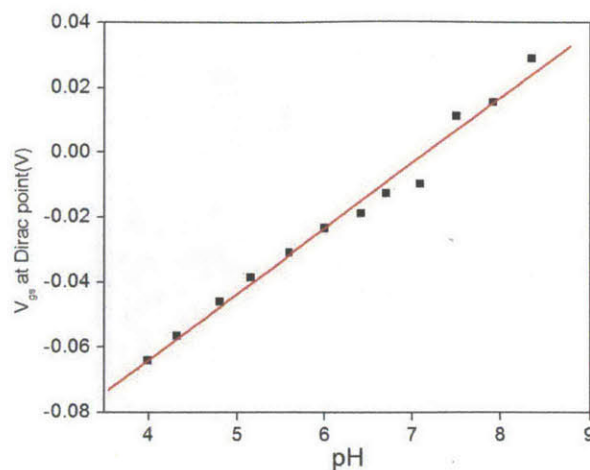


Figure 8: Voltage at Dirac point shift with the pH for the 20x40 μm^2 graphene-on-SiO₂ SGFET with residues on top of the graphene

Thus, the same pH sensitivity found in graphene SGFETs for a graphene surface with or without residues emphasizes that the photoresist residues are not directly with the pH sensing mechanism. This observation opposes the hypothesis that the presence of ionizable acidic groups of organic absorbents such as resist residues or amorphous carbon on top of the graphene surface could create pH-dependent surface charges in the vicinity of graphene, which would be responsible for the electrical response of the graphene devices with pH¹¹.

This observation is also of particular importance for the processing of graphene pH sensors in general since the presence of a reasonable amount of residues will not influence the pH sensitivity. However, it is possible that the electronic noise of the sensor may be increase due to the increase scattering of carriers with residues.

- **pH sensing on PEN substrate**

We have also investigated the pH sensing mechanism on different substrates especially on plastic substrates. The interest of doing graphene pH sensors on plastic substrates is to pave the way to the fabrication of high performance but low cost, flexible and transparent sensors. This work was done in collaboration with Dr. Vinciguerra and Dr. Pappalardo from STMicroelectronics Inc.

As in the previous experiments, the device was immersed in a 10 mM phosphate buffer solution with an ionic strength adjusted to 100 mM with NaCl. Then, aliquots of 0.5 M HCl and NaOH were added to change the pH of the solution. The dependence of the graphene-on-PEN transistor transfer characteristics with pH is shown in Figure 9.

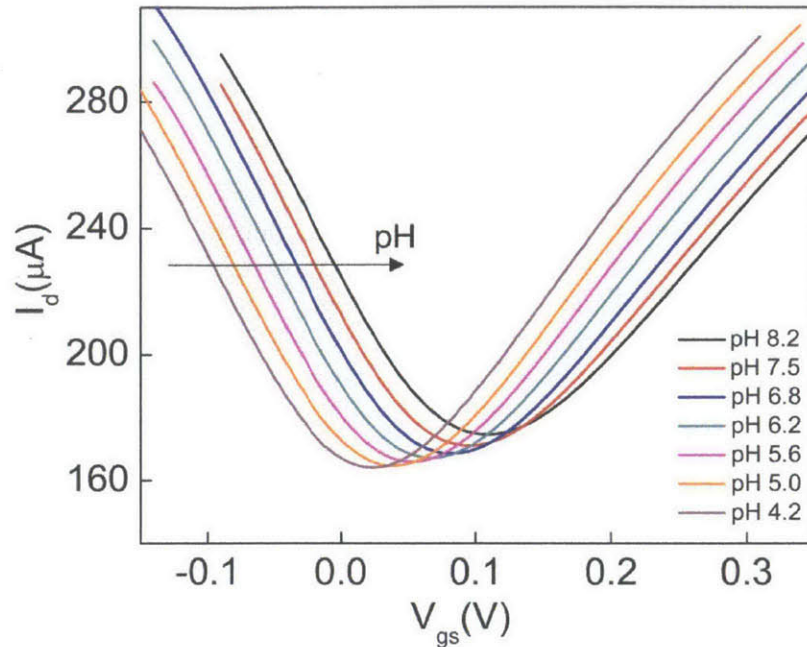


Figure 9: Transfer characteristics of a $50 \times 1000 \mu\text{m}^2$ graphene-on-PEN SGFET at a constant drain-source voltage of $V_{DS}=50 \text{ mV}$, for different pH values.

As shown on Figure 10, the Dirac point shifts linearly with the pH, with a sensitivity of 22 mV/pH.

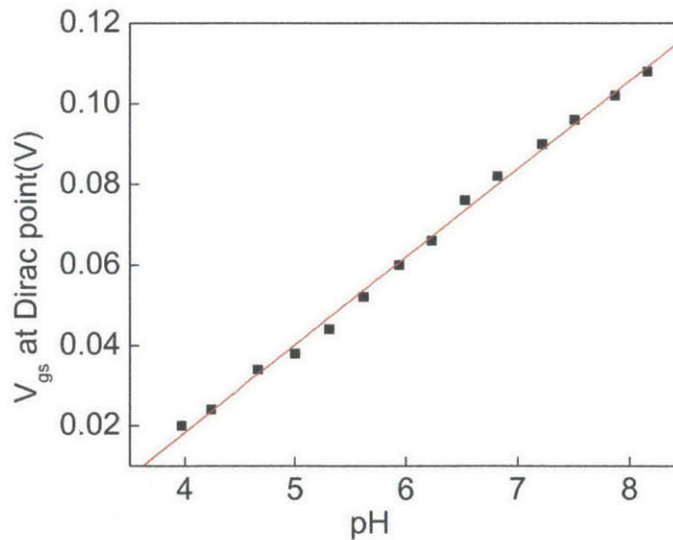


Figure 10: Voltage at Dirac point shift with the pH for the $50 \times 1000 \mu\text{m}^2$ graphene-on-PEN

The similar sensitivity values obtained in the graphene-on-PEN and graphene-on-SiO₂ devices strongly suggest that the nature of the substrate underneath the graphene does not significantly influence the electrical response of the devices to pH. Therefore, the pH response of graphene transistors is not likely to arise from substrate charging effects. The lack of substrate influence on the pH mechanism in graphene sensors is in fact expected since graphene is believed to be impermeable to most gases and liquids^{21, 22}, which would prevent the direct interaction of ions in the electrolyte with the substrate. The lack of substrate influence on the pH mechanism is also in

agreement with the suggested pH mechanism above in this section that would be a surface transfer doping by hydroxide or hydronium ions of the graphene surface. In addition, this mechanism is probably similar to what has been reported for the pH response of single-walled carbon nanotubes (SWNT) ¹².

On the contrary, in the case of Si/SiO₂ SGFETs, there is a very strong influence of the nature of the oxide substrate since the pH sensing mechanism is due to substrate charging effects. For Si/SiO₂ SGFETs, the surface charge density of SiO₂ varies with pH and can yield both a negatively charged (due to SiO⁻) and a positively charged (due to SiOH₂⁺) surface¹⁸. However, if the SiO₂ is replaced by a layer of Al₂O₃, the Si/ Al₂O₃ SGFET has a higher pH sensitivity than the Si/SiO₂ SGFET and even by putting a Ta₂O₅ layer a pH sensitivity of 58 mV/pH can be reached¹⁸. The different substrate charging effect is the reason why the pH sensitivity for Si/SiO₂ sensors is different than the one for Si/Al₂O₃ sensors. The lack of substrate influence on the pH mechanism in graphene sensors is in fact expected since graphene is believed to be impermeable to most gases and liquids^{21, 22}, which would prevent the direct interaction of ions in the electrolyte with the substrate. This mechanism is similar to what has been reported for the pH response of single-walled carbon nanotubes (SWNT) ¹².

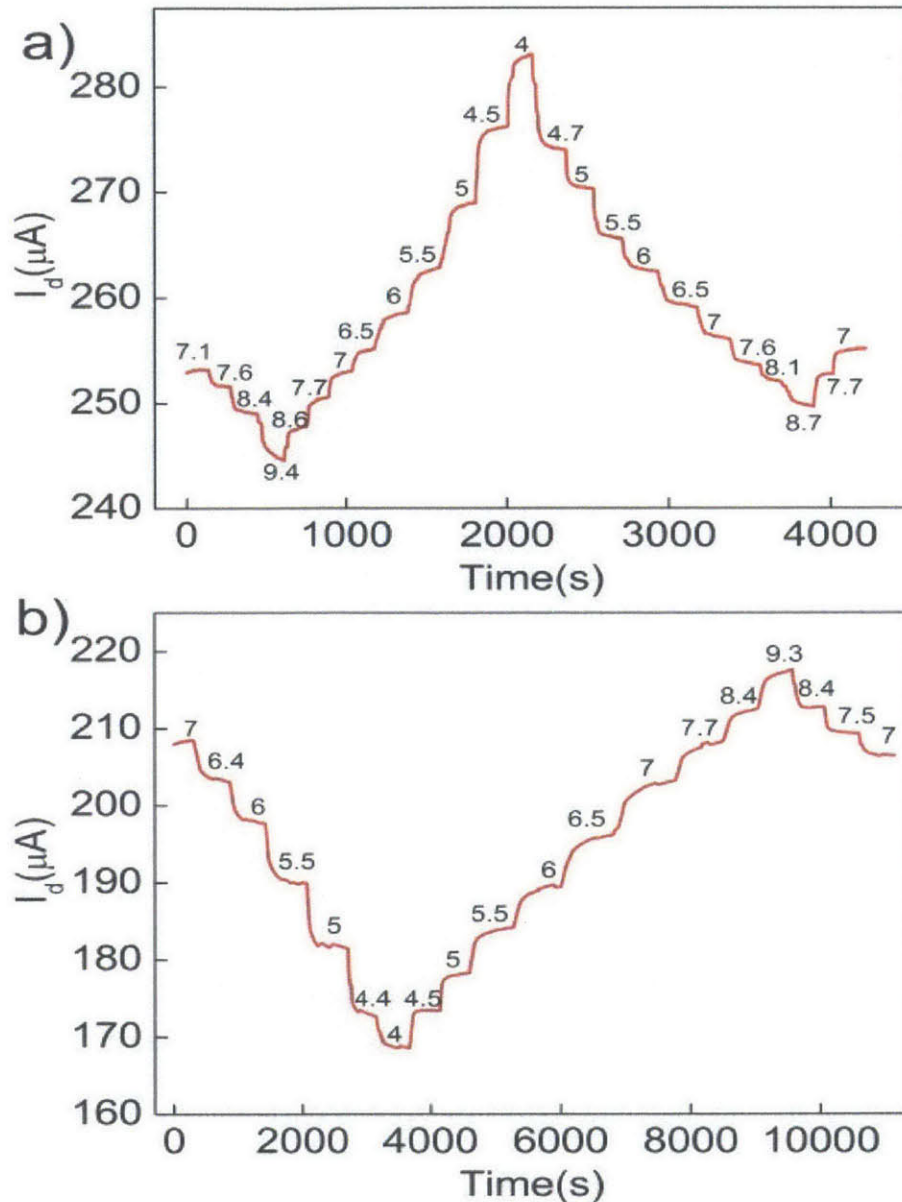


Figure 11: pH monitoring with a $50 \times 1000 \mu\text{m}^2$ graphene SGFET by recording the drain-source current I_D versus time while changing the pH: a) For a gate-source voltage $V_{GS} = 0.22 \text{ V}$ and b) for $V_{GS} = -0.01 \text{ V}$

The use of the graphene-on-PEN devices for real time monitoring of pH is demonstrated in figure 11. In these measurements, the voltage between gate and source was fixed first at $V_{GS} = 0.22 \text{ V}$ and, in a second experiment, to $V_{GS} = -0.01 \text{ V}$ to show pH monitoring in the two conduction regimes (hole and electron conduction regimes) enabled by the ambipolar transport properties of graphene. As shown in Figure 11, the change in pH as a function of time is recorded as a change in the drain-source current I_D . A decrease in pH induces an increase in the I_D value at $V_{GS} = 0.22 \text{ V}$ whereas a decrease in pH induces a decrease in the I_D value at $V_{GS} = -0.01 \text{ V}$, which is consistent with the shift of the transfer characteristics curve when changing pH. It should be noted that the pH sensing exhibits a good reversibility, although there is a small decrease in the current level after going down to very acidic pH.

A new design for these graphene sensors on plastic should be developed which will effectively demonstrate the low cost and flexibility of the sensor by removing the use of a chip carrier. This design will integrate a reference electrode printed directly on the plastic substrate so that we also remove the use of an external reference electrode. The device will then be very compact, low cost and flexible and will use microfluidics as shown in figure 18.

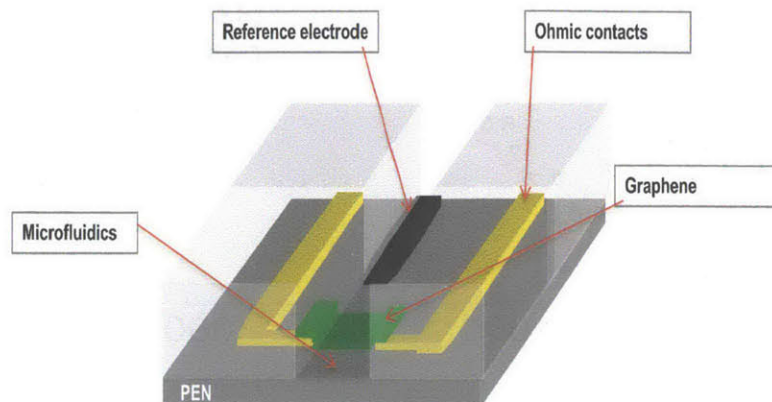


Figure 12: New design for graphene plastic sensors

- **The absence of chemical bonding in the pH sensing mechanism**

We would like to gain more insight into the pH sensing mechanism. In this section, we would like to confirm that no chemical bonding takes place between ions in the solution and the graphene surface. In this section we describe an experiment to test this hypothesis.

In a recent study, Q.H Wang et al demonstrated the influence of the substrate on graphene chemical reactivity and the electron-transfer reaction rates using Raman spectroscopy²³. Indeed, they showed that graphene on SiO_2 and Al_2O_3 is more reactive towards covalent functionalization by aryl diazonium salts than graphene on hexagonal boron nitride or on an alkyl-terminated monolayer like Octadecyltrichlorosilane (OTS) self-assembled monolayer (SAM). To explain the differences in chemical reactivity of graphene on different substrates, they use a model describing the reaction kinetics from electron-transfer theory as a function of the Fermi level of graphene. This model emphasizes the determinant role played by the presence of charged impurities in the substrate and polar surface groups that can induce electron-hole charge fluctuations in graphene. The lower chemical reactivity of graphene on OTS compared to SiO_2 is therefore explained by the fact that the charge fluctuations on SiO_2 are caused by charged impurities in the substrate and polar adsorbates on the surface, so that adding the OTS monolayer decreases the fluctuations by increasing the distance between the graphene and the charged impurities and by reducing the adsorption of polar adsorbates such as water.

Thus, in order to understand if specific adsorption of hydroxide ions or polar adsorbates such as water was not leading to any chemical bonding with the graphene surface during the graphene pH sensing mechanism, we performed pH sensing experiments with an OTS substrate. According to the publication by Q.H Wang et Al, the OTS substrate should reduce the chemical reactivity and the electron transfer reaction rate due to the chemical binding of ions on graphene

surface. If any chemical bonding is taking place with specific adsorption in the graphene pH sensing mechanism, we should therefore observe a decrease in pH sensitivity for graphene on OTS.

On freshly plasma-cleaned SiO₂ substrates with previous deposition of metal contacts on the substrate, Octadecyltrichlorosilane (OTS) (Sigma-Aldrich, 90p%) SAMs were formed in OTS solution (10 mM in toluene) overnight in a closed vial, then rinsed in fresh toluene and blown dry with nitrogen. Then, graphene was transferred on the substrate as described in chapter 2 and the PMMA was removed only by an acetone vapor and acetone flowing treatment. Graphene was then patterned with a O₂ plasma etch and the device was encapsulated with the method that leaves part of the metals exposed to the electrolyte.

The AFM image of the surface of OTS on silicon dioxide is shown in figure 13. The RMS roughness of the surface is 1.97 nm, which is higher than the RMS roughness of silicon dioxide around 0.1 nm.

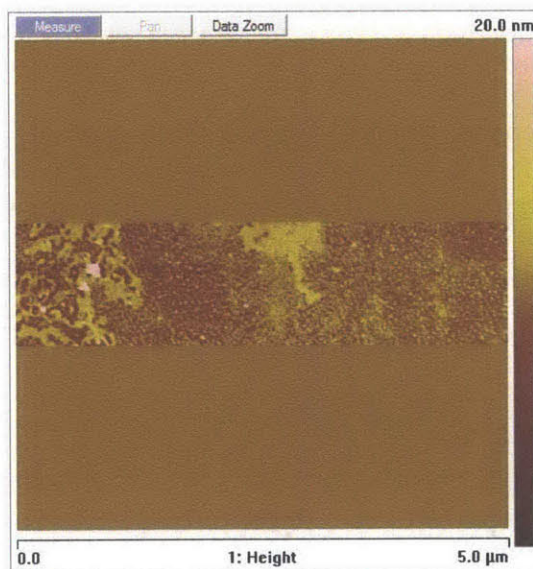


Figure 13: AFM image obtained with a Veeco Dimension 3100 system, of the OTS surface on SiO₂

The device was then immersed in a 10 mM phosphate buffer solution with an ionic strength adjusted to 100 mM with NaCl. Then, aliquots of 0.5 M HCl and NaOH were added to change the pH of the solution. The dependence of the graphene-on-OTS transistor transfer characteristics with pH is shown in Figure 14.

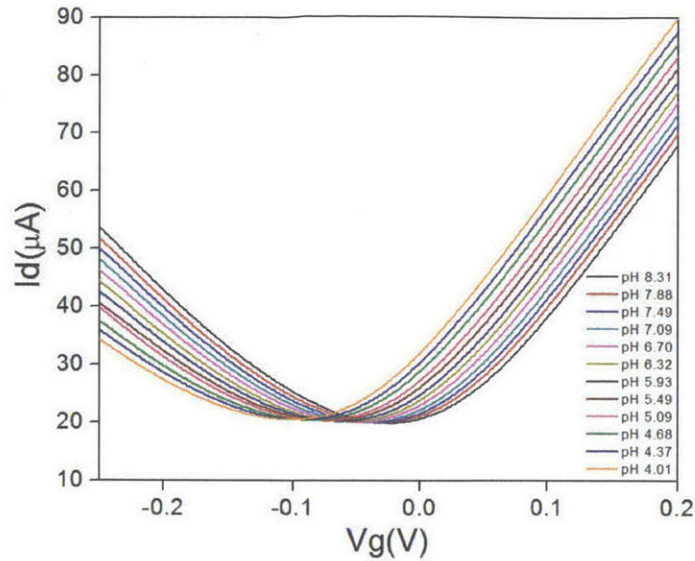


Figure 14: Transfer characteristics of a $20 \times 40 \mu\text{m}^2$ graphene-on-OTS SGFET at a constant drain-source voltage of $V_{DS}=50 \text{ mV}$, for different pH values.

We observe that the graphene is slightly n-doped. This very slight n-doping effect could be attributed to the absence of high temperature annealing in the fabrication and the increased distance with between the graphene and the charged impurities in SiO_2 due to the presence of the OTS layer.

As shown on Figure 15, the Dirac point shifts linearly with the pH, with a sensitivity of 19 mV/pH.

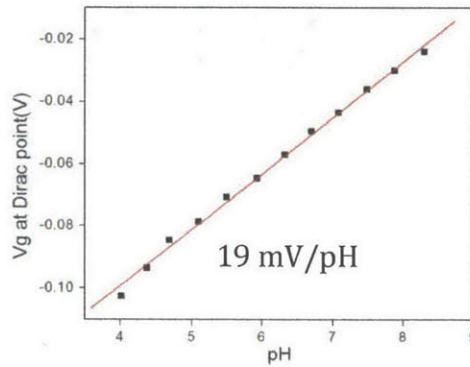


Figure 15: Voltage at Dirac point shift with the pH for the $20 \times 40 \mu\text{m}^2$ graphene-on-OTS SGFET

This pH sensitivity is again similar to the one obtained for graphene on SiO_2 , even though it is slightly lower. This strongly suggests that no chemical bonding is taking place between graphene and hydroxide ions or water in the pH sensing mechanism. Thus, chemical bonding from ions to the graphene surface seems to be ruled out for being a possible sensing mechanism, contrary to the case of Si/SiO_2 SGFETs.

This confirms that it is indeed very likely that a surface transfer doping effect induced by a pH change is taking place, as described earlier. That is why, the presence of the OTS layer does not influence the pH sensing mechanism. This explanation of the pH sensing mechanism account also for the fact that the pH sensing mechanism in graphene is not significantly influenced by the

nature of the substrate underneath graphene or the amount of residues on top of the graphene surface.

In conclusion, in this section, we have demonstrated that graphene can be used as a pH sensor with high sensitivity on silicon dioxide as well as on plastic substrates for flexible and low cost sensors. The pH sensing mechanism is not significantly influenced by the nature of the substrate underneath graphene or the amount of residues on top of graphene. The pH sensing mechanism is very likely due to the adsorption of hydroxide ions at the graphene surface in the electrical double layer that induces an additional p-doping of the graphene sheet without any chemical bonding taking place.

3- Glucose sensing

This work is done in collaboration with Dr. Zhong Jin from Professor Michael Strano's group at MIT. Glucose sensing is of paramount importance in the biosensors industry. Indeed, blood glucose monitoring sensors represent about 60 % of the biosensor market. It is an accurate and invaluable tool for diabetics who need to monitor their glucose level. Therefore, being able to fabricate graphene glucose sensors is a very interesting opportunity for graphene technology.

In our sensing experiment, we use graphene-on-SiO₂ SGFETs that were insulated using SU 8 in order to cover completely the metals. Also instead of a Ag/AgCl reference electrode, and Ag/AgCl wire was used. Glucose sensing cannot be performed directly on bare graphene, as it is the case for pH sensing. Indeed, the experiment of using bare graphene was performed and no glucose detection was observed. Therefore, the first step is to develop the functionalization for glucose sensing. The graphene devices were functionalized with glucose oxidase. Glucose oxidase is an oxido-reductase enzyme that catalyzes the oxidation of glucose in the following reaction:



The glucose oxidase has an active site to which glucose binds and then glucose oxidase starts the catalysis of glucose. The possible mechanism by which graphene functionalized with glucose oxidase could be sensitive to glucose is by the direct transfer of electrons generated from the oxidative reaction of glucose to graphene, as shown in figure 16. Another mechanism that could take place in the same time is the decrease of pH due to the decomposition of gluconate acid into gluconate : $\text{Gluconate acid} \rightarrow \text{gluconate} + \text{H}^+$, since graphene is sensitive to pH, as shown earlier. However, the dissociation constant of the reaction is low and in Si/SiO₂ SGFETs, the sensitivity to glucose due to this decrease in pH is only a few mV/decade²⁴.

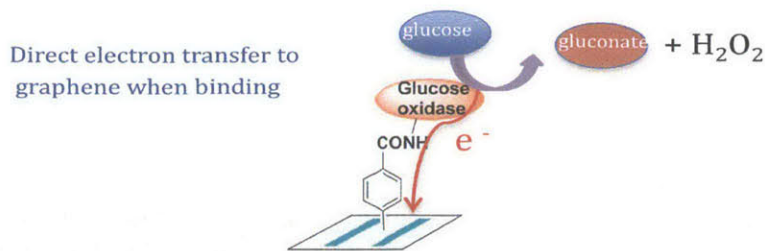


Figure 16: Mechanism of direct electron transfer to graphene when glucose binds to glucose oxidase

Graphene-on-SiO₂ devices were prepared with a SU 8 insulation as described in chapter 2. The devices were then functionalized. The functionalization is a 2 steps process as shown in figure 17: first we covalently attach an intermediary molecule to graphene and secondly, we attach the glucose oxidase to the intermediary molecule. As shown in figure 17, the intermediary molecule attached to graphene is 4-carboxybenzenediazonium tetrafluoroborate. Then the carboxyl group of this molecule binded with an amino group on glucose oxidase, and formed a amide derivative of glucose oxidase fixed on graphene. NHS molecule is N-Hydroxysuccinimide and EDC is ethyl(dimethylaminopropyl) carbodiimide. These two molecules served as coupling agents for the formation of amide.

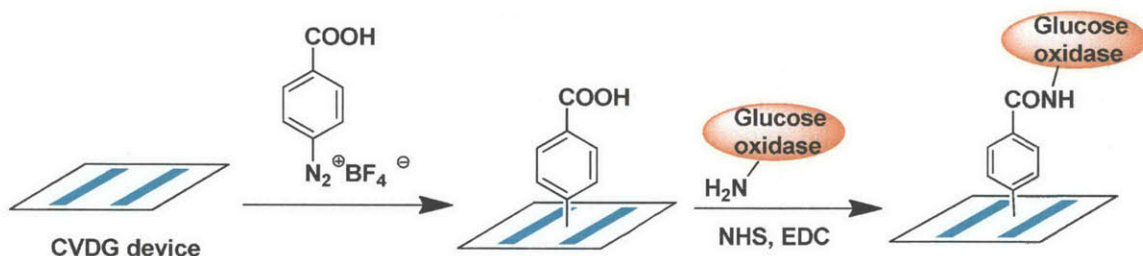
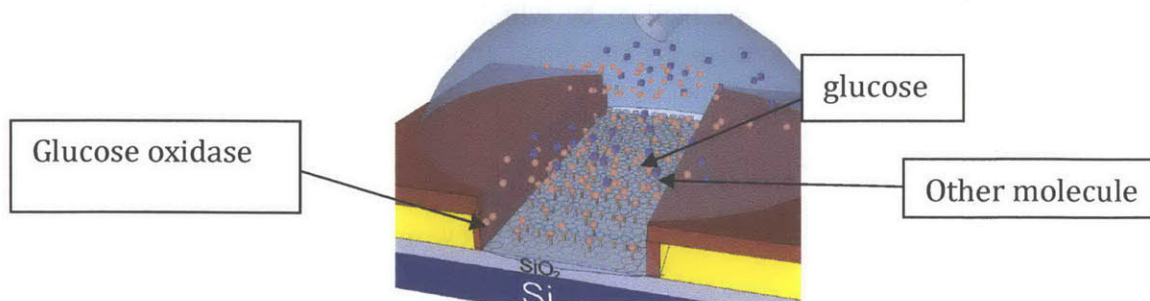


Figure17: a) The different steps of the chemical functionalization of graphene that leads to the attachment of glucose oxidase to graphene, b) Optical image of the device after functionalization

After functionalization, the device is ready to be use as a glucose sensor, as shown in figure 18.



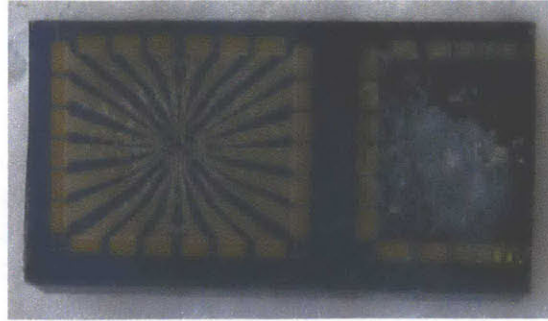


Figure 18: a) Schematics of a graphene glucose sensor, b) Optical image of a device after functionalization

We then proceed to some preliminary glucose sensing experiments. For this purpose, using the same measurement set up as for characterizing the SGFET arrays, the sensor was immersed in a 10 mM phosphate buffer. Then glucose was added to a concentration of 10 mM. The voltage between drain-source is 100 mV. The results of the experiment are shown in figure 19.

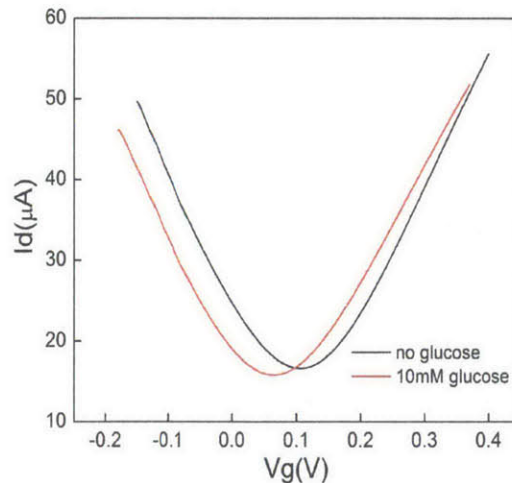


Figure 19: Transfer characteristics of a $30 \times 40 \mu\text{m}^2$ glucose sensor device at a constant drain-source voltage of $V_{ds}=100$ mV in a 10 mM phosphate buffer with and without glucose in 10mM concentration

We can observe a shift of the entire transfer characteristics of the graphene device, especially at the Dirac point, to lower positive voltage with the addition of glucose due to the binding of glucose with glucose oxidase. This clearly emphasizes that the functionalization of graphene with glucose oxidase enables the glucose sensing. This glucose sensing is due to the enzymatic activity of glucose oxidase since bare graphene cannot perform the sensing. Such a negative shift of the transfer characteristics is in agreement with the effect of a direct transfer of electrons generated from the oxidative glucose-glucose oxidase reaction to the graphene that would indeed induce a negative shift of the transfer characteristics. The pH decrease due to the decomposition of gluconic acid can also participate to the negative shift observed. However, the negative shift is significant and such a shift is very not likely due only to this small pH decrease as the decomposition constant at pH 7 is low. Thus, the experiment strongly suggests that our functionalization leads to the direct electron transfer from glucose to graphene. Another glucose sensing experiment using graphene SGFET on SiO_2 was reported by Huang et al¹⁸.

They use a different functionalization of glucose oxidase as well as a different fabrication technology with silver paint for contacting a very large area graphene (8 mm^2 in size compared to $800 \text{ }\mu\text{m}^2$ in our devices). Furthermore, they grow graphene on nickel (we grow on copper foil on the contrary) and the film is quite heterogeneous with only 50 % of the film that is monolayer. In their experiments, Huang et al observed a very small shift of the transfer characteristics²⁵. At the Dirac point, their device exhibits nearly no shift and the binding of glucose seems to only change the characteristics of the saturation regime of graphene without inducing a noticeable shift of the entire transfer characteristics. They suggest that the shift could be due to the products of the glucose-glucose-oxidase reaction but not a direct transfer of electrons to the graphene. Possibly, the pH variation due to the decomposition of gluconic acid may be at stake in their glucose sensing. The differences in functionalization, fabrication technology and quality of graphene in our experiments compared to Huang et al explain the difference in glucose sensitivity in the two experiments and underlines that our high glucose sensitivity is probably due to a direct electron transfer to graphene during the glucose-glucose oxidase reaction.

Recently, Y.H Kwak et al reported glucose sensing on plastic substrate using CVD graphene²⁶. In their experiment, they have a clear negative shift as in our experiment. They also see a very similar shift when they introduce hydrogen peroxide in the solution and suggest that the negative shift of graphene transfer characteristics may be due to the increase in hydrogen peroxide as a product of the glucose-glucose oxidase. In their case, this is true because they use a platinum electrode immersed in the solution to apply the top gate voltage and it was already reported that platinum catalyzes the decomposition of H_2O_2 , which produces two hydrogen ions[ref]. Thus, as graphene is pH sensitive, the shift of the transfer characteristics they observe is very likely due to the decrease in pH caused by the decomposition of H_2O_2 . In our case, we use a Ag/AgCl wire and so the decrease in pH due to decomposition of H_2O_2 on platinum does not take place. Therefore, our sensing mechanism is different from the mechanism used by Y.H Kwak et al. A very interesting future direction of our work will be to use a platinum electrode to see if we can increase significantly the glucose sensitivity of our devices.

In order to quantify the glucose sensitivity of our devices, we performed a glucose sensing experiment by progressively adding some glucose to the solution from a concentration of 0.1 mM to 10mM and recording the transfer characteristics every time, as shown in figure 20.

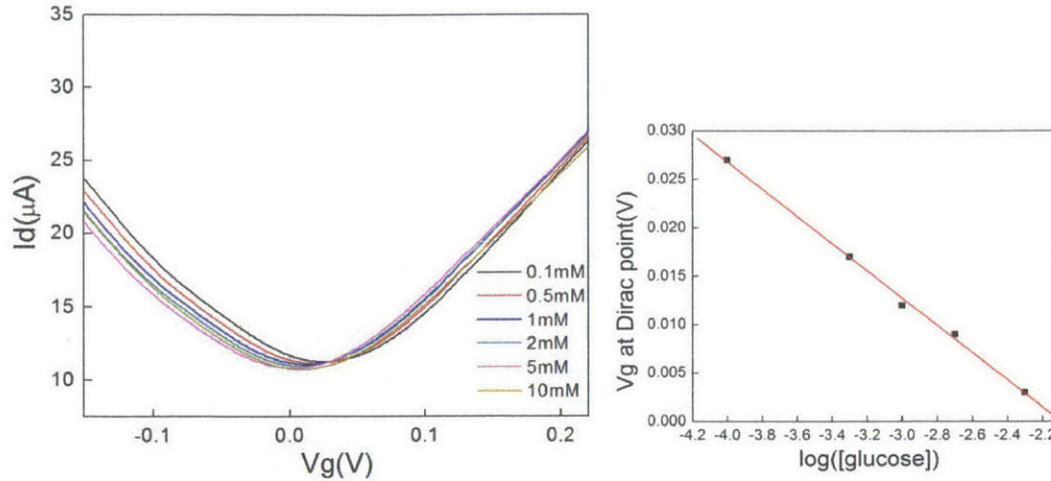


Figure 20: a) The different transfer characteristics of a $30 \times 40 \mu\text{m}^2$ glucose graphene sensor with change in glucose concentration between 0.1mM and 10 mM; b) Top gate voltage at the Dirac point as a function of the logarithm of the glucose concentration, the red line being a linear fit.

As shown in figure 20, the Dirac point shifts towards lower positive voltage when the glucose concentration increases, as a direct electron transfer from glucose to graphene suggests. A linear relationship between the logarithm of the glucose concentration and the shift in the Dirac point is observed. From this relationship, we can extract the sensitivity of the device for glucose at the Dirac point, which is 15 mV/pG, where pG is a unit in the logarithm of the glucose concentration. The same sensitivity was reliably found in many different devices as shown in figure 21 below.

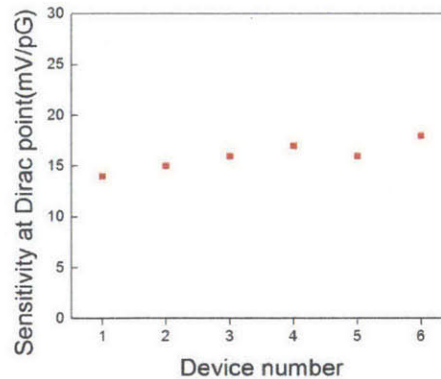


Figure 21: Glucose sensitivity at the Dirac point of several graphene sensors functionalized with glucose oxidase

In addition, more experiments are needed to determine the ultimate glucose concentration detection limit possible with our graphene sensors. In our preliminary experiments, we got a detection limit of 0.1 mM, which is similar to the one in commonly used electrochemical sensors²⁷, and higher than the detection limit for SWNTs network²⁵. It is however still lower than the one in some state-of-the-art electrochemical sensors integrated with functional nanomaterials²⁸.

In summary, we have demonstrated a graphene glucose sensor in CVD graphene using glucose oxidase with a sensitivity of 15 mV/pG at the Dirac point. The shift in the transfer characteristics

with glucose concentration strongly suggests that a direct electron transfer from glucose to graphene via the oxidative reaction with glucose oxidase is taking place. The lowest detection limit was 0.1 mM in these experiments but further experiments with more optimized devices are expected to lower the detection limit even further.

4- E. Coli detection

Food monitoring is becoming a growing concern in developed as well as developing countries around the world in the aftermath of various recent threats like the spreading of deadly Escherichia Coli (E.Coli) bacteria around Europe in 2011²⁹. Biosensors are used for the detection of food pathogens as well as the water supply and it represents a growing sector for biosensors.

In collaboration with Dr Dawn Nida from U.S. Army Natick RDEC, we explore the use of graphene for E.Coli O-157:H7 detection. Escherichia coli O157:H7 is a type of fecal coliform bacteria which is a major hazard in the water supply, causing outbreaks of disease. This strain has some unique characteristics that differentiates it from other strains of E.Coli. First, it is one of the few strains that can cause renal damage, causing death. Secondly, it is persistent in the environment, and, third, it is infective in ever very small doses.

Conventional methods of E. coli O157:H7 detection like the Autoanalysis Colilert (AC) test³⁰ usually take 1-2 days and require hands-on preparation. There is a need to develop a rapid, inexpensive approach to detecting this organism. Biosensor technology offers many advantages for organism detection and quantification including specificity, sensitivity, portability, real time analysis, and simplicity of operation. Different methods of detection with their detection time and limit are summarized in the table below [ref Deisingh].

Method	Approx. detection time	Detection limit
Plating/culturing	1 day to 1 week	Low CFUs
Biochemical tests	1 day to several days	Low CFUs
ELISA	12 h to 2 days	10–100 CFU ml ⁻¹
Fluorescent bacteriophage assay	10 h	10–100 CFU ml ⁻¹
Chemiluminescence enzyme immunoassay	6–8 h	10 ³ –10 ⁴ cells ml ⁻¹
Capillary immunoassay	7 h	0.5–1 CFU ml ⁻¹
Time-resolved fluorescence immunoassay	6 h	10–100 CFU ml ⁻¹
PCR	2–24 h depending on enrichment	10 ² –10 ⁵ CFU ml ⁻¹
Multiplex PCR	24 h	1–2 CFU ml ⁻¹
RT- PCR	6–12 h	10 ⁷ CFU ml ⁻¹
Laser-induced fluorescence	Few hours	Single organism
Fibre optic biosensor	ca 30 min	5.2 × 10 ² CFU g ⁻¹
SPR biosensor	1 h	5 × 10 ⁷ CFU ml ⁻¹
Microarrays	<1 h	55 CFU ml ⁻¹
Molecular beacon	1–6 h depending on enrichment	1–10 ³ CFU ml ⁻¹
Integrated systems (lab-on-a-chip)	16–45 min	10 ² –10 ⁴ organisms ml ⁻¹

Table 22: Summary of methods used to detect E.Coli O-157:H7

A graphene-based detector of E.Coli could be very interesting if its detection time or limit outperform the other sensors. As in the case of glucose sensing, bare graphene cannot be directly used for E.Coli detection and it needs to be functionalized. The functionalization will enable the attachment of the antibody receptor of E.Coli to graphene. Thus, during the detection process, the E.Coli will bind to the antibody. There are two possible mechanisms by which graphene can detect and be sensitive to E.Coli: 1. the E.Coli is a negatively charged bacteria and so by binding to the antibody it will get close enough to the graphene to dope it, and 2.- there is an electron transfer from E.Coli to graphene when the E.Coli binds to the antibody.

For the functionalization of graphene, two approaches were followed: direct surface functionalization of graphene and functionalization of Al₂O₃-coated graphene.

- **Al₂O₃-coated graphene functionalization**

Aluminum oxide was deposited on graphene by oxidizing a 2.5 nm aluminum layer deposited by electron-beam evaporation. The first advantage of functionalizing Al₂O₃- coated graphene is that the graphene remains protected during the entire functionalization process. The second advantage is that the surface functionalization is much more uniform. However this Al₂O₃ layer prevents the direct contact of the analyte with the graphene. In order to functionalize the surface of the sensor, the Al₂O₃ top layer was reacted with a silane containing the moiety of interest (e.g. 3-glycidoxypropyl)trimethoxysilane. Then, the active epoxy groups on the silane couple, depending on the pH, attach to the antibodies: hydroxyl groups at pH 11-12, amine nucleophiles at pH 9, sulfhydryl (most highly reactive nucleophiles with epoxides) at pH 7.5-8.5. As shown on figure 23, the fluorescence confirms that the antibodies have attached to the Al₂O₃ surface via the epoxy groups.



Figure 23: a),b) Confocal fluorescence microscopy image of Al₂O₃ slides functionalized with epoxysilane and a fluorescently labeled anti-0157 antibody (to the 1057 receptor of Escheria Coli), c),d) Al₂O₃ slides without epoxysilane

Functionalization of fabricated devices was also performed as shown on figure 24. A fluorescent dye Alexa 633 was conjugated to Anti-E.Coli antibody in order to be able to map the efficiency of the functionalization. Thus, the functionalization covered well the entire surface of the Al₂O₃-coated graphene.

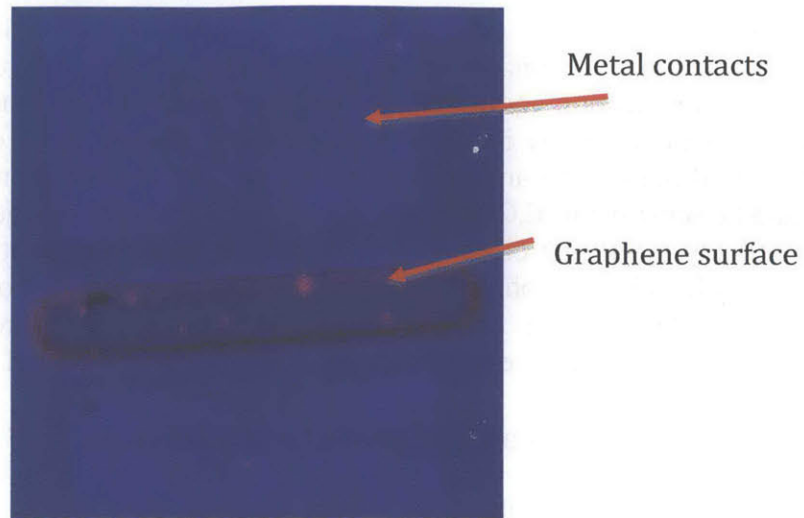


Figure 24: Confocal fluorescence microscopy image of Al_2O_3 coated Graphene-on- SiO_2 transistor functionalized with epoxysilane and then Alexa 633 conjugated to Anti-e.coli antibody. Silicon reflection is false-colored blue, alexa 633-antibody is false-colored red.

The mobility of the graphene layers was measured before and after surface functionalization. The lack of degradation shows that functionalization is gentle enough to preserve the transport properties of graphene.

Some live stained E.Coli (Syto 9) were then incubated in order to assess capture efficiency. A Syto 9 dye was conjugated to the live E.Coli in order to map the capture efficiency of E.Coli. As shown in figure 25, the functionalization managed to bind some E.Coli, shown as green pixels on the fluorescent image. The more green colored edges of the graphene are due to the shape of the SU8 walls that are slightly concave and retain more efficiently the E.Coli.

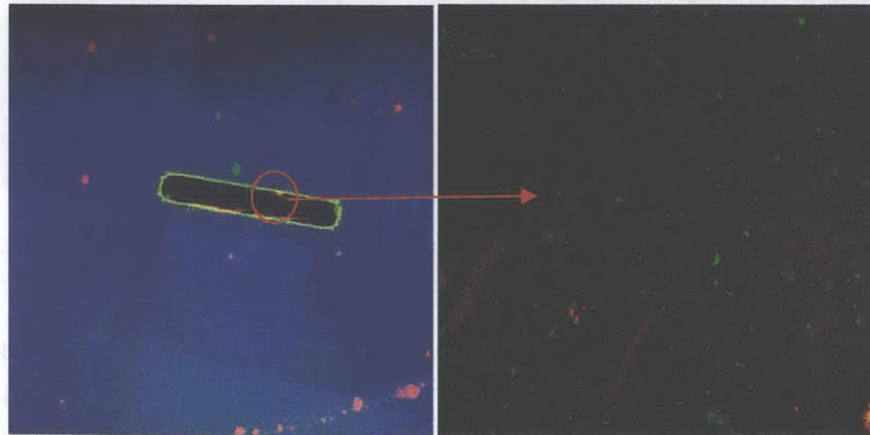


Figure 25: Confocal fluorescence microscopy image of of Al_2O_3 coated Graphene-on- SiO_2 transistor functionalized with epoxysilane and then Alexa 633 conjugated to Anti-e.coli antibody. Live stained e.coli (Syto9) were then incubated with functionalized FETs to establish capture efficiency. Silicon reflection is false-colored blue, alexa 633-antibody is false-colored red and Syto9 stained e.coli cells are false-colored green.

- **Bare graphene functionalization**

For the direct graphene functionalization, there are two possible approaches: covalent or non-covalent functionalization. The covalent approach has the advantage of maximizing the stability, accessibility, and selectivity by controlling the location of the biomolecule and reduces the leaching and dissociation of the biomolecule. To obtain a covalent functionalization, carboxyl acid functional groups are exposed to the graphene surface, which is oxidized using nitric acid reflux, ozonolysis and air oxidation. For the coupling to the antibody, the carboxylic acid couples to the lysine of the antibody. An alternative approach for covalent functionalization is to convert the carboxylic acid to an active ester and react the active ester with the amine of the antibody.

On the other hand, the advantages of the non-covalent functionalization are that it preserves the carbon sp^2 character, it minimizes the number of steps involved in the functionalization and it preserves well the bioactivity of conjugated antibodies/molecules. To perform a non-covalent functionalization, a polymeric (PEG, PEI) or surfactant modification of the surface is done to modify the hydrophobic interactions with proteins and provide some functional groups for antibody tethering (PEI= amine groups).

To characterize the coverage of the surface functionalization, fluorescent confocal microscopy was used, while atomic force microscopy was used to assess antibody positioning as the height will fluctuate between the binding epitope outwards (15nm) versus laying flat (5nm).

Functionalization of fabricated devices was performed as shown on figure 26. A fluorescent dye Alexa 633 was conjugated to Anti-E.Coli antibody in order to be able to map the efficiency of the functionalization.

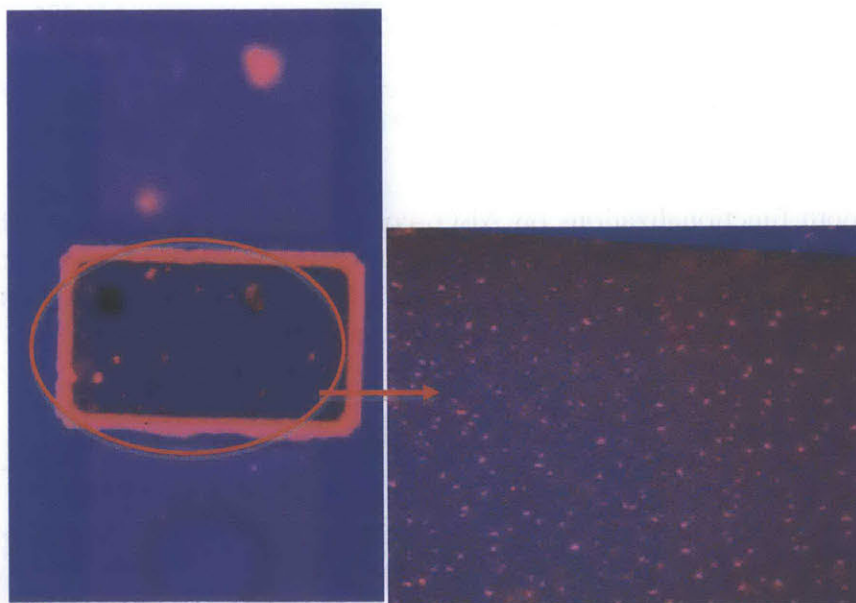


Figure 26: Confocal fluorescence microscopy image of bare Graphene-on-SiO₂ transistor functionalized with epoxysilane and then Alexa 633 conjugated to Anti-e.coli antibody. Silicon reflection is false-colored blue, alexa 633-antibody is false-colored red.

After having completely functionalized the devices, we characterized their the performance for pathogen sensing by introducing different concentrations of E.Coli bacteria and studying the change in graphene characteristics.

Some live stained E.Coli (Syto 9) were then incubated in order to assess capture efficiency. A Syto 9 dye was conjugated to the live E.Coli in order to map the capture efficiency of E.Coli. As shown in figure 27, the functionalization managed to successfully bind E.Coli, shown as green pixels on the fluorescent image. The functionalization on bare graphene seems more efficient than the Al_2O_3 -coated graphene one. However, more samples will be needed to confirm this.

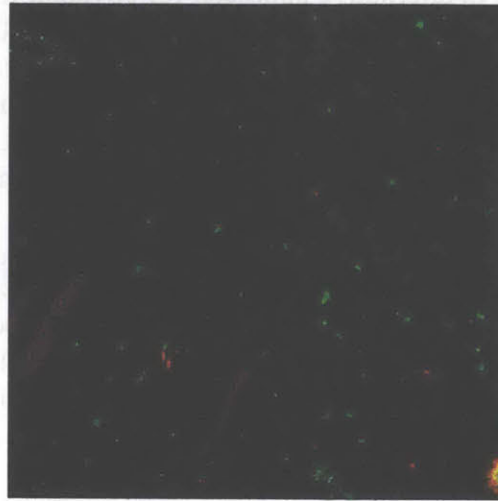


Figure 27: Confocal fluorescence microscopy image of of bare Graphene-on- SiO_2 transistor functionalized with epoxysilane and then Alexa 633 conjugated to Anti-e.coli antibody. Live stained e.coli (Syto9) were then incubated with functionlized FETs to establish capture efficiency. Silicon reflection is false-colored blue, alexa 633-antibody is false-colored red and Syto9 stained e.coli cells are false-colored green.

We prove that both functionalizations on Al_2O_3 -coated graphene and bare graphene manage to capture E.Coli. The next step will consist in measuring the electrical characteristics of graphene with the addition of E.Coli to see if we can achieve the electrical detection of E.Coli. A schematic of the measurement set up we are going to use is shown on figure 28.

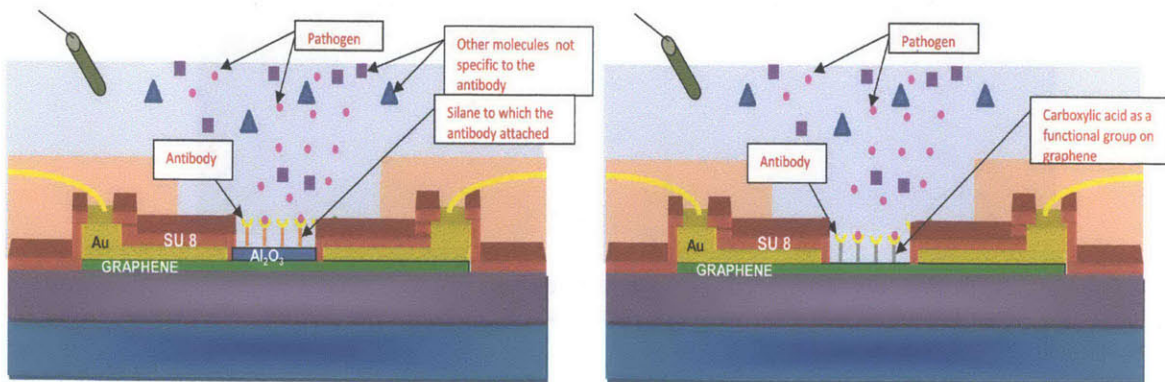


Figure 27: Schematics of the pathogen graphene sensor devices a) with Al_2O_3 coated graphene functionalized with epoxysilane; b) with native graphene functionalized with carboxylic acid

5- Noise characterization in monolayer graphene sensors

In addition to the transconductance, the low-frequency noise of a graphene transistor is a key parameter for sensors because it will have a significant influence on its sensitivity³¹. Indeed, the electronic noise gives the ultimate resolution of the electronic sensor signal output that can be detected since any signal change due to sensing that is within the range of noise will be indistinguishable from the noise perturbations. Noise can therefore limit the actual sensitivity of the device. Furthermore, Si-based electronic devices for sensing applications suffer from relatively high noise, which limits the device sensitivity³². Therefore, it is crucial to find new nanomaterials that could exhibit significant lower noise. Among these materials, graphene is an ideal two-dimensional system that shows very high carrier mobility of both holes and electrons even at room temperature and therefore should exhibit lower noise than silicon based sensors. However, it should be noticed that the high transconductance and sensitivity of graphene SGFETs also implies that any random perturbation in the environment could lead to device current fluctuations and contribute to low-frequency noise.

In this section, we describe our work characterize the noise in monolayer graphene devices. The graphene SGFETs were fabricated on silicon dioxide as described in chapter 2 using the SU 8 protective layer to cover the metal contacts. For the low-frequency noise measurements, the SGFETs were immersed in a 10 mM phosphate buffer adjusted to an ionic strength of 50 mM using NaCl with a Ag/AgCl reference electrode immersed in the liquid. Contrary to all other measurement setups described earlier, the drain-source and gate voltages were applied by a battery-powered setup. The entire set up was put in a Faraday cage in order to shield against external noise. A battery-powered low-noise current pre-amplifier (Stanford Research Systems model SR 570) was then used to amplify the drain-source current ($\times 10^5$). Signal frequencies lower than 0.1 Hz and higher than 300 kHz were than filtered using another battery-powered low-noise amplifier (EG&G Parc Model 113). The noise power spectral density was finally measured with a spectrum analyzer (Stanford Research System SR 760) in a frequency range of 1 Hz to 100 kHz.

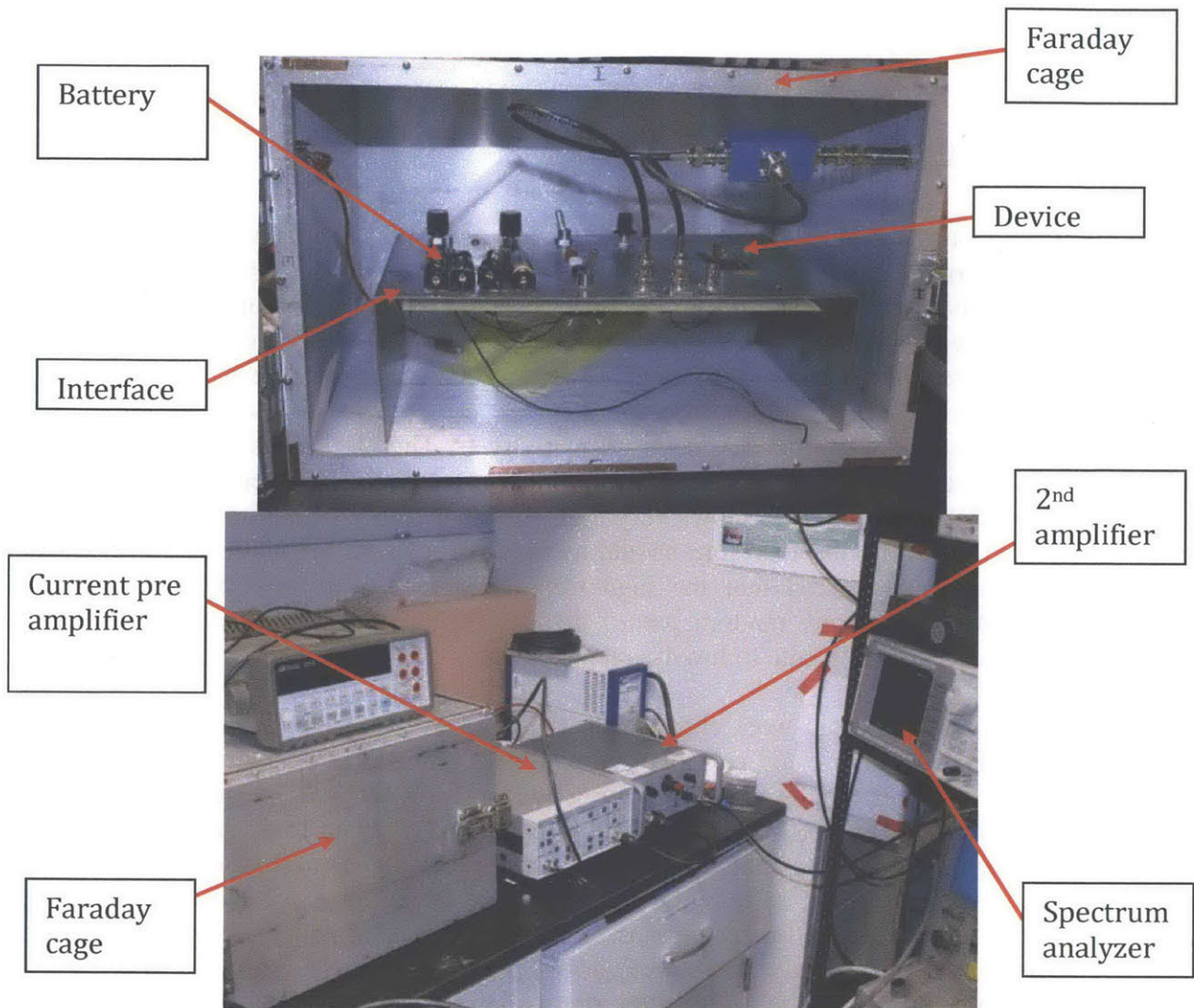


Figure 28: Noise measurement set up. The upper picture shows the inside of the Faraday cage where the graphene device is connected to an interface. The lower picture displays all the instruments used in order to make a noise measurement

In figure 29, the current noise spectral density S_{I_d} is measured for different devices in electrolyte-gated configuration (using the reference electrode). For all the devices, we have found that the current noise spectral density is $1/f$ dependent, where f is the frequency. We have also varied the gate voltage in noise measurements in order to compare the noise at different biases. The noise performance is expected to vary depending on whether the gate voltage bias puts the graphene device in the linear regime close to the saturation regime in the hole or in the electron conduction range where the transconductance and current density are high, or if the gate voltage bias puts the graphene device close to the Dirac point regime, where the transconductance and current density are low.

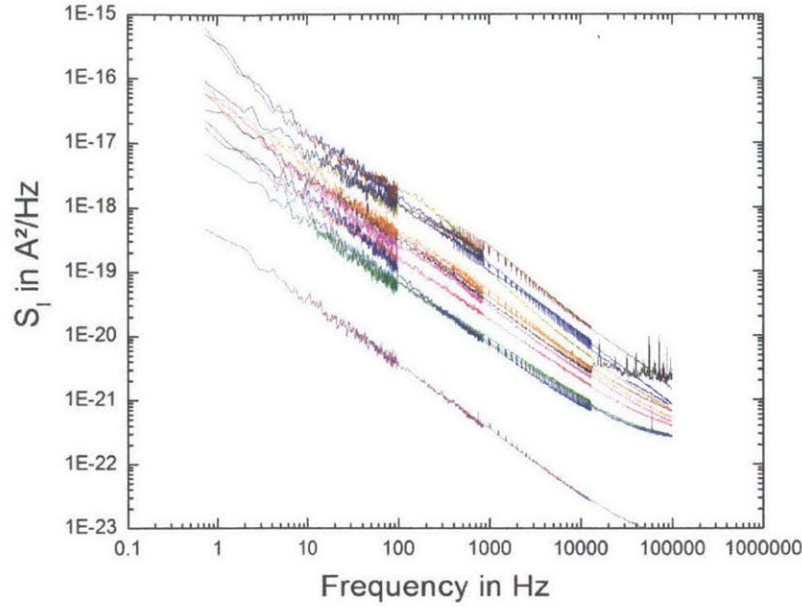


Figure 29: Spectral noise density measurements in 10mM phosphate buffer with ionic strength adjusted to 50mM with NaCl, for sweeping V_g between 0V and 0.8V with $V_{DS}=100mV$

This $1/f$ dependence is often characterized with the empirical Hooge law for electronic devices³³. According to the Hooge law, the noise is inversely proportional to the number of carriers (N) contributing to electronic transport and it can be written: $S_{I_d} = \frac{\alpha_H}{N} \frac{1}{f} I_d^2$. S_{I_d} linear dependence on I^2 stems from the fact that the $1/f$ noise in single layer graphene is due to resistance fluctuations, i.e., $\frac{S_R}{R^2} = \frac{S_I}{I^2}$ ³¹. Here, α_H is the Hooge parameter that characterizes the noise properties of electronic conductors like semiconductors and metals. However, since in device measurements, the number of carriers N is often unknown, the noise amplitude $A = \frac{\alpha_H}{N}$ is therefore commonly used to evaluate the noise performance. The noise amplitude A of 4 graphene devices is shown in figure 30. The noise amplitude was measured for different gate voltages in order to show its gate voltage dependence. The noise amplitude tends to be higher close to the Dirac point for all devices and to be minimal far away from the Dirac point, which is in agreement with the fact the noise amplitude A is inversely proportional with the number of carriers N .

In addition, transistors T2 and T15 have better and similar noise amplitude performance around 10^{-9} Hz^{-1} than the transistors T23 and T7. The main reason is that T23 and T7 were damaged during the SU 8 process even though an aluminum oxide protective layer was used. The current density and transconductance was lower for these transistors than for T2 and T15. For transistors T15 and T2, the values of noise amplitude are in good agreement with reports on low-frequency noise in graphene devices.^{6, 31, 34, 35}

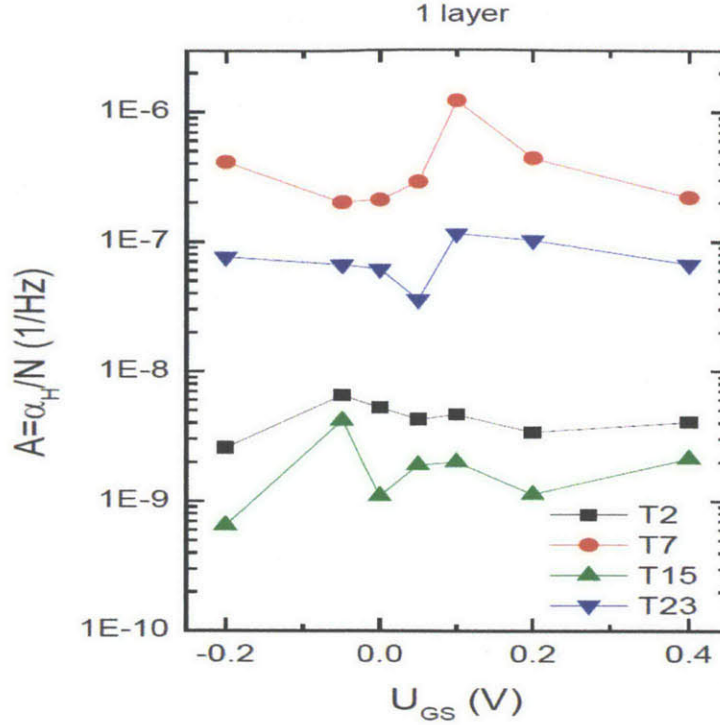


Figure 30: Gate voltage dependence of the noise amplitude $A = \frac{\alpha_H}{N}$, where N is the total number of carriers

As in the Hooge model, we indeed find that the current noise density is proportional to the drain-source current squared, which confirms that the $1/f$ noise is generated by resistance fluctuations. The global noise performance, frequency-independent is then the root-mean square (RMS) noise which is the integration of $\frac{S_{I_d}}{I_d^2}$ over all frequencies.

However, the relevant noise parameter for the device sensitivity is the gate voltage noise spectral density $S_G = \frac{S_{I_d}}{g_m^2}$, which gives the minimum resolution in the gate signal that can be detected by the device ($g_m = \frac{\partial I_d}{\partial V_{gs}}$ is the transconductance). Indeed, in the glucose or pH sensing case, the gate signal represents the surface charge modulation induced by a local glucose or pH variation. It is therefore the variation of the drain-source current caused by a gate signal modulation that must be taken into account in calculating the relevant noise. Thus, the gate voltage spectral density noise was measured at different gate voltages in order to extract the noise at the gate. In figure 31, the RMS of the gate voltage noise power density is calculated at different gate voltages considering the typical bandwidth used in biosensors applications (1 Hz to 5 kHz).

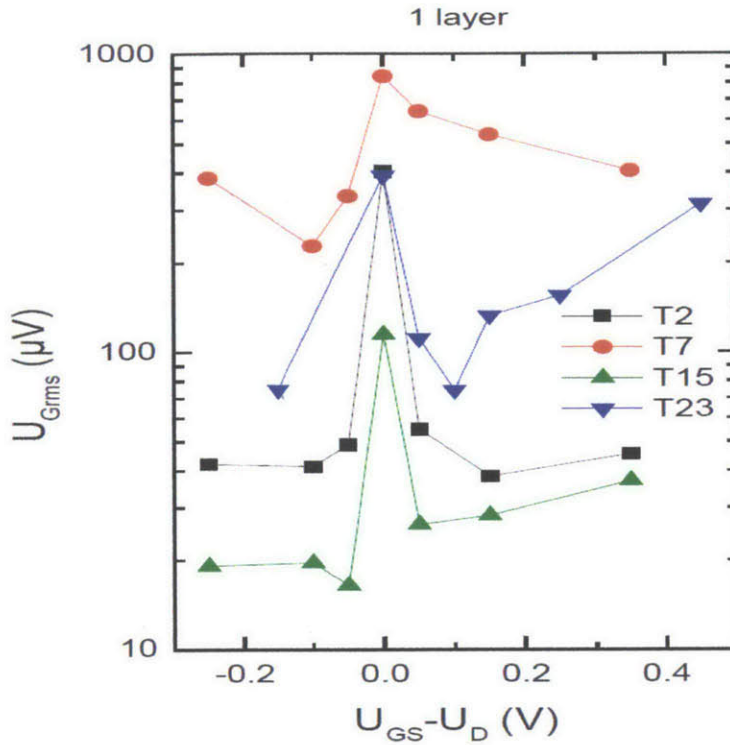


Figure 31: Gate voltage noise spectral density $S_G = \frac{S_{I_d}}{g_m^2}$ at different gate voltages for 4 monolayer graphene devices with U_{gs} the top gate voltage and U_D the gate voltage at the Dirac point

The maximum noise is for all devices at the Dirac point, which results from the minimum of the transconductance at this gate potential. The device with the minimal RMS gate noise is T15 with a noise of 20 μV . This is a very good noise performance compared to conventional Si/SiO₂ SGFETs that typically have one order of magnitude higher RMS gate noise of 200 μV ³⁶. Furthermore, our devices have similar RMS noise value than the state of the art *ultra-low noise* Si/SiO₂ devices^{6, 32}.

The graphene SGFETs, compared to graphene transistors with oxide dielectrics, avoid some sources of noise such as the defects at the graphene-oxide interface since they are directly exposed to an electrolyte, even though the interface with the electrolyte represents itself an additional source of noise. We believe that is the reason why the noise performance of our devices differ from graphene devices using solid gates³¹.

In conclusion, graphene SGFETs exhibit very high performance in terms of noise with an order of magnitude lower noise than in conventional Si/SiO₂ SGFETs. There is however still a large room for improvement. For example, the transconductance could be significantly increased by decreasing the access region length (area of graphene covered by SU 8 that cannot be biased, see chapter 2) and by increasing the carrier mobility especially by transferring graphene on a substrate like hexagonal boron nitride³⁷. Therefore, the noise performance of graphene SGFETs could be increased notably with the transconductance increase and could outperform the best available technologies.

References

- (1) Ristein, J.; Zhang, W.; Speck, F.; Ostler, M.; Ley, L.; Seyller, T. Characteristics of solution gated field effect transistors on the basis of epitaxial graphene on silicon carbide. *J. Phys. D* **2010**, *43*, 345303.
- (2) Wehling, T. O.; Lichtenstein, A. I.; Katsnelson, M. I. First-principles studies of water adsorption on graphene: The role of the substrate. *Appl. Phys. Lett.* **2008**, *93*, 202110-202110-3.
- (3) Hess, L. H.; Hauf, M. V.; Seifert, M.; Speck, F.; Seyller, T.; Stutzmann, M.; Sharp, I. D.; Garrido, J. A. High-transconductance graphene solution-gated field effect transistors. *Appl. Phys. Lett.* **2011**, *99*, 033503.
- (4) Ingebrandt, S.; Yeung, C.; Staab, W.; Zetterer, T.; Offenhausser, A. Backside contacted field effect transistor array for extracellular signal recording. *Biosensors and Bioelectronics* **2003**, *18*, 429-435.
- (5) Offenhausser, A.; Sprossler, C.; Matsuzawa, M.; Knoll, W. Field-effect transistor array for monitoring electrical activity from mammalian neurons in culture. *Biosensors and Bioelectronics* **1997**, *12*, 819-826.
- (6) Dankerl, M.; Hauf, M. V.; Lippert, A.; Hess, L. H.; Birner, S.; Sharp, I. D.; Mahmood, A.; Mallet, P.; Veuillen, J. Y.; Stutzmann, M. Graphene Solution-Gated Field-Effect Transistor Array for Sensing Applications. *Adv Mater* **2010**, *20*, 3117-3124.
- (7) Xia, J.; Chen, F.; Wiktor, P.; Ferry, D.; Tao, N. Effect of top dielectric medium on gate capacitance of graphene field effect transistors: implications in mobility measurements and sensor applications. *Nano letters* **2010**, *10*, 5060-5064.
- (8) Xia, J.; Chen, F.; Li, J.; Tao, N. Measurement of the quantum capacitance of graphene. *Nature nanotechnology* **2009**, *4*, 505-509.
- (9) Dan, Y.; Lu, Y.; Kybert, N. J.; Luo, Z.; Johnson, A. T. Intrinsic response of graphene vapor sensors. *Nano Lett.* **2009**, *9*, 1472-1475.
- (10) Cheng, Z.; Zhou, Q.; Wang, C.; Li, Q.; Wang, C.; Fang, Y. Toward intrinsic graphene surfaces: a systematic study on thermal annealing and wet-chemical treatment of SiO₂-supported graphene devices. *Nano Lett.* **2011**, *11*, 767-771.
- (11) Heller, I.; Chatoor, S.; Mannik, J.; Zevenbergen, M. A.; Dekker, C.; Lemay, S. G. Influence of Electrolyte Composition on Liquid-Gated Carbon Nanotube and Graphene Transistors. *J. Am. Chem. Soc.* **2010**.

- (12) Back, J. H.; Shim, M. pH-dependent electron-transport properties of carbon nanotubes. *The Journal of Physical Chemistry B* **2006**, *110*, 23736-23741.
- (13) Ang, P. K.; Chen, W.; Wee, A. T.; Loh, K. P. Solution-gated epitaxial graphene as pH sensor. *J. Am. Chem. Soc.* **2008**, *130*, 14392-14393.
- (14) Cole, D. J.; Ang, P. K.; Loh, K. P. Ion Adsorption at the Graphene/Electrolyte Interface. *The Journal of Physical Chemistry Letters* **2011**, *2*, 1799-1803.
- (15) Ohno, Y.; Maehashi, K.; Yamashiro, Y.; Matsumoto, K. Electrolyte-gated graphene field-effect transistors for detecting pH and protein adsorption. *Nano Lett.* **2009**, *9*, 3318-3322.
- (16) Wang, X.; Tabakman, S. M.; Dai, H. Atomic layer deposition of metal oxides on pristine and functionalized graphene. *J. Am. Chem. Soc.* **2008**, *130*, 8152-8153.
- (17) Yates, D. E.; Levine, S.; Healy, T. W. Site-binding model of the electrical double layer at the oxide/water interface. *J. Chem. Soc., Faraday Trans. 1* **1974**, *70*, 1807-1818.
- (18) Bergveld, P. In *In ISFET, theory and practice*; IEEE Sensor Conference Toronto; 2003; Vol. 10, pp 1.
- (19) Liu, H.; Liu, Y.; Zhu, D. Chemical doping of graphene. *J. Mater. Chem.* **2010**, *21*, 3335-3345.
- (20) Wehling, T.; Novoselov, K.; Morozov, S.; Vdovin, E.; Katsnelson, M.; Geim, A.; Lichtenstein, A. Molecular doping of graphene. *Nano letters* **2008**, *8*, 173-177.
- (21) Bunch, J. S.; Verbridge, S. S.; Alden, J. S.; Van Der Zande, A. M.; Parpia, J. M.; Craighead, H. G.; McEuen, P. L. Impermeable atomic membranes from graphene sheets. *nano letters* **2008**, *8*, 2458-2462.
- (22) Leenaerts, O.; Partoens, B.; Peeters, F. Graphene: A perfect nanoballoon. *Appl. Phys. Lett.* **2008**, *93*, 193107.
- (23) Wang, Q. H.; Jin, Z.; Kim, K. K.; Hilmer, A. J.; Paulus, G. L. C.; Shih, C. J.; Ham, M. H.; Sanchez-Yamagishi, J. D.; Watanabe, K.; Taniguchi, T. Understanding and controlling the substrate effect on graphene electron-transfer chemistry via reactivity imprint lithography. *Nature Chemistry* **2012**.
- (24) Seo, H. I.; Kim, C. S.; Sohn, B. K.; Yeow, T.; Son, M. T.; Haskard, M. ISFET glucose sensor based on a new principle using the electrolysis of hydrogen peroxide. *Sensors Actuators B: Chem.* **1997**, *40*, 1-5.
- (25) Huang, Y.; Dong, X.; Shi, Y.; Li, C. M.; Li, L. J.; Chen, P. Nanoelectronic biosensors based on CVD grown graphene. *Nanoscale* **2010**, *2*, 1485-1488.

- (26) Hwa Kwak, Y.; Soo Choi, D.; Na Kim, Y.; Kim, H.; Ho Yoon, D.; Ahn, S. S.; Yang, J. W.; Seok Yang, W.; Seo, S. Flexible glucose sensor using CVD-grown graphene-based field effect transistor. *Biosensors and Bioelectronics* **2012**.
- (27) Huang, Y.; Zhang, W.; Xiao, H.; Li, G. An electrochemical investigation of glucose oxidase at a CdS nanoparticles modified electrode. *Biosens. Bioelectron.* **2005**, *21*, 817-821.
- (28) Yogeswaran, U.; Chen, S. M. A review on the electrochemical sensors and biosensors composed of nanowires as sensing material. *Sensors* **2008**, *8*, 290-313.
- (29) Rasko, D. A.; Webster, D. R.; Sahl, J. W.; Bashir, A.; Boisen, N.; Scheutz, F.; Paxinos, E. E.; Sebra, R.; Chin, C. S.; Iliopoulos, D. Origins of the E. coli strain causing an outbreak of hemolytic-uremic syndrome in Germany. *N. Engl. J. Med.* **2011**, *365*, 709-717.
- (30) Lewis, C. M.; Mak, J. L. Comparison of membrane filtration and Autoanalysis Colilert presence-absence techniques for analysis of total coliforms and Escherichia coli in drinking water samples. *Appl. Environ. Microbiol.* **1989**, *55*, 3091-3094.
- (31) Lin, Y. M.; Avouris, P. Strong suppression of electrical noise in bilayer graphene nanodevices. *Nano letters* **2008**, *8*, 2119-2125.
- (32) Voelker, M.; Fromherz, P. Signal Transmission from Individual Mammalian Nerve Cell to Field-Effect Transistor. *Small* **2005**, *1*, 206-210.
- (33) Hooge, F. N. $1/f$ noise is no surface effect. *Physics letters A* **1969**, *29*, 139-140.
- (34) Pal, A. N.; Ghosh, A. Resistance noise in electrically biased bilayer graphene. *Phys. Rev. Lett.* **2009**, *102*, 126805.
- (35) Shao, Q.; Liu, G.; Teweldebrhan, D.; Balandin, A. A.; Rumyantsev, S.; Shur, M. S.; Yan, D. Flicker noise in bilayer graphene transistors. *Electron Device Letters, IEEE* **2009**, *30*, 288-290.
- (36) Voelker, M.; Fromherz, P. Signal Transmission from Individual Mammalian Nerve Cell to Field-Effect Transistor. *Small* **2005**, *1*, 206-210.
- (37) Gannett, W.; Regan, W.; Watanabe, K.; Taniguchi, T.; Crommie, M.; Zettl, A. Boron nitride substrates for high mobility chemical vapor deposited graphene. *Appl. Phys. Lett.* **2011**, *98*, 242105-242105-3.

Chapter 4-Bilayer graphene sensors

The fabrication of bilayer graphene sensors is interesting because these devices could exhibit potentially lower noise than devices fabricated on a single layer of graphene.

Indeed, in electrolyte-gated configuration, there are two major sources of $1/f$ noise. First, a main source of noise comes from the fluctuating presence of ions or dipoles at the graphene/electrolyte interface due to the formation of the double layer and the effectiveness of the ionic screening in the channel. The second source of noise is due to the presence of the underlying oxide, where fluctuating trap charges in the oxide modulate the carrier mobility in the channel and the noise in the graphene sheet depends on the effectiveness of the impurity charges screening.

In our work, we stacked two monolayers graphene in order to make bilayer graphene by CVD and there is therefore no coupling between the two graphene layers that can be considered as independent. Two possible screening effects taking place in this bilayer system could induce a lower noise than in monolayer. One is the screening of the ions in solution by the top graphene layer (facing the electrolyte) on the bottom layer (closer to the substrate) and the second effect is the screening of the charged impurities in the substrate by the bottom graphene layer on the top layer.

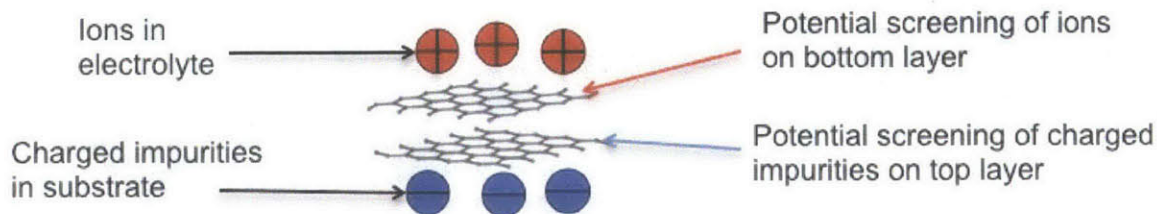


Figure 1: Schematic of the bilayer graphene system of two stacked monolayer with the possible screening effects that could reduce the noise in bilayer

As shown in figure 1, since the bottom graphene layer (closer to the substrate) is separated from the electrolyte by the top graphene layer (facing the electrolyte), the bottom graphene layer could be less sensitive to the noise effect induced by the ions and dipoles in the electrolyte contact due to a screening effect by the top graphene layer. Therefore, the graphene bottom layer could have lower noise than monolayer graphene. Likewise, since the top graphene layer is separated from the substrate by the bottom graphene layer, the top graphene layer could be less sensitive to the noise effect induced by the substrate due to a screening effect by the bottom graphene layer. Therefore, the graphene top layer could also have lower noise than monolayer graphene. Thus, both graphene layers in our bilayer graphene devices could potentially exhibit lower noise than single layer graphene devices and so could therefore the bilayer system as a whole.

In addition, it is worth noticing Lin et al demonstrated that there is a strong suppression of the $1/f$ electronic noise in bilayer transistors compared to single layer ones ¹. However, Lin et al use bilayer graphene that was A-B stacked and this coupling between the two layers gives rise to a unique field-dependent band structure that is expected to be responsible for the suppressed electronic noise. However, in our bilayer system where there is no A-B stacking order, this suppression effect of the electronic noise may not take place due to the fact that the band structure of our bilayer is closer to monolayer than A-B stacked bilayer as the two graphene layers are considered to be uncoupled.

1- Fabrication process

In order to fabricate bilayer devices, we first grow graphene on two separate copper foils as described in Chapter 2. Then, a PMMA layer is spin coated on one of the copper foil and after etching away the copper, the graphene-PMMA film is rinsed in water as described in Chapter 2. The graphene-PMMA film is then transferred onto the other copper foil where graphene was already grown onto it. By this process, we can obtain a copper foil with two graphene layers stacked one onto the other and covered by a PMMA layer. After etching away the copper, cleaning the film with hydrochloric acid and rinsing the bilayer graphene-PMMA film in water, the film was transferred onto a silicon dioxide wafer with already deposited metal contacts on it. The device is then processed as described in chapter 2 with a SU 8 insulation layer that covers the metal contacts.

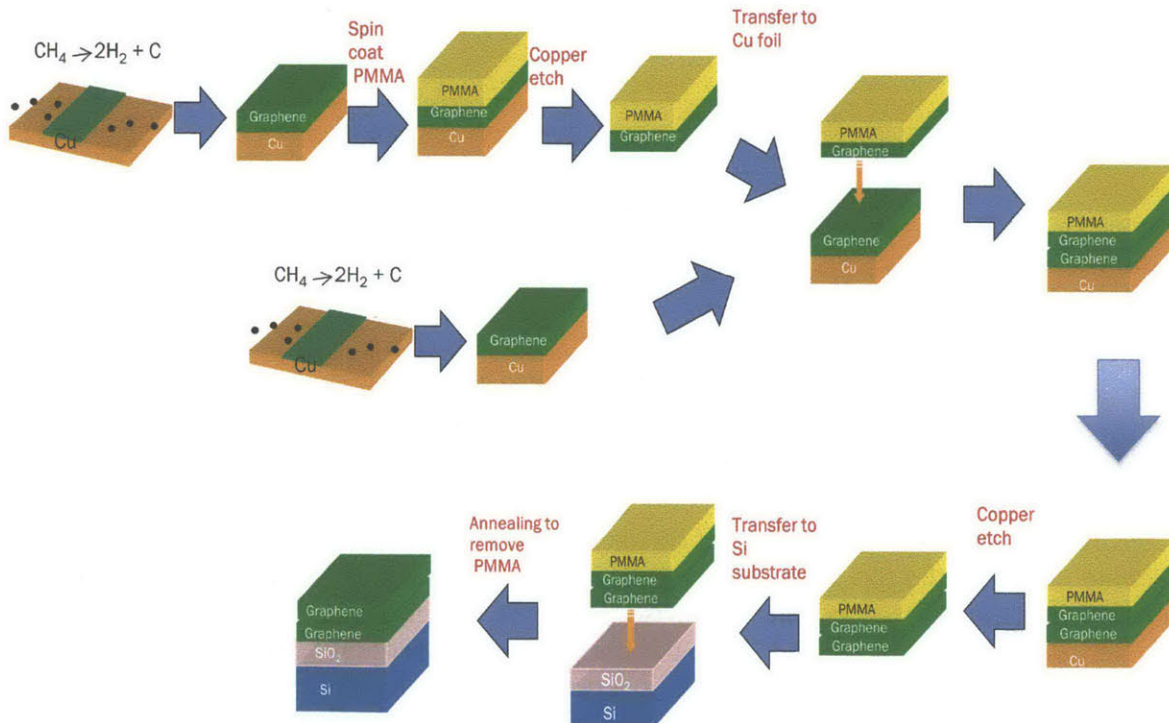


Figure 1: Schematic of the transfer process for bilayer graphene on silicon dioxide

An alternative fabrication process would have been to transfer onto a Si/SiO₂ substrate a first graphene monolayer and remove the PMMA layer. Then, subsequently transfer a second graphene monolayer on top of the first graphene film on the Si/SiO₂ substrate. However, the method is less advantageous than the one we use because PMMA residue on the first graphene layer would be sandwiched in between the two graphene layers and will not enable an intimate contact and stacking of the two layers.

2- Bilayer graphene sensor characterization

As described by the fabrication process, we use bilayer graphene with an arbitrary orientation between the two layers since we stacked two independent monolayers of graphene onto each other. This bilayer sheet is really different from the conventional bilayer graphene that is usually obtained by exfoliation² and where the two layers have an A-B stack orientation. The A-B stacking induces a very different band structure for bilayer exfoliated graphene compared to monolayer with a band gap opening that can be induced with an electrolyte gated configuration². On the contrary, the two layers in our bilayer system are not coupled and they have the same band structure as monolayer graphene. Thus, the electrical characteristics of our bilayer sensors are expected to be quite similar to the ones in monolayer graphene with the hole and conduction regime separated by a minimum conduction point.

Figure 2 shows the transfer characteristics of a bilayer device compared to a monolayer device, for a 10 mM phosphate buffer solution pH 7.2.

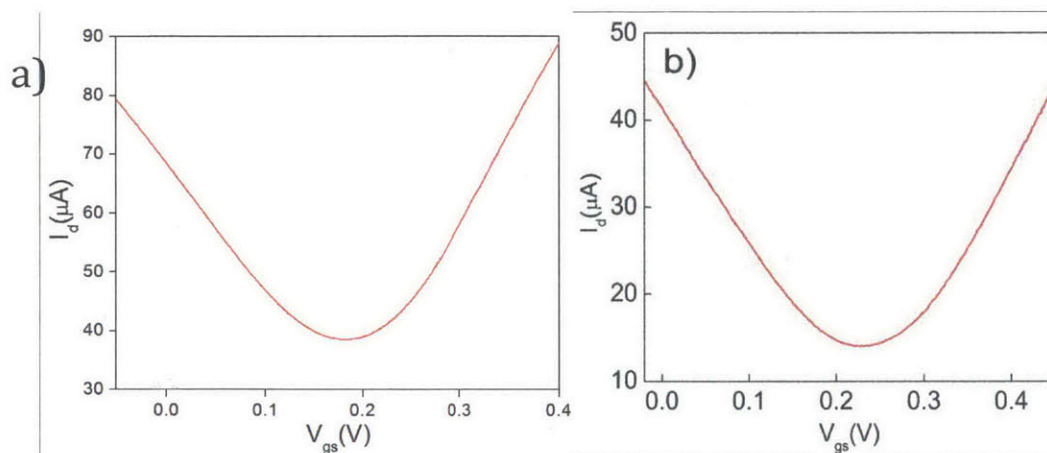


Figure 2: a) Transfer characteristics of a $30 \times 40 \mu\text{m}^2$ bilayer graphene-on-SiO₂ SGFET. b) Transfer characteristics of a $20 \times 40 \mu\text{m}^2$ monolayer graphene-on-SiO₂ SGFET for $V_{ds} = 50 \text{mV}$

As expected the transfer characteristics of the bilayer graphene-on-SiO₂ SGFET are similar to the ones of monolayer graphene-on-SiO₂ SGFET with a hole and electron regimes separated by a minimum conductivity point, i.e. the Dirac point³. This was also observed in back gate measurements elsewhere³. The Dirac point in bilayer devices is slightly shifted to lower voltages compared to monolayer devices. This shift underlines that the bilayer devices are slightly less p-

doped. This shift can be due to two screening effects taking place. The first one is the screening effect of charge impurities of the substrate by the bottom graphene layer on the top graphene layer. As found elsewhere⁴ this screening effect is indeed limited for the first two layers but becomes significant after the third layer in multilayer graphene. Thus, this screening effect is expected to be weak. The other screening effect is a screening of the ions in the solution by the top graphene layer that is in contact with the electrolyte on the bottom graphene layer. Again this screening effect is weak since the bilayer devices are only slightly less p-doped.

The conductivity in bilayer devices is about twice higher than in monolayer, which is expected since we have two independent monolayers stacked together. Indeed, the minimum conductivity point in bilayer devices is about 4 times higher in conductivity than the monolayer one. This was also similarly observed elsewhere³. The maximum transconductance $g_m = \frac{\partial I_d}{\partial V_{gs}}$ of the bilayer device is 220 μS in the hole conduction regime and 320 μS in the electron conduction regime. When normalized by the transistor width, the maximum transconductance of the transistor is then 8 $\text{mS}\cdot\text{mm}^{-1}$. In order to compare transconductance with the monolayer graphene device, the same length of device is needed since with an increase in device length, the transconductance decreases. As the monolayer transistor in Chapter 3 is 20 μm in length compared to 30 μm for the bilayer transistor shown in figure 2, we measure the transfer characteristics of another bilayer device with 20 μm in length. This maximum transconductance value of this device is 11.1 $\text{mS}\cdot\text{mm}^{-1}$ and is a little more than twice higher than for monolayer devices (5 $\text{mS}\cdot\text{mm}^{-1}$). This is consistent with the fact that our bilayer system consists of two uncoupled monolayer graphene and that therefore the transconductance is twice higher than in monolayer graphene.

The field effect carrier mobility of the transistor μ_{FE} can be calculated using $\mu_{FE} = \frac{1}{C_{int}} \frac{d\sigma}{dV_{gs}}$, where C_{int} is the interfacial graphene/electrolyte capacitance and σ is the conductivity. Since both layers are completely uncoupled and if we assume for simplicity that there is no screening effect of the electrochemical double layer by the top graphene layer for the bottom graphene layer, we can consider the two graphene layers to be capacitors in parallel. Therefore the carrier concentration is the same in the two layers of graphene. The interfacial capacitance of the bilayer system is then the combination in series of the double layer capacitance and two equal quantum capacitance of a monolayer graphene: $\frac{1}{C_{int}} = \frac{1}{C_{DL}} + \frac{2}{C_Q}$ where C_{int} is the interfacial capacitance, C_{DL} the double layer capacitance and C_Q the quantum capacitance of a monolayer graphene, as shown in figure 3.

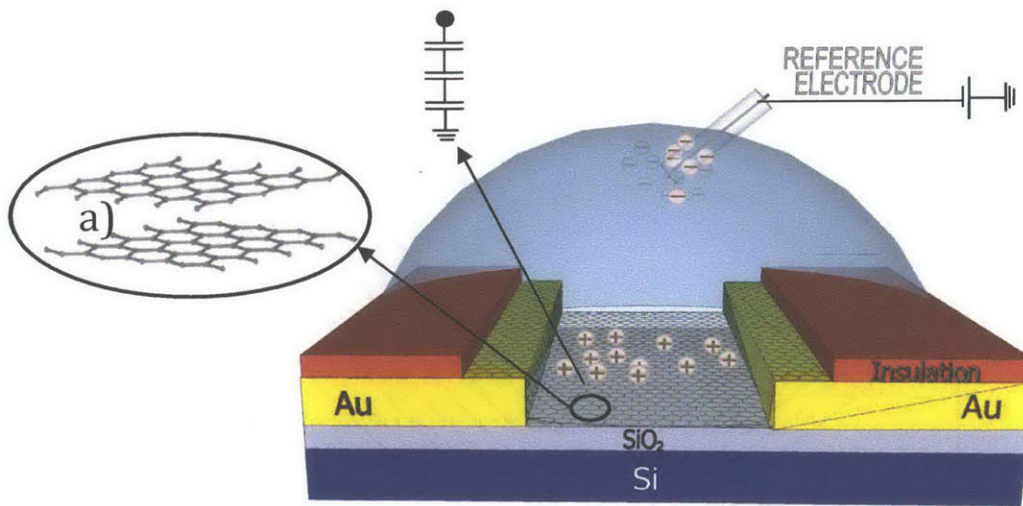


Figure 3: Model of the bilayer graphene SGFET with the double layer and the two quantum capacitances of both graphene layers in series

Following an interfacial capacitance model for monolayer graphene but introducing two quantum capacitance of same value, we can extract a maximum hole mobility for our bilayer system of $1240 \text{ cm}^2 \cdot \text{V}^{-1} \cdot \text{s}^{-1}$ and an electron mobility of $2010 \text{ cm}^2 \cdot \text{V}^{-1} \cdot \text{s}^{-1}$. The carrier mobility obtained for the bilayer system are in agreement with the usual mobility obtained for the monolayer device, even though the electron mobility in bilayer device tend to be a bit higher than for the monolayer device. Indeed, the maximum hole mobility in monolayer is usually around $1100\text{-}1200 \text{ cm}^2 \cdot \text{V}^{-1} \cdot \text{s}^{-1}$ and the electron mobility around $1600\text{-}1700 \text{ cm}^2 \cdot \text{V}^{-1} \cdot \text{s}^{-1}$. The fact that the carrier mobility in the bilayer system is similar to what was obtained for a monolayer system is quite expected since the two monolayers in the bilayer device are completely uncoupled.

3- pH sensing

The dependence of the bilayer graphene-on-SiO₂ transistor transfer characteristics with the pH was evaluated. For these measurements, the device was immersed in a 10 mM phosphate buffer solution with an ionic strength adjusted to 100 mM with NaCl. Then, aliquots of 0.5 M HCl and NaOH were added to change the pH of the solution.

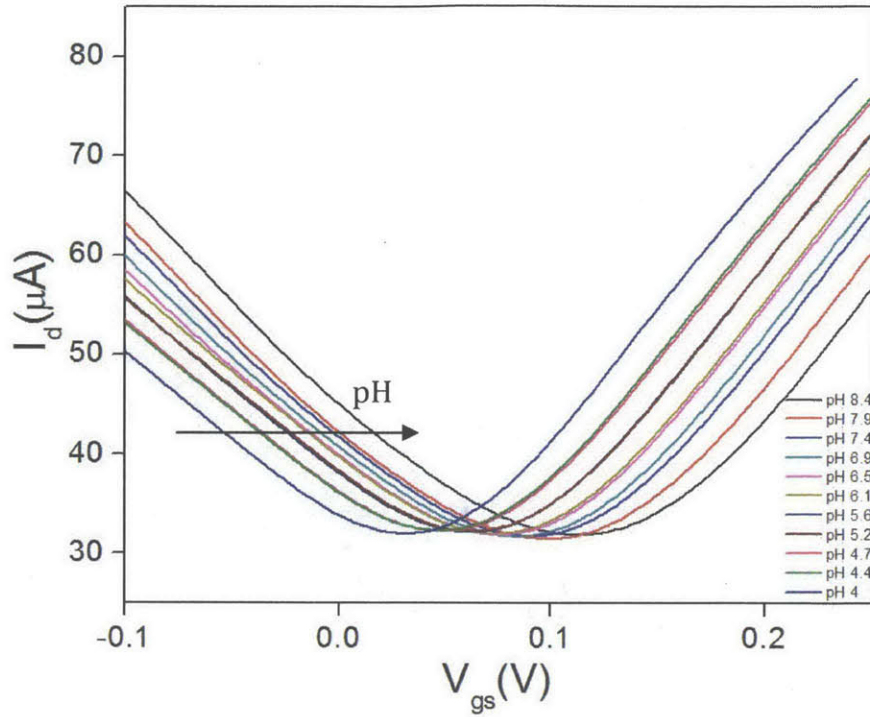


Figure 4. a) Transfer characteristics of a $30 \times 40 \mu\text{m}^2$ bilayer device at a constant drain-source voltage of $V_{ds}=50 \text{ mV}$, for different pH values. b) Voltage at Dirac point shift with the pH for a $30 \times 40 \mu\text{m}^2$ bilayer graphene SGFET

As in the case of monolayer devices, the Dirac point in the bilayer graphene transistor shifts towards more positive voltages when the pH is increased. Therefore, the same pH mechanism is at stake in bilayer and monolayer devices. The shift of the Dirac point is due to the increase in negative charge close to the graphene when the pH increases. The physical adsorption of ions at the surface of graphene with doping effect of the graphene sheet as described in Chapter 3 is in agreement with this result. This pH-induced doping would dope monolayer and bilayer graphene in a similar fashion.

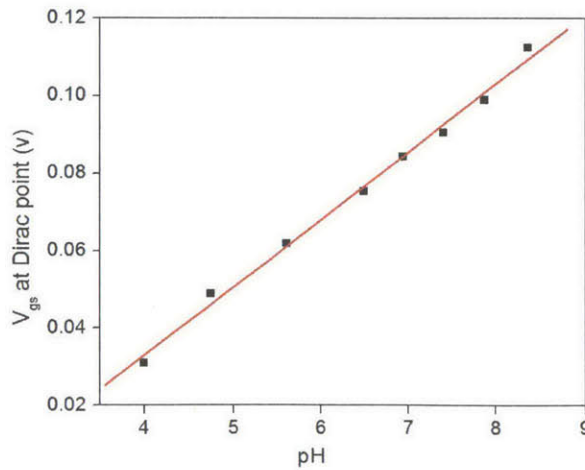


Figure 5: Voltage at Dirac point shift with the pH for the $30 \times 40 \mu\text{m}^2$ bilayer graphene-on- SiO_2 SGFET

As shown on Figure 5, the Dirac point shifts linearly with the pH, with a sensitivity of 18 mV/pH. This pH sensitivity is 18 % lower than the pH sensitivity of 22mV/pH found for monolayer devices. The quite similar pH sensitivity in bilayer and in monolayer graphene emphasizes that the same pH mechanism is taking place. However, bilayer devices seem to be a little less pH sensitive. This lower sensitivity could be explained by the fact that the physical adsorption of hydroxide ions when increasing pH does not have as much an influence on the bottom graphene layer as on the top layer due to the screening effect of ions in solution by the top graphene on the bottom graphene layer.

Additional experiments are needed to first confirm the slightly lower pH sensitivity of bilayer devices by measuring the pH sensitivity on many different bilayer devices. Secondly, experiments should be designed to understand in depth the mechanism for the lower pH sensitivity of bilayer graphene.

In conclusion, bilayer graphene devices exhibit high pH sensitivity, though slightly lower than monolayer devices, and therefore could be used for high performance pH monitoring applications.

4- Noise in bilayer graphene devices

As mentioned in chapter 3, in addition to the transconductance, the low-frequency noise of a graphene transistor is the other key parameter for sensors because it will have a significant influence on the sensitivity¹. One of the possible advantages of bilayer graphene devices compared to monolayer devices is that they could exhibit lower 1/f noise. As mentioned earlier, a lower noise in bilayer devices could be explained by two possible screening effects: a screening of ions in the double layer by the top graphene layer on the bottom layer that would reduce the noise influence by ionic fluctuations of the electrolyte on the bottom graphene layer; and, a screening effect by the bottom graphene layer on the top layer that would reduce the noise influence by charge impurities fluctuations of the substrate on the top graphene layer. Here we measure the noise in 4 different bilayer devices as well as 4 monolayer devices for comparison with size 20x40 μm^2 .

First, noise measurements were performed in the dry state, which means that the devices were not immersed in any electrolyte but exposed to the air. The back gate configuration was used and the top gate voltage was applied through the silicon on the back of the sample. The top gate voltage was set at 0V. In figure 6, the current noise spectral density S_{I_d} is measured with a spectrum analyzer for 4 different bilayer and 4 different monolayer devices in dry state. For all devices, we found that the current noise spectral density is 1/f dependent, where f is the frequency.

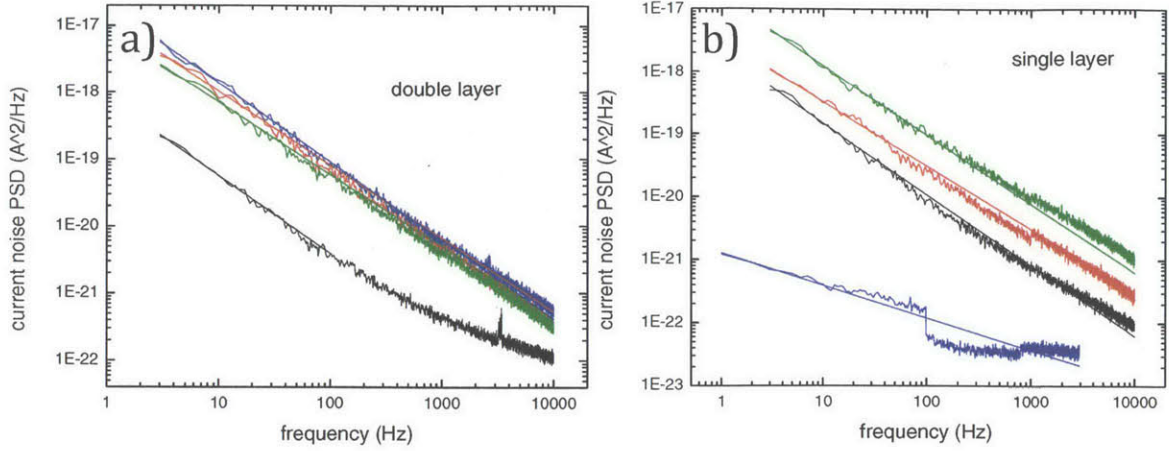


Figure 6: Spectral noise density measurements in dry state and back gate, for $V_{GS} = 0V$ with $V_{DS} = 100mV$, for a) 4 bilayer graphene devices, b) for 4 monolayer graphene devices.

As described in chapter 3, the $1/f$ dependence is often characterized with the empirical Hooge law for electronic devices⁵. According to the Hooge law, the noise is inversely proportional to the number of carriers (N) contributing to electronic transport and it can be written: $S_{I_d} = \frac{\alpha_H}{N} \frac{1}{f} I_d^2$, with α_H the Hooge parameter that characterizes the noise properties of bilayer and monolayer graphene. Using the Hooge model, we can deduce from the spectral noise density, the noise amplitude $A = \frac{\alpha_H}{N}$, commonly used to evaluate the noise performance. In figure 7, the noise amplitude of the 4 different bilayer and 4 different monolayer devices is plotted as well as the drain-source current I_D for $V_{GS} = 0V$.

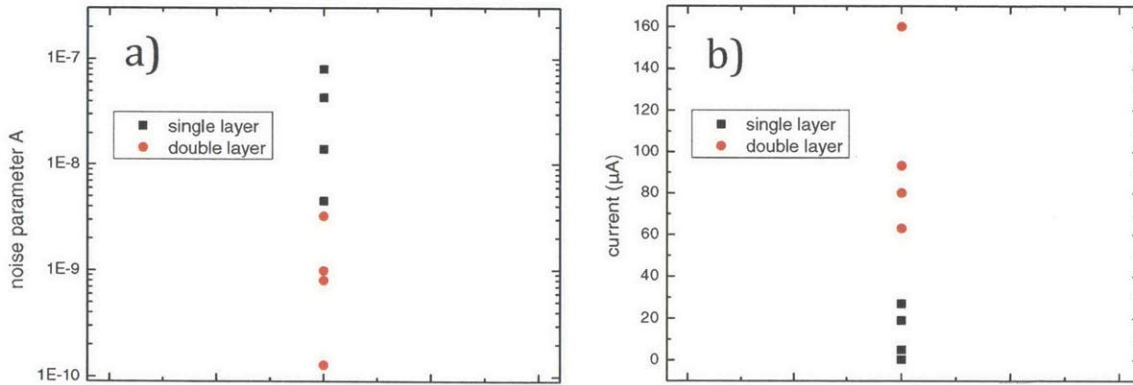


Figure 7: a) noise amplitude deduced from the noise spectral density measurement, b) drain-source current I_D for $V_g = 0V$ with $V_{ds} = 100mV$ for 4 different bilayer and 4 different monolayer devices.

As expected and shown in figure 7 b), we can see that the bilayer devices have more than two times higher drain-source current than monolayer. We see also that there is some dispersion in the drain-source current among bilayer and monolayer devices. The reason for the dispersion can be attributed mainly to the SU 8 processing step that sometimes degrades the graphene quality for some of the devices. However, clear trends can be drawn thanks to the use of 8 different devices. Figure 7 a) shows that the noise amplitude also is on average an order of magnitude lower in bilayer devices than in monolayer devices. This emphasizes that in the dry state, the

noise performance of bilayer devices is significantly better than monolayer devices. Thus, bilayer graphene made of stacked monolayer have lower $1/f$ noise in dry state. However, only the noise performance of bilayer devices in electrolyte-gated configuration is of interest for chemical and biosensing applications.

Therefore, the bilayer and monolayer graphene-on-SiO₂ SGFETs were immersed in a 10 mM phosphate buffer adjusted to an ionic strength of 50 mM using NaCl with a Ag/AgCl reference electrode immersed in the liquid. The noise measurement set up used was exactly the same as described in chapter 3. The spectral noise density of all devices was measured in a frequency range of 1 Hz to 100 kHz. We also vary the gate voltage in noise measurements V_g between -0.2 V and 0.4 V in order to compare noise with different biases. The devices exhibit the expected $1/f$ dependence.

Using the Hooge model $S_{I_d} = \frac{\alpha_H}{N} \frac{1}{f} I_d^2$, the noise amplitude $A = \frac{\alpha_H}{N}$ is extracted from the measurement as shown in figure 8.

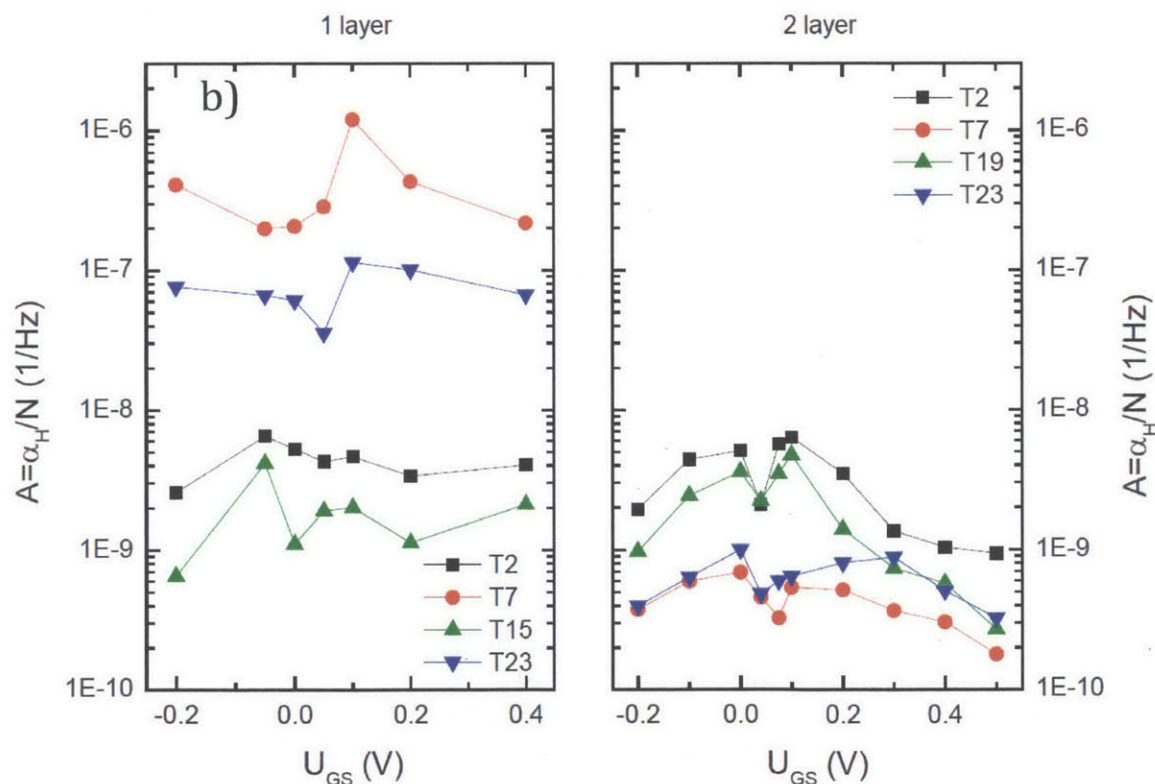


Figure 8: Gate voltage dependence of the noise amplitude $A = \frac{\alpha_H}{N}$, where N is the total number of carriers, a) for monolayer graphene devices, b) for bilayer graphene devices

On average, the bilayer devices exhibit more than 3 times lower noise amplitude than the best low noise monolayer graphene devices. In addition, the bilayer devices exhibit more reproducible noise amplitude than monolayer devices with values around $3 \cdot 10^{-10} \text{ Hz}^{-1}$. However, regarding device sensitivity, the relevant noise parameter to evaluate chemical sensors is the gate

voltage noise spectral density $S_G = \frac{S_{I_d}}{g_m^2}$, which gives the minimum resolution in the gate signal that can be detected by the device. In figure 9, the RMS of the gate voltage noise power density is calculated at different gate voltages considering the typical bandwidth used in biosensors applications (1 Hz to 5 kHz).

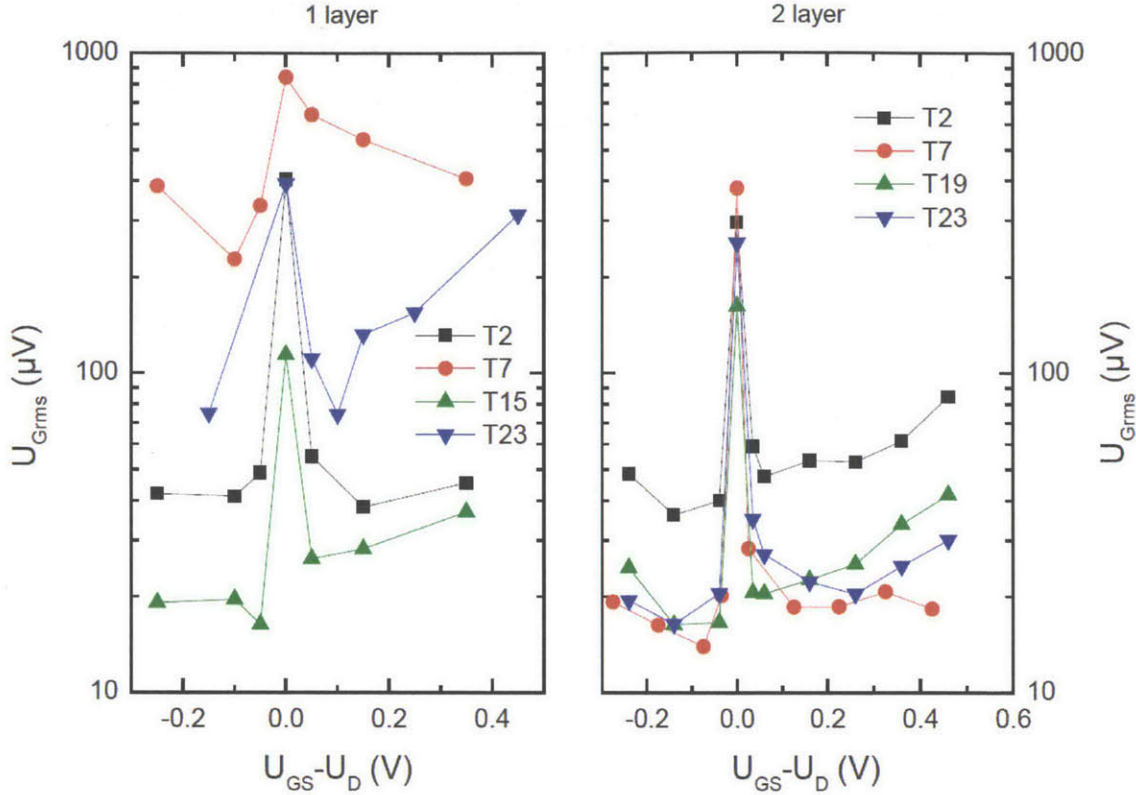


Figure 9: Gate voltage noise spectral density $S_G = \frac{S_{I_d}}{g_m^2}$ at different gate voltages for 4 monolayer graphene devices with U_{GS} the top gate voltage and U_D the gate voltage at the Dirac point

On average, the RMS of the gate voltage noise power density of bilayer devices is four times lower than the monolayer devices. The bilayer devices exhibit more reproducible values of RMS of the gate voltage noise power density than monolayer devices. Three bilayer devices exhibit values around 15 μV whereas the best monolayer device has a 20 μV noise. Thus, bilayer devices have reproducibly better noise performance but their noise is not significantly lower than the best monolayer devices.

Therefore, the two screening effects mentioned earlier did not have a significant impact on noise performance but only a weak effect that induces a slightly lower noise in bilayer devices than monolayer devices. More experiments would be needed to get more reproducible noise performance in monolayer devices as well as optimizing the bilayer fabrication process to lower further its electronic noise.

In conclusion, bilayer graphene is a promising candidate for chemical and biological sensing applications because it exhibits high pH sensitivity close to the one found in monolayer graphene and also bilayer graphene has reliably very high noise performance, better than monolayer. Optimization of the design of bilayer devices could potentially improve the noise performance further. It would be also very interesting in the future to characterize and compare the noise performance of bilayer graphene with A-B stacking since it has a very different band structure that in dry state leads to a strong suppression of $1/f$ electronic noise^{1, 2}. Another interesting direction of the work would be to increase the number of graphene layers stacked on each other in order to see if it decreases the noise of the device further as the screening effects between layers mentioned earlier become more significant.

References

- (1) Lin, Y. M.; Avouris, P. Strong suppression of electrical noise in bilayer graphene nanodevices. *Nano letters* **2008**, *8*, 2119-2125.
- (2) Yamashiro, Y.; Ohno, Y.; Maehashi, K.; Inoue, K.; Matsumoto, K. Electric-field-induced band gap of bilayer graphene in ionic liquid. *Journal of Vacuum Science & Technology B: Microelectronics and Nanometer Structures* **2012**, *30*, 03D111-03D111-5.
- (3) Yu, T.; Kim, C.; Yu, B. Highly Conductive 3D Nano-Carbon: Stacked Multilayer Graphene System with Interlayer Decoupling. *arXiv preprint arXiv:1103.4567* **2011**.
- (4) Wang, H.; Wu, Y.; Ni, Z.; Shen, Z. Electronic transport and layer engineering in multilayer graphene structures. *Appl. Phys. Lett.* **2008**, *92*, 053504-053504-3.
- (5) Hooge, F. N. $1/f$ noise is no surface effect. *Physics letters A* **1969**, *29*, 139-140.

Chapter 5: The policy implications of moving from research to commercialization in the biosensor market

In previous chapters, we showed that graphene exhibits high performance and great potential for many applications in chemical and biological sensing applications. Research for the integration of graphene and other carbon-based materials (e.g. carbon nanotubes) into a biological sensor (biosensor) is part of a general effort worldwide focused on the discovery of radically new biosensors through the convergence of nanotechnology, biotechnology and bioelectronics. However, there is a high risk that the benefits of graphene sensors or other radically innovative sensors will not be soon available to society due to issues related to regulation. In this Chapter we study the policy implications of the commercialization of biosensors.

1- Policy controversies around the commercialization of biosensors

The biological and medical sensors (commonly called biosensors) market encompasses all sensors that either rely on biological materials or processes to produce a signal, like a glucose sensor, or any sensor that measures a biological process, like a blood pressure sensor. Nowadays, the biosensor market is going through a technological revolution with the convergence of nanotechnology, biotechnology and bioelectronics and it will bring many new devices that could revolutionize medicine. For example, early detection of cancer could be achieved with biosensors designed to detect early cancer biomarkers and determine drug effectiveness at various target sites. This could lead to a lot more efficient way to treat cancer, since the earlier cancer can be detected, the better the chance of a cure¹. Although biosensors are used in a wide variety of fields such as environment monitoring or biodefense, its main applications are in the medical field especially for point of care testing (medical testing at or near the site of patient care). However, commercialization of the revolutionary innovations of biosensors faces serious hurdles due to the stringent regulation for market approval. This regulatory challenge is of crucial importance because it may seriously hamper the innovations in the field to reach the market. Therefore, crucial policy issues have been raised mainly around risk shielding and evaluating the FDA regulation: can we shorten and optimize the market approval without compromising the high safety standards of America's health? But also regulatory harmonization is a major concern especially for the industry: should FDA align its regulation to the European one that seems more attractive to the biosensor industry in order to stay competitive? Finally, ongoing discussions exist about improving FDA regulation through an adaptive regulation with

earlier approval and limited-launch, living-licensing process as well as about the need for standardization of the use of biosensors in industry and government institutions.

After reviewing the biosensor field with its on-going technological revolution, the FDA regulation for medical devices will be explained. Then, the negative impacts of regulation on the industry will be described. Risk shielding, regulatory harmonization and evaluating the FDA regulation in the biosensor market will be discussed. Finally, policy recommendations will be proposed aiming at making the regulation more efficient and supportive of innovation while maintaining the high standards for safety in the US.

2- The biosensor technological revolution

- **The biosensor market**

The biosensor market is a 9 billion dollars market today with a very rapid growth around 12% estimated to reach 16 billion dollars by 2017. It has 6 different market segments: the point of care testing (46%), the home diagnosis (20%), environmental monitoring (13%), research laboratories (11%), process industries monitoring (7%) and biodefense which is the market for all technologies to protect and fight against a biological warfare that is a growing market since the anthrax case in the US (3%)²(Frost & Sullivan 2010). It is essentially concentrated on medical applications with point of care testing and home diagnosis representing more than 65 % of the market. The blood glucose sensor market is by far the most significant one in medical devices with 70 % of the market.

- **Technological revolution**

Biosensors represent a large and expanding field thanks to the development of a wide variety of technologies. For example, the detection principle of biosensors technologies can rely on electrical or optical detection but also on piezoelectric or thermal detection. Therefore, many very different technologies with various technical advantages have been developed for many applications with specific requirements. However, for the last two decades, the commercialization and success of biosensors have been limited because they did not exhibit superior enough technical performance³. Indeed, they were competing with other technologies already in use with similar prices and quite comparable technical performance. Biosensors did not exhibit superior advantages especially in light of the 3 main technical requirements: sensitivity, selectivity and fast response. Sensitivity of a sensor corresponds to its minimum concentration level detection of an analyte whereas its selectivity corresponds to its capacity to be specifically sensitive to the targeted analyte and insensitive to other molecules. The sensor response corresponds to the time required for detection and transmission of the signal.

In the last decade, the parallel development of nanotechnology, biotechnology and bioelectronics has led to current demonstration of technological breakthroughs for biosensors with new materials and new principles, and it will lead to plenty of new research opportunities. Indeed, tremendous breakthroughs have been demonstrated recently that reach the possible limits of detection with sensitivity up to single molecule detection, as well as excellent selectivity and

extremely fast response. For example, carbon nanotubes^{4,5} and graphene⁶, new carbon materials, for biosensors have exhibited single molecule detection and extremely fast response. Although these breakthroughs are still at the research state, their development into commercial technologies will lead to an unprecedented boom of disruptive technological innovations for biosensors in the next decade⁷. Indeed, the use and integration of microelectronics fabrication and micro fluidics technologies for biosensors has enabled the miniaturization required for implantable sensors as well as the development of sensor arrays for multiple analyte detection on a same chip. The miniaturized implantable sensor technology with wireless communication has already impacted the point of care diagnosis. Its predicted mass implementation will change the way of doing point of care diagnosis and treating chronic diseases. Their use in medical applications could also considerably reduce the cost of diagnosis. Finally, a boom of new applications for biosensors are being developed in genomic and proteomic research, which could considerably expand the market².

Thus, the convergence of nanotechnology, biotechnology and bioelectronics will lead to an explosion of revolutionary technological innovations in the field of biosensors over the next decade. It could very likely bring about a revolution in medical care in prevention and diagnosis of diseases as well as treatment with tremendous benefits for America's health⁸.

However, although the technological biosensor revolution is arguably on its way, it is still uncertain whether the benefits of its commercialization will reach the American citizens in the near term. Indeed, commercialization of these new innovative chemical sensor and biosensor technologies from the biosensor revolution that now meet the high technical requirements for commercialization, has continued to lag behind research by several years³. The difficulty for innovations to reach the market needs to be corrected through better policies to support innovation. For this purpose, we need to understand first the key drivers and restraints that exist in the biosensor market.

3- Key drivers and restraints in the market

Since more than 65% of the biosensor market is dedicated to medical applications where most of the innovations are being created, we will focus especially on this part of the market.

- **Key drivers**

There are key factors in the biosensor market that drive the huge investment in research for innovations and push for its commercialization. First, the continuous development of nanotechnology is a main key driver because it has facilitated nano-engineered biosensors. The improvement in process techniques and enhancement in biosensor functionalities have resulted in the expansion of applications and their extension to newer tests. An important driver is also the large number of applications in which biosensors are used and the increasing number of new applications. Indeed, their application ranges from medical diagnostics like small, cheap biosensors for the sensing of all sorts of biomarkers or glucose for diabetics⁹ to security and defense applications with the detection of dangerous virus like Ebola or of explosives¹⁰. In all these applications, the need for an efficient, compatible and user- friendly biosensor is

imperative. The rise of genomic and proteomic research will drive the creation of new applications for biosensors. Another important factor is the increasing awareness about maintaining good health, which makes consumers to periodically check their blood chemistry. With the increase in incidence of diseases such as diabetes, the need for using biosensors for sensing or monitoring blood glucose levels regularly has significantly increased. Several assay tests have moved to home diagnostic monitoring settings. The development of newer rapid assay biosensors has facilitated such tests. With the increased importance of real time in-vivo sensing, biosensors have great potential for growth in both the point-of-care and home diagnostic markets. Finally, new investments in R&D are also a key market driver. Thus, the U.S. Congress in the early part of 2009 had sanctioned \$1.1 billion in funds for comparative effectiveness research as part of its economic stimulus program¹¹. The main goal of comparative effectiveness research is to bring down the costs of drugs, devices, and treatments and make them available to all. Comparative effectiveness research looks at different treatment options for the same condition. Such research provides physicians and patients with information on which they can base their clinical decisions.

- **Two significant restraints in the US**

These drivers represent strong incentives for successful investment in the development of biosensor technologies. However, two subsequent high barriers and restraints need to be overcome for successful commercialization: high development costs^{2,3} and a long and uncertain FDA market approval^{11,12}. This has led to a commercialization of innovation that lags behind research by several years, resulting in a low technology transfer from laboratory to market^{2,3} especially due to a regulatory failure to support innovation. We are going to first describe the negative impact of this regulatory failure on the biosensor market and then we will explain how the regulation in the US is partially responsible for this situation.

- **Negative trends in the US**

The different barriers and restraints, especially regulation in the US, have negative impacts in the biosensor market in the US that are alarming since a shrink of investments by venture capitalists as well as an outflow of capital outside the US towards Europe and emerging countries are starting to be observed.

Venture capitalist funding plays a crucial role in the biosensor market in order to bring to market disruptive revolutionary technologies with potentially tremendous benefits for America's health. However, the venture capitalist investments have dropped 37% since 2007 so that commercialization of this kind of innovation is endangered. It is true that the financial crisis has severely impacted the venture capitalist world that has dropped 27%, but the shrink in the biosensor market by 37% is more severe and does not show the recovery expected and observed in other high tech markets¹³. In addition, in 2010, total venture capital investing increased 19% while investment in medical devices fell 9%. This shrink is therefore not conjectural but structural. It has been related to the too long and uncertain FDA market approval process to overcome for a successful commercialization of biosensor that makes the investment too risky to insure a decent return on investment. Venture capitalism is considered one of greatest strength of the American innovation system compared notably to Europe and its decrease in the biosensor market highlights the regulatory failure and the urgency to solve it.

Another negative consequence of the restraints in the US market is the fact that market approval is traditionally sought in Europe before going to the US^{13,14}. Indeed, new entrants in the market routinely start getting approval in Europe thanks to a more efficient, collaborative and shorter market approval, especially in terms of clinical trials. In addition, marketing to emerging countries also before the US is predicted to happen by 2020. As for example, Explora Med, a medical device incubator has developed a strategy of going outside the US for first clinical studies and out of 6 new products, only one reached the US market first, compared to 3 in Europe¹⁴. Therefore, the benefits of medical devices go to European citizens about 3 to 4 years before approval in the US and “medical tourism” from American citizens seeking to buy the devices is getting more and more frequent. Even worse is the fact that more and more companies are considering not entering the US market because it is too difficult to obtain approval, depriving American citizens of technological benefits¹⁵. A meaningful example is the case of Mr Stirling, a venture capitalist that runs Synecor, a medical device company incubator in North Carolina and investor in Spinal Kinetics, a company that does not plan to spend the money in clinical trials in the US but in Europe¹³.

Finally, as a logical consequence of seeking first approval in Europe, the concern comes from the outsourcing of R&D and production to Europe. It is a growing reality as about 40% of respondents to a survey by the Medical Device Manufacturing Association in October 2011 indicate that they were investing less in US medical devices and investing more in European start-ups¹⁶. Illustrative examples are starting to become more common like the case of Biosensors International, a medical device company, which shut down its operation in Southern California because it took too long to get FDA approval for its new cardiac stent¹³. Another example is Spinal Kinetics, cited above, that is moving its manufacturing to Germany. Thus, the negative economic trends observed in the biosensor market in the US make the situation quite alarming and the sources of these trends need to be analyzed. As mentioned earlier, two subsequent high barriers and restraints need to be overcome for successful commercialization: high development costs and a long and uncertain FDA market approval. The regulation in the US is the main cause for the negative trends in the market observed in the US and the quite different regulation in Europe explain its attractiveness for investments.

4- Two high barriers: development costs and regulatory approval

- **High development costs**

The first barrier that investors face when funding a new biosensor technology at the research level is the process of development that represents a very high cost over a long time. The cost of developing a biosensor ranges vastly and on an average can cost as high as \$25 million to \$30 million³. If high costs of development are easily justified for example in the pharmaceutical industry thanks to high return on investment expected with certain high volume products, on the contrary, in the biosensor industry, the high cost of development is a difficult to justify due to the uncertainty around the number of units sold² as well as the price competition by existing old technologies that drive revenues and profits of biosensors down. In addition, even in the case of

a high demand, the researchers are sometimes not successful at producing biosensors that meet the high expectations of the market and its consumers. Indeed, the difficult technical problems to overcome are the demonstration of selectivity, sterilization, reproducibility and reliability of the sensor over long times at a competitive cost³. This adds an additional risk to the investment since failure to meet one of these technical standards will result in the discard of the sensor technology. Finally, an additional technical requirement demanded by users of biosensors is to increase the life spans of the analytes. Even if this may aid the growth of the market initially, the long-term effects are likely to be negative. With replacement rates shortening, future revenue growth may be in jeopardy².

Thus, the high development costs and the need to meet the challenging technical requirements imposed by consumers³ make the development of new biosensors a risky investment. However, funding from government agencies for initial stages of high-risk technology R&D can be secured to facilitate and incentivize the investment. These funding are however limited to the Department of Defense small business innovation research (SBIR) program and to the Military, where they have very unique and specific interests². More funding from institutions with more medical-oriented interests like the NIH should be created.

However, as the research efforts become focused and an increasing number of biosensors that meet the demand of the market are developed, the higher sales volumes are likely to support the high R&D expenses.

Therefore, the high development costs for biosensors is a first barrier to investment but it is very likely that it is surmountable with the increase in sales volumes in the future thanks to the strong market drivers described above. However, if the investment for development of a new biosensor turns out to be successful, the biosensor innovation still faces a daunting secondary barrier for commercialization: the regulatory approval. As explained below, the FDA regulation is not adapted to the biosensor market and it faces important challenges to support innovation by approving reliably in a sensible time the innovative biosensors while ensuring the high safety standards in the US. We believe these regulatory issues are the main cause of the deleterious trends observed in the US market.

- **The FDA market approval**

Regulation for biosensors goes under the general regulation of medical devices established under the Food, Drug and Cosmetic Act (FD&C Act) in 1976. Under the FD&C Act, FDA needs to ensure the safety and effectiveness of medical devices. The regulation is based on a risk classification with three levels:

- Class I: for devices without a potential unreasonable risk to health and are submitted to a “general controls” test requirement
- Class II: for devices with a greater risk of harm than class I and are submitted to a “specific controls” test requirement
- Class III: for devices that raise a potential unreasonable risk to health and are submitted to a “premarket approval” (PMA) test. Genuinely novel devices are directly classified as class III devices.

Biosensors, more than other medical devices, tend to be novel devices since they usually

integrate innovations in nanotechnology. Therefore, biosensors tend to fall under class III due to their novelty but an important aspect of the regulation is the reclassification possibility as class I or II under what is defined as the 510(k) pathway. The 510(k) pathway is a significantly shorter process to get market approval than the normal pathway that is the pre-market approval process. In order to get access to the 510(k) pathway, it needs to be shown that the device exhibits “substantial equivalence” to already approved devices. 90 % of devices are actually approved through the 510(k) pathway. However, in the future, the convergence of nanotechnology, biotechnology and electronics will provide many new biosensors that will fall more and more under the pre market approval process.

The pre-market approval (PMA) is composed of 3 phases: phase I is the preclinical trial usually on animals, phase II is the pilot trial with clinical trials on a representative portions of the population and phase III is the pivotal trial with clinical trials on a greater number of patients. The process takes between 5 and 10 years and costs between 50 and 150 \$ millions. The 510(k) process is significantly shorter and comprises at most the phase I of the PMA. Its costs is between 10 and 50 \$ millions. Finally, based on the results of the trials, FDA makes a risk-benefit assessment to decide on approval^{3, 11}.

The 510(k) pathway and the PMA process as currently designed and implemented are not adapted to support innovation by approving reliably in a sensible time the innovative technologies while ensuring safety. Indeed, according to the survey by the Medical Device Manufacturing Association mentioned above¹⁶, the two third of life science investors are reluctant to invest in the industry because of regulatory challenges. Therefore, the approval process seriously hampers the commercialization of innovation and had very negative consequences for the biosensor market in the US, which could soon lead to the loss of leadership in the field for the US essentially in benefit of Europe.

- **Issues with the FDA regulation**

The main issue with the US regulation leading to the negative impacts that will be described later is the too stringent, lengthy and unpredictable approval process in the US, both from 510(k) pathway as well as the pre-market approval^{11, 13}. Since 2007, FDA has toughened and slowed down its approval process in reaction to criticism that its former approvals for some products had been lax, leading to a spate of recalls of some unsafe medical devices, like implanted defibrillators and hip replacements. Indeed, from 2007 to 2010 the average time to approve a medical device application increased 43 percent and the average time to obtain a pre-market approval (PMA) application increased 75 percent¹⁶.

However, maintaining such a line in a weakened economy could be very detrimental to the industry and profound changes are needed.

The approval process is firstly too lengthy with too long clinical trials and delays in moving to the next step in the process. The all-or-nothing approach of FDA for market approval with the trend of toughening and slowing down the process in order to presumably ensure more safety and effectiveness has led to this length extension in the process. However, it is obviously crucial to wonder if the very tough criteria of the US regulation are not an essential prerequisite to ensure the high safety standards in the US? Comparing the results of the European and the US

regulation resolves this primordial question. The same medical devices have been approved in both Europe and the US as well as the same recalls of devices for additional proofs of safety have been made as shown by two studies by PWC and AdvaMed^{11, 17}. And yet, the European approval process is twice shorter than the US one^{11, 14}.

Therefore, the results in terms of safety of both regulations have been the exact same, which clearly emphasizes that the longer and tougher US regulation does not lead to better safety standards. Therefore, it underlines that the additional safety requirements of US regulation may be superfluous and unnecessary since they hamper innovation by lengthening the process of approval and making it more costly without leading to better safety. The need to prove effectiveness as well as safety under the Food, Drug and Cosmetic Act, compared to Europe where only proof of safety is required, helps also to make the market approval process longer.

In addition, FDA's lack of adequate resources and investment to keep up with rapidly evolving technologies is also responsible in part for this lengthy process. The healthcare reform that will give more responsibilities to FDA could aggravate this financial issue. The need for more staff as well as investment in state-of-the art technologies is becoming critical. Therefore, it takes half less time in Europe to get approval for the same technology. This lengthy approval process costs a lot of money and loss-of-profits for companies in part due to the erosion of the market exclusivity of their patent on the technology. And yet, a faster approval does not lead to a degradation in safety since the same devices get approval in the US and in Europe and the same number of recalls have occurred in both places, as mentioned by a study by PricewaterhouseCoopers (PWC)¹¹.

Another issue with the approval process is the uncertainty around the approval decision. This is essentially due to a lack of transparency in the decision making process. Indeed, another PWC study shows that FDA changed its position on at least one review in more than 60% of approval processes¹¹. This lack of predictability and these changing decisions are in part linked with the fact that politics has too much influence on the approval process, as 60 % of the respondents agree on it. The lack of adequate review resources contributes significantly to the uncertainty around FDA's decisions. Thus, 40 % of respondents to the survey think that FDA denied some products because of inadequate review resources and only 22% of respondents disagreed with this conclusion¹¹. Finally, the unpredictability is also due to the communication during the development process between FDA and the industry that falls short on both sides. The FDA usually fails to provide enough feedback during the process. The industry is not consistent in scheduling presubmission and end-of-phase meetings with FDA, and FDA does not always encourage these meetings. The industry usually lacks awareness of major FDA initiatives.

Therefore, the uncertainty surrounding FDA's approval decision adds a layer of risk on investments for commercialization of biosensors. Many companies already starting approval process in Europe, will delay and in worst cases refuse to invest money to get US approval in a logical risk-adverse decision faced with the uncertainty in the US approval process.

Finally, the premarket approval process is especially getting tougher and longer, which very seriously hamper the commercialization and even the development of disruptive innovations in medical devices and even more in biosensors. This concern is specifically relevant in the field of biosensors where revolutionary innovations with the convergence of nanotechnology and biotechnology usually will require taking the PMA process. The very long (between 5 and 10

years) and tough approval is excessive for biosensors. The fact that the number of premarket approval is considerably decreasing from 48 in 2000 to 19 in 2011, the lowest level since 1983, emphasizes the more stringent position adopted by FDA¹³. This is obviously a strong deterrent for investors to even start investing in the development of the more novel and radical biosensors technologies.

Thanks to the favorable environment for innovation with the excellence of the research done in academic and private institutions, the US still keeps the leadership for innovation in the biosensor market and medical devices market in general with some 32 of the 46 medical technology companies with annual sales exceeding \$1 billion based in the United States¹³. However, recent trends are alarming with investments and production moving to Europe because the too tough and long FDA regulation, contrary to the European one, is a deterrent for companies to spend the money and take the risk to get market approval in the US. Some policy recommendations can be made to rectify this regulatory failure and invert the trends in a positive way in order to maintain the US leadership in the biosensor market.

5- Policy recommendations

- **Recommendations to lessen the burden of high development costs**

The high development costs of biosensors due to the high technical requirements that they need to meet are not likely to decrease. However, as an increasing number of demand-oriented biosensors are developed and become more widespread as well as incorporated in operational standards, the higher sales volumes will very likely support the high R&D expenses. Two policy recommendations can be made here in order to ease the difficulty of investments in the development process. A first one is to remove a new tax that could be detrimental to innovation in the biosensor field. Indeed, the Patient Protection and Affordable Care Act imposes a new excise tax of 2.3 percent on most of medical devices, biosensors included, effective in 2013. It will be levied on the total revenues of a company, regardless of whether a company generates a profit, starting in 2013. Thus, many companies will owe more in taxes than they generate from their operations, especially smaller manufacturers that are responsible for the overwhelming majority of innovation in the medical device industry¹⁸. Consequently, the tax is estimated to induce in the future a \$2 billion dollars cut per year in R&D, ie \$20 billion over 10 years, in the entire medical device industry¹⁹.

This reform is probably going to severely harm innovation in the biosensor market. Defenders of the tax reform claim that the costs of this "innovation tax" will be offset due to an increased pool of insured beneficiaries receiving treatment with the Patient Protection and Affordable Care Act. However there is no data or studies that show that it is going to be the case. In fact, since the majority of products impacted are used in acute care settings where there are legal obligations to treat a patient, the effect of expanded coverage is not likely to increase utilization¹⁸. Recognizing the risk of investment in the high development costs of biosensors, the excised tax should be repealed for the case of biosensor technologies in order to support innovation and avoid the flow of investment to Europe and a more important shrink of venture capitalist funding.

On the contrary, subsidies and tax credits should be granted to the most innovative biosensor technologies in order to create some incentives for investments in the development of these biosensors. Some of the funds for example of the Federal Coordinating Council for Comparative research, founded and funded for \$ 1.1 billion should be used to subsidize development process of these technologies. The mechanism for subsidies should be copied on the Clean Energy and Recovery Act that subsidy 1% of the innovative projects that were likely to have the most impact on the economy. This Act enabled to bolster the clean energy sector with expected creation of 700 000 jobs in 2012²⁰ and likewise a similar subsidy plan in the biosensor field should boost the innovation in the sector.

The second recommendation is to impose or incentivize through regulation the standardization of the use of biosensors in government institutions and industries in order to foster their widespread use. Indeed, the development of new biosensors are gradually leading to standardization of equipment, type of biomolecule, and test processes in the areas of drug discovery, biodefense, environmental monitoring, and narcotic detection²¹. However, despite significant innovations in biosensors, there is still a low degree of technical change in industry and government institutions²². The degree of technical change is measured in accordance with the introduction of newer technologies in the market year round. An increase in the rate of technical change is important for the introduction of newer products, leading to a quicker market penetration. Thus, the low degree of technical change in the biosensor market limits the end-user base and therefore the growth in revenues to justify the investment in the high development costs. This low degree of technical change is essentially due to the fact that, in some cases, alternative analytical techniques can roughly do the work of a biosensor. An integrated biosensor usually has significant advantages over alternative diagnostic methods, but it may cost as much or even more. Thus, many companies and institutions use non- biosensor technology where biosensors can be used in a lot more successful way and open up new opportunities, especially because the switching cost to biosensor can be a deterrent as people are used to old technologies and usually don't want to make the effort of changing the equipment²².

Therefore, the creation of regulation to impose the standardized use of biosensors would foster their widespread use by replacing older technologies. For example, creating government regulation to impose the standardized use of biosensors in the early detection of some diseases like cancers in hospitals would both benefit the quality of prevention thanks to higher sensitivity and rapid monitoring of biomarkers by biosensors. Doing early detection of cancer is still not implemented in most hospitals, which implies that most cancers are detected when they are at advanced stages. Implementing early detection of cancer could considerably reduce healthcare costs and greatly increase the chances of cure for the patient¹. The regulation here could considerably speed up the standardized adoption of biosensors for early cancer detection. Likewise, FDA could impose the use of biosensors for biomarkers monitoring in clinical trials since they enable a rapid monitoring. . In addition, advertising and informing about the advantages of biosensors as well as the new innovations in the field by federal agencies like FDA or EPA would also help to promote the use of biosensors. For example, EPA has already published much information about the advantages of biosensors for environmental monitoring and FDA should pursue a similar informational policy. Likewise, FDA should inform and promote every semester the new innovative biosensors on the market like for example, a new developed biosensor which is a hand-held probe for real-time breast cancer diagnosis using RF

spectroscopy developed by Dune medical devices that could significantly help the detection and even surgery of breast cancer especially for older people²².

Thus, these policy recommendations would represent a strong signal for investors that higher volume sales are to be expected thanks to the new policies and therefore it would further help to support the high R&D expenses.

- **Recommendations to improve the FDA regulation**

The first and most important change is to optimize the market approval process through regulatory harmonization with Europe, which has a two-times shorter market approval process. Indeed, from 2007 to 2010, in the US, the average time to approve a medical device application increased 43 percent and the average time to obtain a pre-market approval (PMA) application increased 75 percent¹⁶. Therefore, there is an urgent need to align with European standards that are better adapted to support innovation by approving reliably in a sensible time the innovative technologies while ensuring safety. As we describe earlier, the safety results of both the US and the European regulation are the same with the approval of the same devices. However, the European regulation is twice shorter and the entire market approval process is more understood by the industry.

The longer US regulation entails significant additional costs for the industry that is more and more reluctant to invest in the US market approval. Therefore, there is a crucial need to shorten the US approval process and this should be made possible without any degradation in safety since Europeans have done it. In this outlook, the first and most straightforward policy recommendation to shorten the process is to remove the FD&C Act requirement of proving the effectiveness of the device for the case of biosensors, and more generally of medical devices. This would be an efficient policy to shorten the process and focus on the safety demonstration of the device. This will speed up the market approval process and so will enable new biosensors to start making revenues and reimbursing the investment at an early stage. Indeed, the absence of effectiveness demonstration in the European regulation is one of the reasons that make the European approval process twice shorter.

An specific example of this is the case of the GuardWire device by Medtronic. In the European Union (EU), the GuardWire device was awarded CE marking by demonstrating safety and performance (i.e., the ability to aspirate material during the stenting procedure) in a 22-patient, single arm study. In the United States, this device was designated Class II. To demonstrate safety and effectiveness (defined as the ability to reduce complications associated with stenting of saphenous vein grafts) the FDA required an 800-patient, multicenter, randomized trial comparing distal protection to usual care (no protection). As a result, the GuardWire was available in the EU at least two years before U.S. physicians had access to the technology²³.

Is this policy recommendation compromising safety of American citizens? We believe the answer is no. Indeed, effectiveness of the device is completely unrelated to safety and that is why it should not be a requirement. An additional proof of this is that European safety is as good as the American one, as mentioned earlier, even though there is no effectiveness requirement in the European regulation and devices come earlier on the European market^{13, 14}. However, we can

still wonder if it is really needed or not to have effectiveness demonstration requirements for biosensors, even though it does not affect safety of the technology. This policy controversy needs to be resolved looking at the tradeoff of effectiveness versus bringing quickly the benefits of technologies without costly delays. On the one hand, it would be better that all biosensors were 100 % proven effective but on the other hand, there are significant delays associated with effectiveness demonstration. These delays have two negative consequences. First patients in the US get innovative devices that can help significantly improve their health two to three years in average after their European counterparts²⁴. Secondly, delays induce great costs for companies that decide in some cases not to market in the US, depriving American citizens from their innovations.

In light of this compromise, there are two reasons why the effectiveness demonstration should be removed. First, biosensors are generally much more passive medical devices than drugs. In case the biosensor is not effective, the patient's health does not obviously get better but it does not get worse either. Indeed, biosensors are not therapeutic in the sense that they are a detection tool or a help for a better treatment but do not represent a treatment for cure. Therefore, if biosensors are not effective, the patient does not benefit from this additional tool but his health is not affected. That is why, drugs, on the contrary, absolutely need to be effective because if they are not, the patient is receiving a useless treatment and suffering from the fact that instead of being cured, his situation is usually worsening since the disease is aggravating. For example, in some cancers, you can use biosensors to detect biomarkers close to a tumor and see if the treatment you are using is effective^{9,22}. If the biosensor is defective, first the doctor does not have the additional information about the efficacy of the treatment on the patient but the treatment to cure the patient is typically not affected by this deficiency.

On the contrary, if the drug to treat the cancer is not effective, the patient health is getting worse significantly as the cancer grows. The doctor could have prescribed another more effective treatment and so here the ineffectiveness of the drug has harmed irreversibly the patient. Thus, a drug needs to be absolutely effective because otherwise it is significantly harming the patient whereas for a biosensor, its ineffectiveness means that the patient does not benefit from this additional tool but his health is not affected. Therefore, the impact of biosensor ineffectiveness is not significant. The second argument to justify the removal of effectiveness demonstration is that it is pretty straightforward to figure out that a biosensor is ineffective and the market that already requires very high technical standards will be quick to dismiss the technology³. Indeed, tests on standard samples can quickly show that a biosensor is not effective. Therefore, post-market surveillance of effectiveness will be quick and effective at removing inefficient biosensors if the market has not already dismissed them.

For these two reasons and the deleterious consequences of delays induced by effectiveness demonstration requirement, it is recommended that the effectiveness demonstration requirement be removed, as it is the case in Europe.

Nevertheless, post-approval demonstration of effectiveness and market surveillance should be required to the industry in order to maintain quality products on the market that are effective.

Another important reason that makes the market approval process of biosensors too lengthy is the zero risk and all-or-nothing attitude showed by FDA in the last decade¹¹. This approach has

led to major delays asking for always larger clinical trials than in Europe and the number of PMA of medical devices has fallen from 48 in 2000 to 19 in 2011, lowest level since 1983. The industry has intensely criticized the FDA approach and asked for a laxer approval decision and an anticipated risk/benefit analysis to be considered. The policy controversy here focus around the tradeoff between ensuring the highest safety before approval with trying to make risks tend to zero and bringing quickly the benefits of technology to the market without costly delays. FDA has decided to adopt the zero-risk approach without considerations of the 3 year delay compared to Europe in order to bring benefits of new medical devices to American citizens as well as the large costs these delays caused to industry with the outflow of capital outside the US that is induced. FDA's approach to overlook the consequences of its delays would be probably justified if it insured better safety results that really protect better America's health.

However, as mentioned earlier, the safety results of the European and US regulation are the same with the same devices approved and the same recalls. And yet, European decision for approval is laxer than the US one and based on a risk/benefits analysis¹³. Thus, the zero risk attitude does not lead to an increment of higher safety. The reason for this is that the actual cause of a recall is very often outside the scope of the approval process. The most frequent causes of recalls are isolated lot-related subcomponent failures; manufacturing issues such as operator error, processing error, or in-process contamination; latent hardware or software issues; and packaging or labeling issues. In addition, company communications that describe incorrect and potentially dangerous procedures used by some medical personnel are also considered a recall, even though the device is not faulty²⁴.

Taking this in consideration, our policy recommendation is to implement a more adaptive and laxer approval process taking into account risk/benefits analyses for the biosensor market since it enables to bring benefits of innovation quicker to patients as well as remove the costs associated with delays to the industry without any degradation of safety standards. The all-or-nothing FDA's approach should be replaced with a limited-launch, living-license process as soon as a reasonable risk/benefit analysis can be done from the studies. This process would be based on gradual accumulation of data over time and conditional incremental approvals beginning with evidence from smaller populations. This adaptive regulation is a lot more adapted to the biosensor market because by doing a limited launch for people that would most benefits from the technology, FDA can monitor and detect these potential additional safety issues that lead to recalls and that are very unlikely to be possible to detect during the approval process even in the current zero risk approach of FDA. Indeed, usually these additional safety issues when they appear will be detected with the beginning of mass marketing during the limited launch²⁴.

Especially for the PMA process, getting a limited market approval before completion of phase III in PMA should be given provided that phase II of the PMA process give very usually enough insurance to do a reasonable risk/benefit analysis. Post market surveillance for safety should be then required in this case in order to identify any new safety issues that might be identified.

In addition to making the process shorter, another important aspect of the regulation that needs to be improved is the uncertainty surrounding the FDA decision-making process that makes the investment in biosensors riskier.

This uncertainty comes in part from an inadequate level of FDA's resources as emphasized by

the PWC study¹¹ showing 40 % of respondent think that FDA denied some approvals due to a lack of resources. Increasing the Medical Device User fees would be a good policy recommendation since most respondents to the PWC study consider these fees as not excessive and would be ready to increase them if that could make the process review better¹¹.

The Medical Device User Fee Act (MDUFA) was first established by congress in 2002 and it was allowed again until 2017 on October 1st 2012. The MDUFA allows FDA to collect fees from industry and represents a commitment between the U.S. medical device industry and the FDA to increase the efficiency of regulatory processes in order to reduce the time it takes to bring safe and effective medical devices to the U.S. market. The fees are collected when medical devices companies register their establishment and list their devices with the agency, whenever they submit an application or a notification to market a new medical device in the U.S. The fees give FDA more financial means for their reviews and therefore speed up the process. Under MDUFA III, the FDA is authorized to collect user fees that will total approximately \$595 million (plus adjustments for inflation) over five years. Most of the fees are limited to the pre-market approval PMA process, which is logical since the process is longer and require more review means. However, the contribution of fees towards the 510(k) pathway should be increased proportionally because this pathway is the one taken by 90 % of devices.

Furthermore, MDUFA are essentially used for hiring more staff. As these fees are considered as non excessive, a policy recommendation is to increase fees required from industry in order for FDA to maintain the scientific and technological advances required for clinical trials of the more and more complex technologies coming as in the case of biosensors. Indeed, industry would be inclined to pay more fees if they could see clearly that it would improve the review process¹¹. This increase in fees would then be easily balanced by the gains in reducing the costs of FDA delays and the risk of investment perceived with FDA process. Having state-of-the art scientific knowledge and technologies could significantly accelerate clinical trials and their review since FDA will be able to understand and assess new technologies without having to delay clinical trials as it is the case today in order to keep up with the advance presented by the technology.

In addition, even though these fees come directly from industry, there are not perceived as creating any conflict of interest as respondents to the PWC survey suggest. The reason for it is that when FDA collects the fees, the money goes to the general fund of Medical Device User Fees that contributes generally to improve the FDA process. Therefore, the money is not tied with any specific request for approval and a company could not try to exert pressure to accelerate a particular approval process it is involved in. Increasing them will therefore not reduce FDA's credibility. However the industry, in order to be willing to accept an increase in the fees, call for even more transparency by FDA in the purpose and use of the fees in order to ensure that these fees are efficiently used to improve the review process. Finally, in the case where FDA still does not have the technical capabilities in house to perform efficiently the approval process, it could rely on 3rd party to conduct some parts of the process like clinical trials. This approach could reduce significantly delays due to FDA's inability to conduct the process. This is commonly used in Europe with the use of Notified Bodies that are independent third parties nominated and monitored by Member State' authorities. They carry out pre- and post-market conformity assessment and certification of medical devices based on the requirements of the EU Directives. This approach has been successful in Europe at compensating the limited resources in some areas of the European Medical Agency without delaying the process and while maintaining

the high safety standards of Europe²⁵.

In addition, the uncertainty around FDA procedures and its decision making process should be reduced. Indeed, the PWC survey shows that FDA changed its position on at least one review in more than 60% of approval processes. This uncertainty contributes to increase the risk associated with investment in biosensors since the industry does not consider the approval process as being reliable enough with clear expectations about all requirements in the process. A more predictable process in its requirements and procedures could be obtained by a stronger collaboration between the FDA and the medical device industry.

A better collaboration will be enhanced by an open and clear communication during all the steps of the approval process between the FDA and the industry. The scheduling and encouragement of more meetings between FDA and the biosensor company should be organized at all stages of the market approval from pre submission to end-of-phase meetings. FDA should work to solidify submission requirements and improve communications during the development process as well as industry should ask for more guidance. The regulator should pay attention to encourage industry participation in review meetings, especially later in the product approval process when delays and failures are more costly. Finally, FDA should provide more guidance to industry about the review process and also communicate more effectively its major initiatives. Indeed, for example, half of the industry lacks awareness of the high-priority FDA programs like the Critical Path plan or the Sentinel System plan¹¹. The industry also should make the effort to get updated frequently with FDA new initiatives. A monthly publication of FDA's guidelines for approval process with possible current changes would definitely help industry keeping up with requirements. The collaboration could be even pushed forward by having industry help FDA develop guidance documents by participating in agency-sponsored work groups and reviewing and commenting on drafts and proposals. Thus, these initiatives for an increased collaboration and communication between FDA and the industry will definitely reduce the uncertainty perceived by the industry in the decision making process and therefore make the investment for market approval less risky.

Finally, the last policy recommendation made to improve even further the regulation for biosensors is the creation of a Biosensor committee inside FDA. As mentioned earlier, the most radical innovations in the biosensor field will come from the convergence of nanotechnology, biotechnology and microelectronics. Therefore, FDA could find very difficult to review the safety of a technology that gather technologies from all these three fields, which could lead to considerable delays as FDA consult and gather expertise from these fields. The creation of a Biosensor Committee could definitely avoid these delays. The committee will gather experts from the nanotechnology, biotechnology and bioelectronics fields in order to assess the new technologies. This will be an efficient way of doing a relatively fast approval while insuring very high safety standards. Medical Devices User Fees coming from biosensor companies could directly fund this committee.

• Conclusion

In conclusion, despite the fact that the biosensor field is going through a technological revolution that gives birth to radical innovations that could considerably improve America's health, there is

a risk that American citizens will not enjoy soon the benefits of them since these innovations struggle too much to reach market. If the key market drivers are strong for the commercialization of these innovations, their successful commercialization faces two subsequent high barriers: high development costs and a too lengthy and uncertain FDA market approval. The FDA regulation is not adapted to support innovation by approving reliably in a sensible time the innovative technologies while ensuring the high safety standards in the US. On the contrary, the European regulation with the same safety results as in the US but a two times shorter process is better adapted. The consequences of the ill-adapted FDA regulation are very negative with a shrink of venture capital funding and an outflow of capital from the US to Europe which enable European people to get access to new technologies 3 years before American people. The situation has become critical and led to a regulatory failure, which calls for urgent changes.

Therefore, policy recommendations can first be made to decrease the burden of development costs by removing the new excise tax of 2.3% enacted by the Patient Protection and Affordable Care Act as well as incentivize through regulation the standardized use of biosensors for higher operational standards. Nevertheless, the main policy recommendations aim at harmonizing the US regulation on the European one and make it even better to support innovation. First, FDA approval should remove the effectiveness of device demonstration requirement as done in Europe as well as adopting an adaptive regulation with a limited-launch, living-license process instead of an all-or-nothing approach. This will reduce considerably the length of the process to be in agreement with the European one without compromising the high safety standards required in the US. In addition, in order to reduce uncertainty around the FDA decision making process and the requirements for the approval process, the Medical Device User fees should be increased so that FDA can hire more staff and keep updated with state-of-the art technologies. A stronger collaboration between FDA and the industry should also be achieved with reciprocal feedback to make the process more understandable. Finally, a Biosensor committee should be created in order to assess new biosensor technologies that will be at the interface between nanotechnology, biotechnology and bioelectronics. Following these policy recommendations should restore a well suited regulation that supports innovation while ensuring the high safety American standards as well as it will enable the US to keep the leadership in the biosensor market.

References

- (1) Bohunicky, B.; Mousa, S. A. Biosensors: the new wave in cancer diagnosis. *Nanotechnology, Science and Applications* **2011**, *4*, 1-10.
- (2) Frost & Sullivan An Analytical Review of World Biosensors Market. **2010**, *N810-32*.
- (3) Kalorama Information, L. Information Market Intelligence report: Medical and Biological Sensors and Sensor Systems. **2006**.
- (4) Balasubramanian, K.; Burghard, M. Biosensors based on carbon nanotubes. *Analytical and bioanalytical chemistry* **2006**, *385*, 452-468.

- (5) Frost & Sullivan World Emerging Sensors Markets. , M678-32.
- (6) Shao, Y.; Wang, J.; Wu, H.; Liu, J.; Aksay, I. A.; Lin, Y. Graphene based electrochemical sensors and biosensors: a review. *Electroanalysis* **2010**, *22*, 1027-1036.
- (7) Jianrong, C.; Yuqing, M.; Nongyue, H.; Xiaohua, W.; Sijiao, L. Nanotechnology and biosensors. *Biotechnol. Adv.* **2004**, *22*, 505-518.
- (8) The Korea Times Cheap Biosensors to Bring Medical Revolution. **2007**.
- (9) Mascini, M.; Tombelli, S. Biosensors for biomarkers in medical diagnostics. *Biomarkers* **2008**, *13*, 637-657.
- (10) Yanik, A. A.; Huang, M.; Kamohara, O.; Artar, A.; Geisbert, T. W.; Connor, J. H.; Altug, H. An optofluidic nanoplasmonic biosensor for direct detection of live viruses from biological media. *Nano letters* **2010**, *10*, 4962-4969.
- (11) PricewaterhouseCoppers and Biocom Improving America's Health V. **2010**.
- (12) Schoonmaker, M. In *In The US Approval Process for Medical Devices: Legislative Issues and Comparison with the Drug Model*; Congressional Information Service, Library of Congress Washington, DC: 2005; .
- (13) The New York Times Medical Treatment, Out of Reach. *Feb 2011* .
- (14) PricewaterhouseCoppers Medical Technology Innovation Scorecard The race for global leadership. **January 2011**.
- (15) Harvard Executive Consultants Regulatory Environment
http://www.harvardexecutiveconsultants.com/Regulatory_Environment.html.
- (16) Area Development Online Market Report: Medical Device Market Stays Steady in 2012. *April 2012* .
- (17) Medical Design Blog EU vs. US: Study sheds a new light on an old debate, **2011**.
<http://blog.medicaldesign.com/perspectives/2011/01/>.
- (18) Medical Device Manufacturers Association Health Care Reform, Device Tax
<http://www.medicaldevices.org/issues/Health-Care-Reform,-Device-Tax>.
- (19) Pacific Research Institute Obamacare's Tax on Medical Devices: Cuts R&D by \$2 Billion a Year. *2012* .
- (20) The White House Blog Progress on Green Jobs from the Recovery Act, **2010**.
<http://www.whitehouse.gov/blog/2010/01/14/progress-green-jobs-recovery-act>.

- (21) Sensors Mag Strong Growth Predicted for Biosensors Market, **2010**.
<http://www.sensorsmag.com/specialty-markets/medical/strong-growth-predicted-biosensors-market-7640>.
- (22) Frost & Sullivan Biosensors in Medical Diagnostics (Technical Insights). **2006**.
- (23) Applied Clinical trials Online Medical Device Development: U.S. and EU Differences. **2006**.
<http://www.appliedclinicaltrials.com/appliedclinicaltrials/article/articleDetail.jsp?id=363640&pageID=1&sk=&date=>
- (24) Issues in Science and Technology Online Medical Devices: Lost in Regulation
http://www.issues.org/27.3/p_citron.html.
- (25) Eucomed Medical Technology A new EU regulatory framework for medical devices. **2011**.

Conclusion

In this thesis, we have investigated the potential of graphene sensors for chemical and biosensing applications. Graphene is indeed considered as a promising candidate for biosensing because it is all surface 2D material with very high carrier mobility. These properties should enable graphene to combine the two crucial characteristics of a sensor's performance: a very high sensitivity as well as a low noise.

Here we have focused on the design of a graphene solution-gated FET technology because a SGFET has numerous advantages compared to conventional electrode-based sensors such as intrinsic signal amplification, simple electronic read-out and straightforward integration with microelectronics. Using graphene grown by CVD on copper, we demonstrate and test a fabrication process to integrate graphene with SGFET technology on silicon dioxide. We further optimize the fabrication process to clean the graphene surface of any photoresist residues on top of it. In addition, we demonstrate the integration of graphene on plastic substrates in order to pave the way for flexible high performance but low cost sensors.

Then the graphene sensors on different substrates are characterized. Graphene-on-SiO₂ SGFETs exhibit a transconductance around 5 mS.mm⁻¹ and graphene-on-PEN SGFETs a transconductance around 1 mS.mm⁻¹. This is an order of magnitude higher transconductance than conventional planar silicon SGFET technology.

Subsequently, the use of graphene SGFET as pH sensor is demonstrated on SiO₂ as well as PEN substrate. The pH sensitivity is quite high around 20 mV/pH. In addition, we demonstrate that the pH sensitivity is not significantly influenced by the nature of the substrate or the amount of residues on top of the graphene surface, which simplifies the design and fabrication process of graphene pH sensors. Experiments shows that no chemical bonding between the ions in solution and the graphene surface is involved in the pH sensing mechanism that is likely due to the adsorption of hydroxide ions that dopes the graphene surface by surface transfer doping.

Graphene SGFETs are also used to make glucose sensors arrays. We develop a functionalization of graphene that enables to attach glucose oxidase to the graphene surface. The binding of glucose to glucose oxidase likely leads to a transfer of electrons from glucose directly to the graphene surface that dopes the later. This doping induces a shift of the entire transfer characteristics of a graphene SGFET, which enables to sense glucose. The sensitivity is found reliably to be 15 mV/pG and the lower detection limit is 0.1 mM. However an optimization of the functionalization and fabrication process should lead to a lower the detection limit.

We also characterize the noise of graphene SGFETs. Graphene devices exhibit a 1/f noise that follows the Hooge model. After calculating the noise amplitude, we characterize the noise density of the device at the gate. The best performance of monolayer device is found to be 20 μV, which is very good in comparison of the noise of planar silicon SGFET that is an order of magnitude higher.

Therefore, graphene SGFETs are very high-quality sensors with high sensitivity and low noise and their commercialization is promising.

Then, we investigated the potential of bilayer graphene for sensing applications. Indeed, bilayer graphene could potentially exhibit better noise performance than monolayer graphene and therefore be a better candidate for sensors. For this purpose, we design a transfer method that enables to stack two monolayer graphene layer grown by CVD onto a silicon dioxide substrate in order to form bilayer graphene. The bilayer devices are then characterized and exhibit similar transfer characteristics as monolayer devices. However, bilayer devices exhibit twice higher transconductance as expected since the two layers of graphene are uncoupled in our bilayer. We demonstrate pH sensing with bilayer devices with pH sensitivity of 18 mV/pH at the Dirac point, which is slightly lower than monolayer devices. The noise performance of bilayer devices is then measured and compared to monolayer devices. The noise performance of bilayer sensors is reliably better than in monolayer device, which makes bilayer graphene also a very promising candidate for sensing applications.

Finally, although graphene exhibits high performance and great potential for many applications in chemical and biological sensing applications, there is a high risk that the benefits of graphene sensors or other radically innovative sensors will not be soon available to American citizens essentially because of an ill-adapted regulation by FDA of biosensors. The FDA regulation is not adapted to support innovation by approving reliably in a sensible time the innovative technologies while ensuring the high safety standards in the US. The consequences of this regulatory failure are very negative with a shrink of venture capital funding and an outflow of capital from the US to Europe. Policy recommendations are made to restore the US leadership in the biosensor market, especially the implementation of an adaptive FDA regulation with a limited-launch, living-license process in which the effectiveness requirement is removed.

As a final thought, if graphene potential for biosensing applications is demonstrated at the research level in this thesis, the commercialization of graphene sensors will require the demonstration of secondary but very needed properties of graphene sensors like stability, biocompatibility, reliability and selectivity.